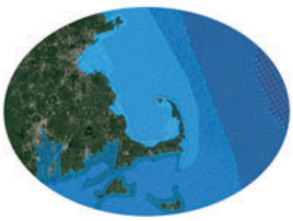

Simulations of 2018 Hydrodynamics and Water Quality in the Massachusetts Bay System using the Bays Eutrophication Model

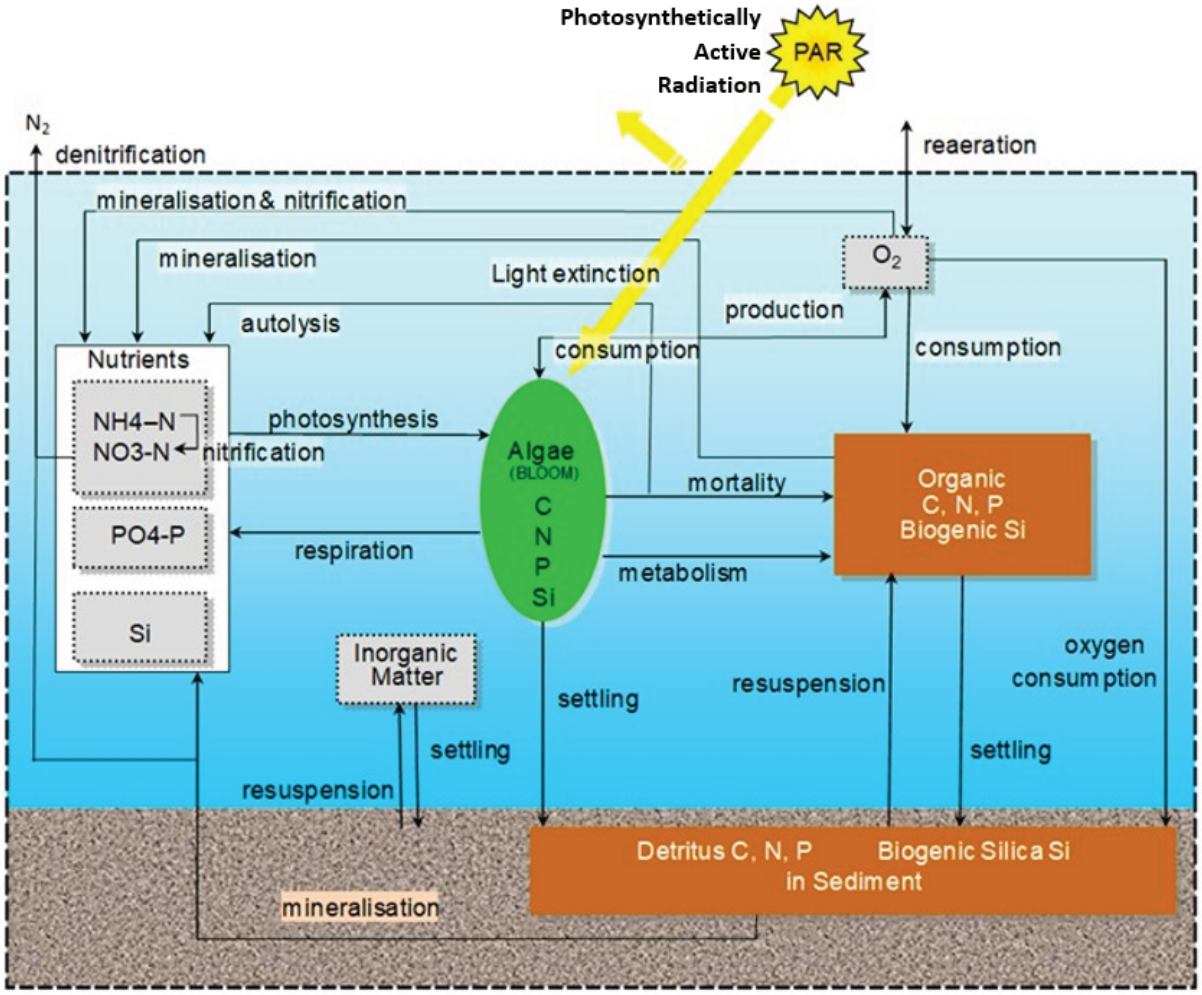

Massachusetts Water Resources Authority
Environmental Quality Department Report
2022-06

Citation:

Deltares, 2022**. Simulations of 2018 Hydrodynamics and Water Quality in the Massachusetts Bay System using the Bays Eutrophication Model.** Boston: Massachusetts Water Resources Authority. Report 2022-06. 89 p.

MWRA Environmental Quality Department reports can be downloaded from http://www.mwra.com/harbor/enquad/trlist.html.

Summary

Background. This report presents hydrodynamic and water quality model results for the Massachusetts Bays system (Massachusetts Bay, Cape Cod Bay, and Boston Harbor) during 2018. Treated effluent sent from the Massachusetts Water Resources Authority (MWRA) treatment plant through a 15 km (9.5 mi) long tunnel and released at an outfall offshore in Massachusetts Bay contains nutrients. Nutrients are necessary and important to support healthy and diverse marine ecosystems. However, excess nutrients can cause eutrophication, the overgrowth of phytoplankton (microscopic marine algae) which degrades water quality and can harm marine life by depleting oxygen when it decays. To address potential eutrophication and other concerns, MWRA maintains an extensive bay and harbor field monitoring program, which this modelling complements. The hydrodynamic model simulates temperature, salinity, and currents, and is the foundation for the water quality model, which simulates key eutrophication parameters including nutrients, chlorophyll (a measure of phytoplankton), and oxygen.

Results for 2018. Consistent with field observations, the model did not show effects of effluent on chlorophyll or oxygen, nor indications that eutrophication was occurring. Hydrodynamic results for 2018 agree well with available observations and capture the geographic and vertical structure, and temporal variability, of temperature and salinity distributions and density stratification, as well as tidal and non-tidal currents. The 2018 water quality simulation captured general patterns in observed seasonal variations, geographic distributions, and vertical structure for many variables. This included the late spring reduction in near-surface dissolved inorganic nitrogen (DIN) due to phytoplankton uptake, and its replenishment after mixing in fall due to cooling and storms. It also included seasonal dissolved oxygen variations, with peak values in spring at shallow depths due to colder water and phytoplankton growth, and late summer minima at depth where stratification inhibits reaeration by air-sea exchange. In addition to those more bay-wide patterns, in the model as in observations, DIN was elevated persistently within about 10 km (6 mi) of the outfall and intermittently as far as about 20 km (12 mi) away, mainly due to nitrogen from ammonium in the treated effluent. The model captured the observed vertical structure of this effluent influence, which reached the surface through the winter months and remained at depth from about May through October when the bay was stratified.

In 2018, surface heat flux and winds were generally in ranges typical of past years, as was river flow with the exception of relatively high flow during fall. Skill metrics and model results were in similar ranges as past simulations. Overall, the water quality model accurately represented observed vertical gradients and temporal dynamics of key variables, including light conditions, dissolved inorganic nitrogen, particulate organic carbon, and dissolved oxygen. The phytoplankton community structure in the model was generally similar to past years and consistent with available 2018 observations, including low *Phaeocystis* except for an increase mainly in Cape Cod Bay during springtime.

Overall, the 2018 simulation supports the conclusions from field monitoring, that eutrophication was not a concern and bay-wide ecological function was not appreciably influenced by the outfall.

Special studies. Simulations to refine nitrogen budgets and characterize effluent dilution using this model, which was updated in recent years, confirmed prior understanding. In nitrogen budgets the fluxes in to the bays from Gulf of Maine waters dominate. Dilution is typically about 100-500 within Massachusetts Bay and higher father away, for example in Cape Cod Bay.

Contents

List of Figures

List of Tables

1 Introduction

The Massachusetts Water Resources Authority (MWRA) has established a long-term monitoring program to evaluate the impact of its sewage treatment plant effluent on the water quality and ecosystem function of Massachusetts Bay, Cape Cod Bay, and Boston Harbor. The monitoring program primarily consists of a series of ongoing field observation surveys and includes complementary water quality modeling as required by the discharge permit. The water quality simulations are carried out using the Bays Eutrophication Model (BEM; Deltares, 2021). This report presents simulation results for the 2018 calendar year. The content of this report is derived from internal Deltares document 11203379-005-ZKS-0003 dated 4 August 2022, except for the material in section 6 on refined nitrogen budgets and on effluent dilution, which is from internal Deltares document 11203379-008-ZKS-0012 dated 12 May 2022 and internal Deltares document 11203379-008-ZKS-0013 dated 13 May 2022, respectively.

1.1 Background on oceanographic processes influencing water quality

Massachusetts Bay and Cape Cod Bay (Figure 1-1) comprise a temperate coastal embayment system. Readers unfamiliar with the geography and/or the current understanding of the physical and biological oceanographic processes characterizing the system are referred to the introductory summaries found in sections 1.2 and 1.3 of MWRA Technical Report 2011-13 (Zhao et al., 2012), in the annual MWRA water column monitoring reports (e.g., for calendar year 2020, Libby et al., 2021), and in references cited by them. (All MWRA Technical Reports, including those just cited, are available online at http://www.mwra.state.ma.us/harbor/enquad/trlist.html.) A brief summary follows here. In this subsection the focus is on processes and influences other than effluent from the MWRA outfall, which has been shown in past studies to have a minor system-wide effect.

System hydrodynamics are characterized by a persistent general circulation pattern driving the flow of offshore Gulf of Maine waters into Massachusetts Bay via the Western Maine Coastal Current off Cape Ann, then southward before returning offshore just to the north of Cape Cod, with a portion of the flow first passing through Cape Cod Bay to the south (Figure 1-1). Rough estimates of the water residence time are about a month based on the surface currents, somewhat longer at mid-depth or deeper, where currents are weaker, and also longer in Cape Cod Bay than in Massachusetts Bay. While this slow general circulation is important in determining long-term average transport pathways, superposed on it are stronger and more variable wind-driven currents, and oscillatory tidal motions. Temperatures follow the characteristic temperate seasonal pattern of minima in late winter and peaks in late summer. Salinities are freshest inshore and in the upper several meters; in addition to the influence of offshore oceanographic conditions, they vary mainly in response to riverine inputs including primarily those brought by the Western Maine Coastal Current and the Merrimack River outflow to the north, and to a lesser extent the smaller amounts delivered via Boston Harbor. There is a seasonal cycle in vertical structure that includes transitions between well-mixed conditions, present from fall through early spring due to higher winds and atmospheric cooling, and strong density stratification during the late spring and summer due mainly to increased surface temperatures resulting from atmospheric heating.

The biology of the system is plankton-based and exhibits clear seasonal cycles that are tied closely to those hydrodynamic features, but with more pronounced spatial and interannual variability. Phytoplankton abundance typically peaks most strongly during bloom-favorable conditions in the late

winter and early spring, as temperatures rise, light increases, and nutrients remain plentiful near the surface due to the active vertical mixing. Following the transition from spring to summer, near-surface nutrient concentrations become depleted as density stratification impedes the vertical mixing that replenishes them. Zooplankton abundance and biomass generally peak in late summer, following the spring increase in phytoplankton prey levels. Primary productivity is commonly sustained at modest levels through summer and typically there is a second increase in phytoplankton during fall, when vertical mixing increases again and delivers nutrients to the surface while temperature and light conditions are still favorable before winter. Dissolved oxygen concentrations are influenced by a combination of biological and physical processes; the net result is a seasonal peak in late spring, due to phytoplankton production increasing winter levels already high due to strong reaeration, then steady decreases to a late summer minimum due to respiration and reduced reaeration. The summer oxygen minimum is lower at depth, where stratification limits reaeration.

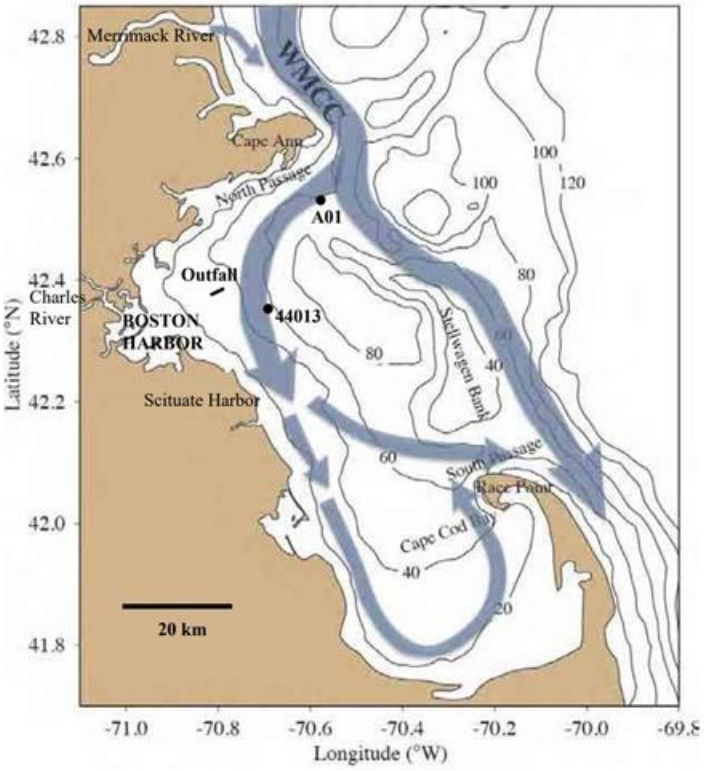

Figure 1-1 Geography, bathymetry, schematic long-term mean circulation. WMCC = Western Maine Coastal Current. A01 = Oceanographic mooring (Northeastern Regional Association of Coastal and Ocean Observing Systems). 44013 = Weather buoy (National Data Buoy Center). Contours = water depth in meters. Figure from Zhao et al. (2017), adapted from Xue et al. (2014).

1.2 Summary of observed 2018 conditions

To provide context for descriptions of model simulations of 2018 throughout this report, a brief summary is given here of observed 2018 conditions based on monitoring results (Libby et al., 2019). River flow for the year 2018 overall was higher than typical, although Merrimack River flow was lower than typical during the spring freshet period from April to June. In early March there was a very intense and long duration Nor'easter storm, with sustained winds of nearly 20 m s^{-1} and wave heights up to 10 m at the peak of the storm. Nutrient concentrations were in the range of past years, including the seasonal cycle with drawdown in spring and replenishment in fall. Annual total phytoplankton

abundance and chlorophyll concentrations were lower than typical, in part because strong bays-wide winter/spring diatom or *Phaeocystis* blooms were not observed. There was, however, a moderate *Phaeocystis* bloom in Cape Cod Bay during April. Zooplankton abundances were higher than typical, with the dominant copepod species reaching abundance maxima for the 1992-2018 period at many Massachusetts Bay stations. Upwelling-favorable southwesterly winds in June/July led to cooler surface waters offshore (at station F22) but not further inshore. June upwelling raised deep oxygen concentrations, such that the minima later in summer were not as low as otherwise would have been the case. There was a late summer Nor'easter storm which resulted in warmer water at depth, consistent with downwelling driven by the storm, at both nearfield and offshore stations; late summer bottom water temperatures at nearfield station N18 were warmer than the 1992-2017 maximum.

2 Methods

A complete model description is documented in MWRA's technical report 2021-02 and its appendices (Deltares, 2021). The model is set up in the Delft3D Flexible Mesh Suite, developed by Deltares. Technical details on the model set-up, its grid and forcing is presented in Appendix A of Deltares (2021). A description of the software package and underlying hydrodynamic and water quality equations are available in Section A1 of Deltares (2021), and in Deltares (2019a, b). The model has been calibrated for the years 2012-2016, as described in Appendix B of Deltares (2021). The results of the model validation are given in the main report body of Deltares (2021).

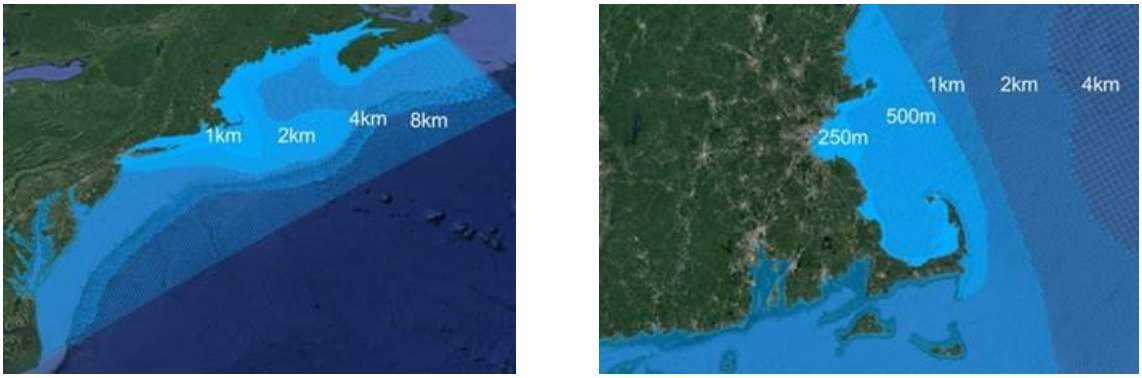

Figure 2-1 Model grid of the entire model domain (left) and zoomed-in for Massachusetts Bay (right).

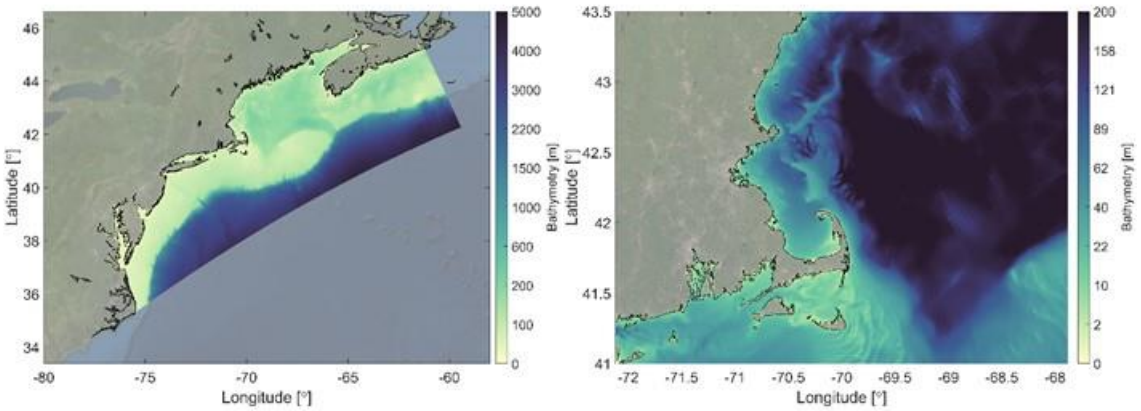

Figure 2-2 Model bathymetry of the entire model domain (left) and zoomed-in for Massachusetts Bay (right).

The model domain is large in order to best handle influences of offshore boundaries, as explained in Deltares (2021); it covers the entire Gulf of Maine region as well as the coastal region to the south, down to and including Chesapeake Bay (Figure 2-1 and Figure 2-2). Model performance in comparison to field measurements has been demonstrated most carefully in the area of Massachusetts Bay nearest the outfall, using MWRA observations (Deltares, 2021). The horizontal resolution is roughly 8km at the open ocean and is gradually refined toward the coast, with a maximum resolution of 250m in Boston Harbor and along the surrounding coastline, including at the outfall location.

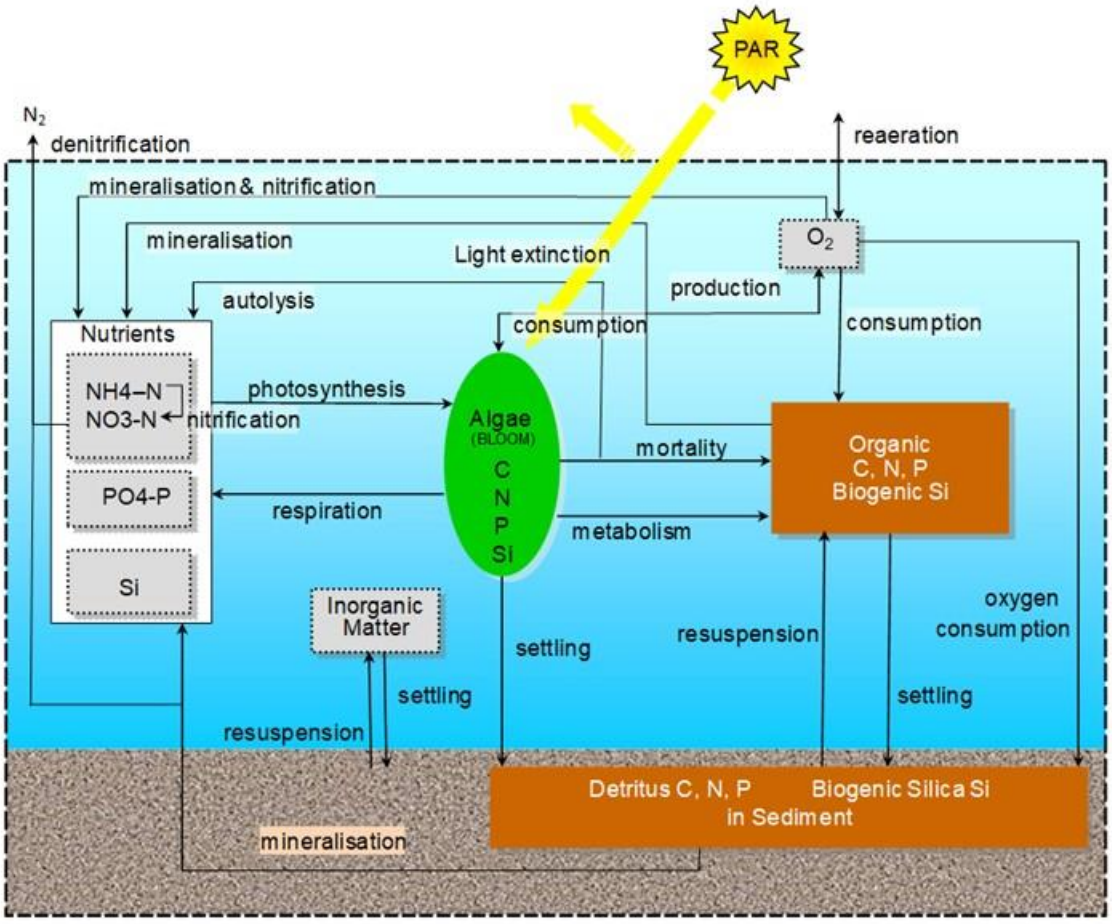

Figure 2-3 Schematic overview of all state variables and processes. Reproduced from Deltares (2021). Note that Inorganic Matter, Algae and Detritus affect light extinction in the water column.

Figure 2-3 provides an overview of the simulated state variables and processes for the water quality component. Four functional groups of pelagic phytoplankton are simulated (“Algae” in the figure): diatoms, dinoflagellates, other flagellates, and *Phaeocystis*.

The monitoring stations used to assess model performance and the transects along which water quality variables are examined are mapped in Figure 2-4. Model-observation comparison time-series are plotted for a representative selection of eight stations: N01 in the Northern Mass Bay, F22 with a greater oceanic influence, F23 near the outlet of Boston Harbor, N18 close to the MWRA outfall, N07 southeast of the outfall, F13 and F06 toward the south shore, and F02 in Cape Cod Bay.

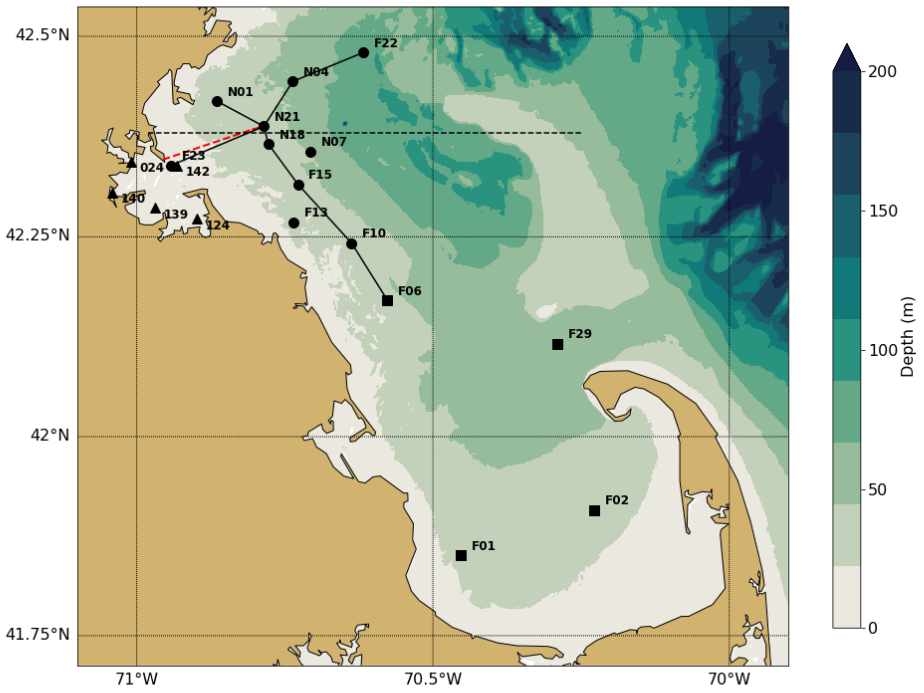

Figure 2-4 Location of MWRA monitoring locations (circles=Northern stations, squares=Southern stations, triangles=Harbor stations). The red dashed line indicates the tunnel to the outfall diffusers. The black lines are the West-East and North-South transects used for model-observation comparisons. The horizontal black dashed line represents the transect through the outfall, on which model results are presented in later figures.

2.1 Updated methods

In the 2018 BEM run, some minor changes to the methods as used for the 2017 BEM run (Deltares, 2022a) were implemented. This concerned the initialization of the water quality model. Where all previously reported simulations were initialized using products from the Copernicus Marine Environment Monitoring Service and given a 2-year spin-up, the 2018 run was simply restarted from the 2017 simulation.

3 Forcing

3.1 Wind, heat flux, solar radiation, and rivers

3.1.1 Wind

In Figure 3-1 the main characteristics of the monthly-mean wind forcing for the simulated year 2018 are compared to the means of the previous years (1997-2017) for the A01 mooring location off Cape Ann (Figure 1-1). Ranges of the standard deviation and of the minimum and maximum values are also shown.

The seasonal pattern of the vector-averaged velocities (top frame) showed some strong deviations from the long-term mean. Winds in February had a more northward component than usual. In March the southward component was much stronger than the long-term mean. In June and July, the wind was slightly more northwestward than the usual northeastward direction. September showed a stronger than usual westward component, and October and November were directed more to the east than typical.

Wind speeds (second frame) were similar to the long-term mean, but slightly below average in May and June. The months of March and November were above average with average wind speeds of about 9 m/s. Monthly-mean wind stress magnitudes (third frame) show a similar pattern.

North-south wind stresses (bottom frame) are an indicator for upwelling. Southward wind stress was close to the long-term extreme maximum amplitudes in the months January and March. June and September had an unusually weak (negative values of smaller magnitude) southward wind stress, indicating relatively strong upwelling.

3.1.2 Heat flux

A comparison between time series of the calculated net air-sea heat flux (including solar radiation) for 2018 and for the previous years is given in Figure 3-2. A moving average with a window of 3 days is applied to visualize the instantaneous values. The time series of the net flux includes the ranges of the standard deviation from the mean and of the minimum and maximum values. The cumulative flux (middle frame) is presented without any filtering.

The seasonal pattern in 2018 (top frame) showed an overall negative heat flux in winter (loss of heat from the surface, cooling of the ocean) and an overall positive heat flux in summer (heating of the ocean). The net heat flux started the year below average in January but quickly caught up with above average values in February and early March. October had a net flux below the long-term mean.

After January, the cumulative flux (middle frame) stayed above average until the end of October. The year closed with about 0.4 GJ m^{-2}, which is close to the long-term mean. The cumulative heat flux anomaly (bottom frame) was about 18 GJ m^{-2} for the year.

3.1.3 Solar radiation

The solar radiation from the meteorological forcing product is given in Figure 3-3. In general, the solar radiation in 2018 was similar to the average of the previous 20 years. There was however a negative anomaly (less solar radiation from mid-February onward (bottom frame, blue line). This led to a negative anomaly of solar radiation at the end of 2018 of about 0.14 GJ m^{-2} (bottom frame, blue line), so on an annual-mean basis, 2018 had less incident surface radiation than a typical year.

The higher net surface heat flux in 2018 than a typical year occurred despite the lower than typical incident radiation in 2018. Every year there is a net influx of solar radiation of about 5.5 GJ m^{-2}. Since the net air-surface heat flux is about 0.4 GJ m^{-2}, around 5 GJ m^{-2} is lost through other air-sea heat fluxes every year. These fluxes are either evaporative, convective turbulent fluxes or long wave radiation.

3.1.4 Rivers

In Figure 3-4 the volume transport for Merrimack River is presented. The figures include the daily-averaged discharges (top frame) for the simulated year 2018 and for the previous twenty years (1997-2017). Ranges of the standard deviation and of the minimum and maximum values are given as well.

The discharge of the Merrimack River started the year above average in January and in late February to early March. During the following months it was similar to the long-term mean, until November and December when several large discharge events occurred. This was clearly visible in the total discharged volume as well (middle frame), ending the year above average. The cumulative anomaly of the discharged volume (bottom frame) was 2 km^3.

The combined volume transport for the rivers discharging directly to Massachusetts Bay and Cape Cod Bay is presented in Figure 3-5. These rivers are Saugus, Mystic, Charles, Neponset, North, and Jones. The combined discharge was above average in the first three months. Around June this was below the long-term mean, resulting in a cumulative flux close to the average. In the last part of the year from half September onward the discharge was constantly above average. This resulted in a positive anomaly of the discharged volume (bottom frame) of 0.3 km^3 at the end of the year.

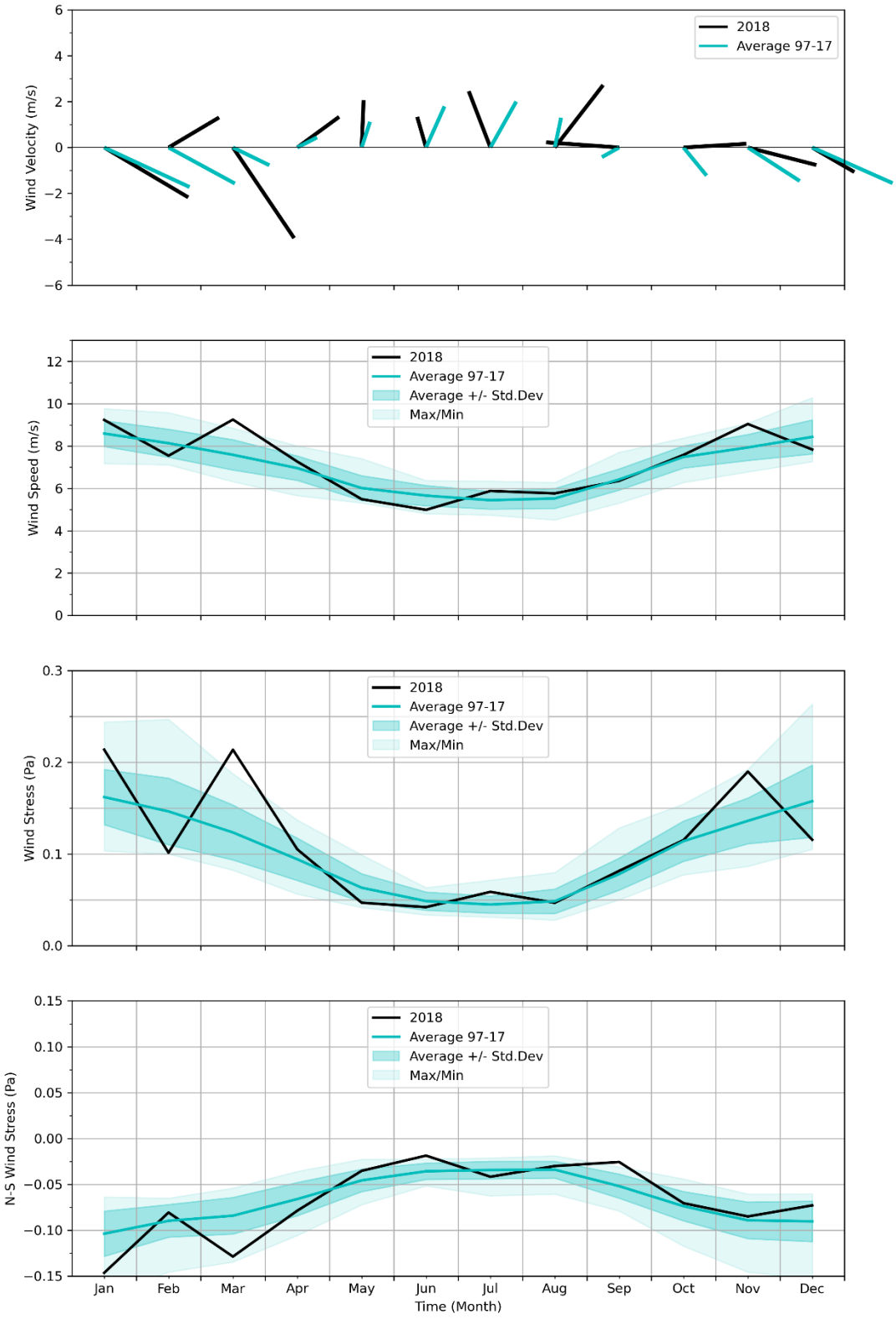

Figure 3-1 Surface wind forcing, monthly averages, compared to prior 20-year period.

Top frame: Vector-averaged wind velocities. Second frame: Wind speed. Third frame: Wind stress magnitude. Bottom frame: North-south component of wind stress, an indicator for wind-driven upwelling.

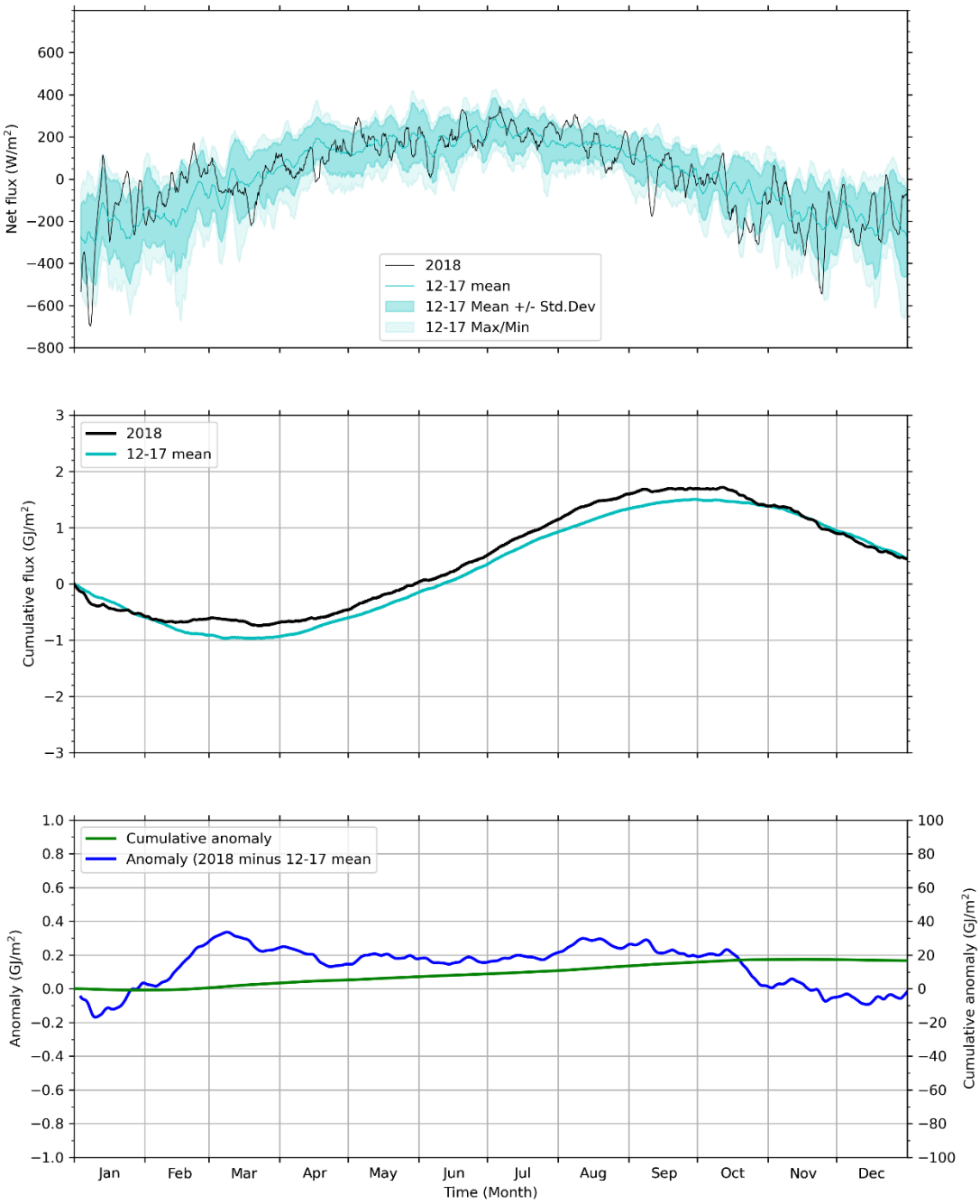

Figure 3-2 Surface heat flux, compared to prior 6-year period.

Top frame: Net heat flux into ocean. Middle frame: Cumulative net heat flux starting from January 1. Bottom frame: Anomaly (blue, left axis) and cumulative anomaly (cumulative sum of daily mean anomaly; green, right axis) of 2018 net cumulative heat relative to 2012-2017 average. The 2012-2017 reference period has been used because direct simulation output is available; it is shorter the 20 years used for the long-term mean.

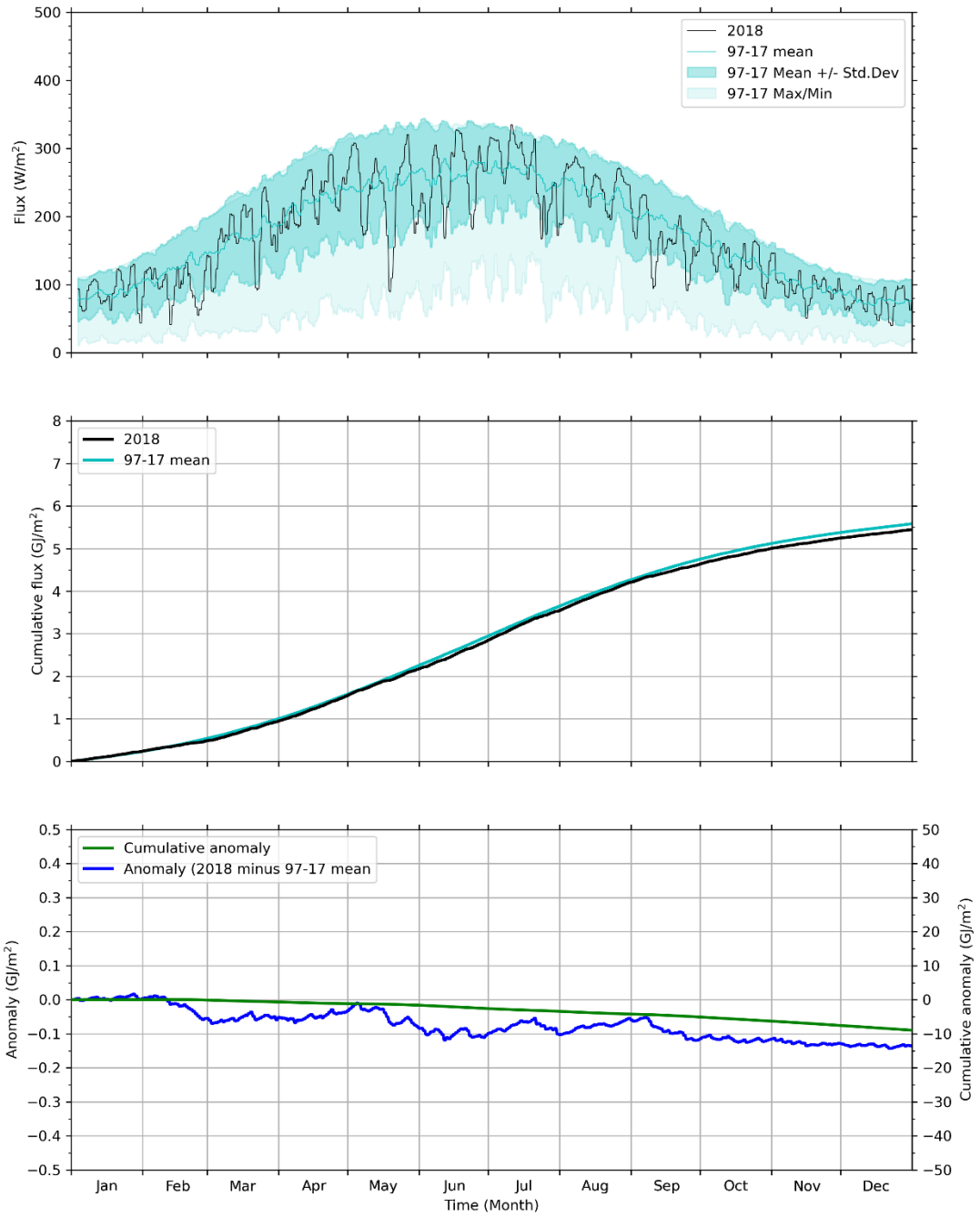

Figure 3-3 Solar radiation, compared to prior 20-year period.

Top frame: Solar radiation into ocean. Middle frame: Cumulative solar radiation starting from January 1. Bottom frame: Anomaly and cumulative anomaly (cumulative sum of daily mean anomaly) of 2018 cumulative solar radiation relative to 1997-2017 average.

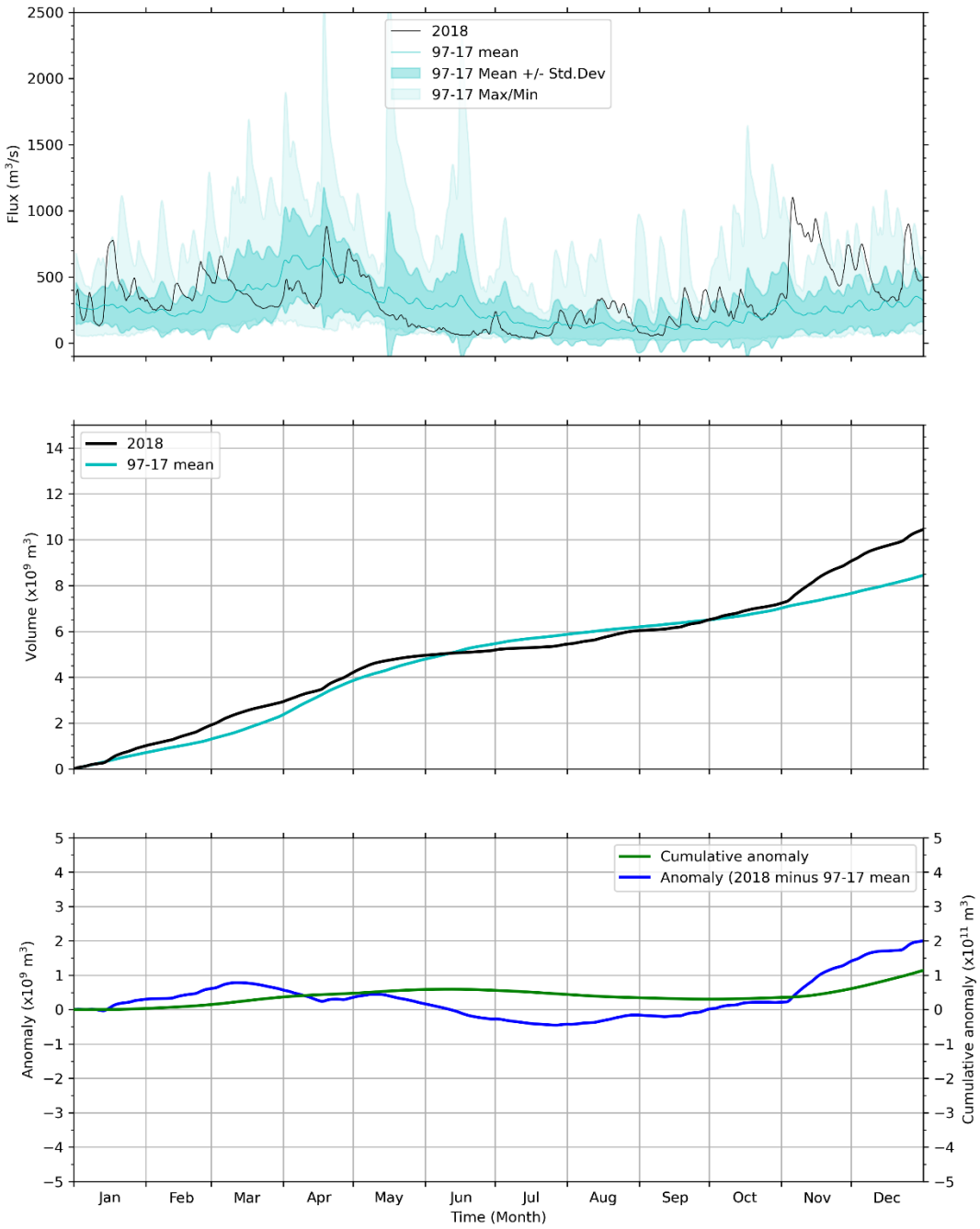

Figure 3-4 Merrimack River daily/cumulative flux and anomaly relative to previous 20 years.

Top frame: Merrimack River volume flux. Middle frame: Cumulative flux relative to January 1. Bottom frame: Anomaly and cumulative anomaly (cumulative sum of daily mean anomaly) of flux in 2018 relative to 1997-2017 average.

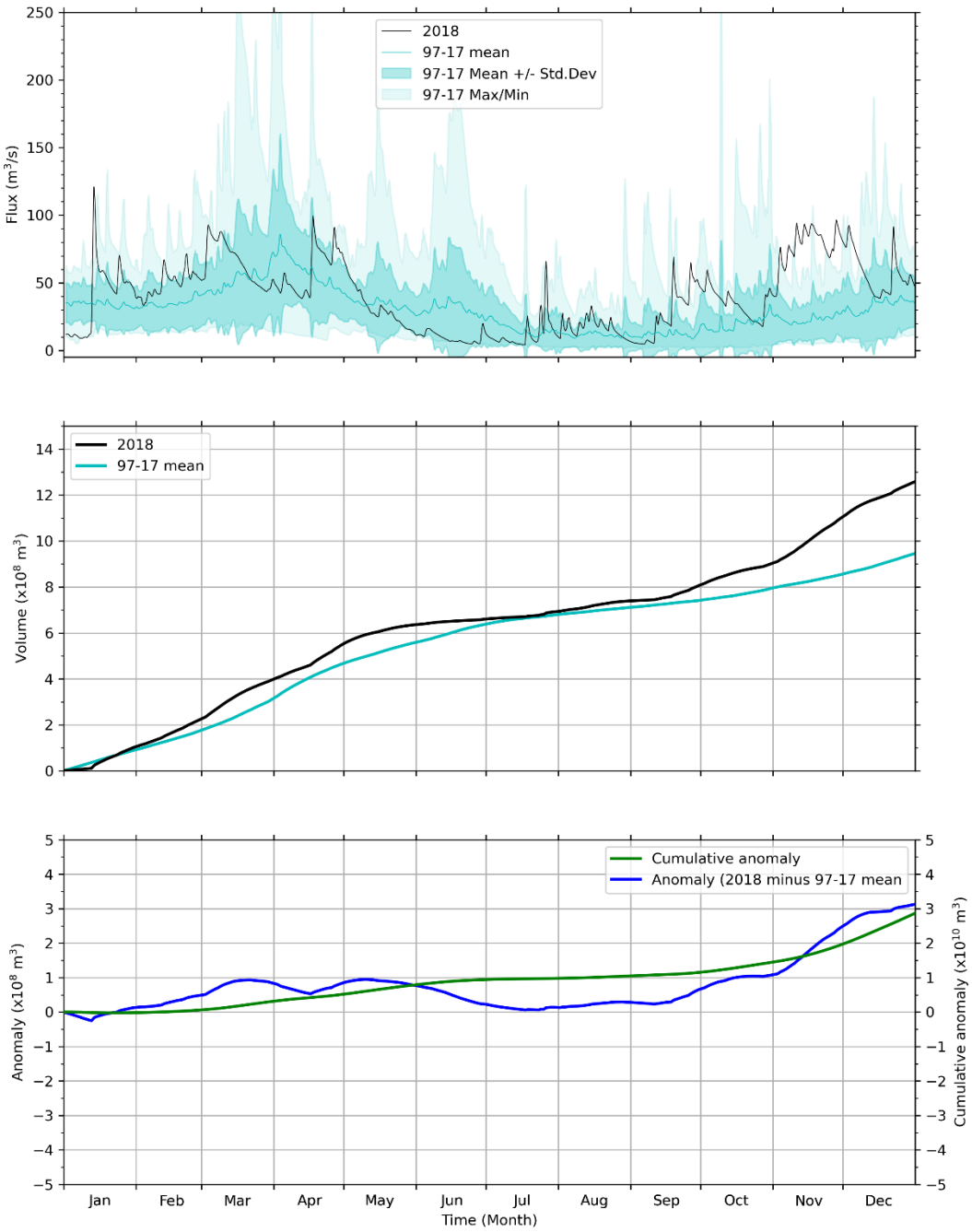

Figure 3-5 Summed discharge of all modeled rivers (Saugus, Mystic, Charles, Neponset, North, and Jones) flowing directly in to Massachusetts and Cape Cod Bays.

Presented as in Figure 3-4.

3.2 Loading of organic carbon, nitrogen, and phosphorous

Loads directly entering Massachusetts and Cape Cod Bays from rivers, the Deer Island treatment plant, and the atmosphere are shown in Figure 3-6. Loads entering the system through its offshore boundary are marked “oceanic input”, for example originating from rivers to the north including the Merrimack.

Model results show that oceanic input was the dominant source of organic carbon (OC), nitrogen and phosphorus (both in organic and inorganic forms), accounting for 99%, 93% and 96% of their total inputs, respectively (Figure 3-6). The simulated oceanic input of total nitrogen (TN) was comparable to the estimates based on the simulation of 1992 conditions from Hunt et al. (1999), reported by Zhao et al. (2017). The latter indicated that 93% of the TN entering the Mass Bay originated from the Gulf of Maine.

Rivers were the second largest source of OC, accounting for 86% of the non-oceanic input. MWRA loads constitute the main non-oceanic source of TN and total phosphorus (TP). These occur mainly in the inorganic form for nitrogen and in the organic form for phosphorus. Atmospheric deposition accounted for approximately 10% of the non-oceanic TN inputs. Finally, rivers are the smallest source of TN and TP to Massachusetts and Cape Cod Bays, representing 9% and 6% of their non-oceanic inputs, respectively.

The 2018 OC loads from the MWRA effluent were slightly higher than in the preceding years 2013-2017. The 2018 TN and TP effluent loads were in the middle of the range of loads from the preceding years 2012-2017.

River loads were about 66% (OC), 53% (TN) and 54% (TP) higher in 2018 than they were in 2017. This is mostly the result of the higher than average river discharges.

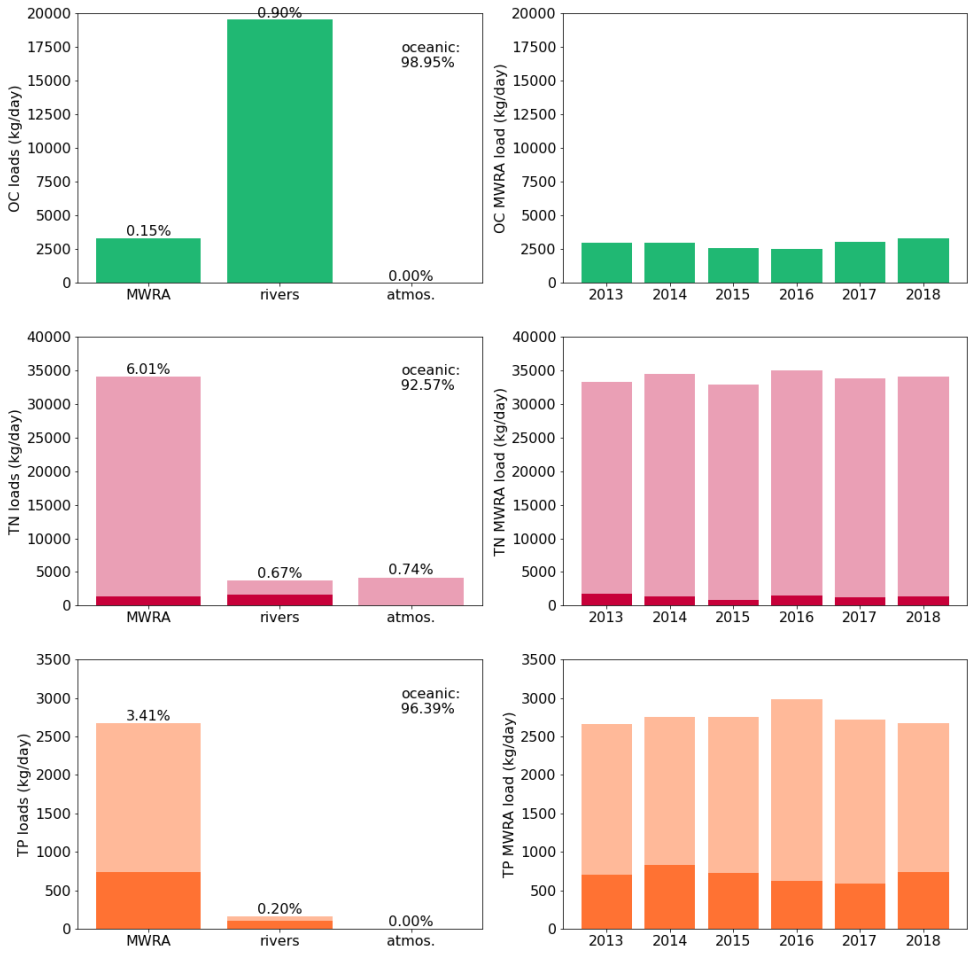

Figure 3-6: Organic Carbon (OC), Total Nitrogen (TN) and Total Phosphorus (TP) loads to Massachusetts and Cape Cod Bays in 2018. In the TN and TP plots, the darker sections of the bars represent the organic fractions. Left: loads from non-oceanic sources; percent of total is shown at top of each bar, and percent oceanic input (offshore boundary) shown at upper right. (Percentages correspond to summed organic and inorganic fractions.) Right: Deer Island Treatment Plant loads since 2013. OC=organic carbon; TN=total nitrogen; TP=total phosphorus.

4 Hydrodynamic Model

In this section the performance of the hydrodynamic model is discussed, and model results are compared to measurements.

4.1 Statistical assessment of model skill

The model skill was assessed for surface and bottom temperature and salinity by means of a statistical analysis. Three quantitative skill measures (correlation, normalized standard deviation Std*, and normalized unbiased root mean square error uRMSE*) were determined, based on simulation results and vessel-based observations of MWRA surveys. The result is presented in four pairs of Taylor diagrams in Figure 4-1. The left column shows the 2012-2016 validation period (Deltares, 2021) and the right column shows the 2018 simulation. See also the box below for further details and an explanation of the statistics in the diagrams.

Temperatures had correlation of over 0.99 and 0.95, Std* of 0.90-1.05 and 0.75-1.15, and uRMSE* of under 0.15 and 0.35, at the surface and bottom respectively. The performance at both the surface and the bottom slightly improved compared to the validation result.

The skill of simulated salinity varied more per observation station in 2018 than in the validation period. There were values for correlation of 0.40 or greater and 0.20 or greater, for Std* of 0.40-0.65 and 0.55-1.30, and for uRMSE* of up to 0.90 and 1.50, at the surface and bottom respectively. The performance at the surface slightly improved compared to the validation result. At the bottom, the performance slightly reduced. The performance at the bottom was similar to the validation results with the exception of station F02.

Overall, the figures presented here serve to verify that the performance of the hydrodynamic model in the simulations of 2018 did not deviate substantially from its performance during the 5-year validation period. For completeness, Taylor diagrams broken out for individual years 2012-2016, are presented in Appendix A of the Annual BEM Report on 2017 (Deltares, 2022a).

How to read a Taylor diagram

A Taylor diagram consists of a combination of three quantitative skill measures:

- Correlation Coefficient, represented in the plot by the azimuthal angle or blue lines.
- Normalized Standard Deviation (Std*), the Standard Deviation of the model results, normalized (*) by the standard deviation of the corresponding measurements. This ratio represents the relative amplitude of the modeled and observed variations, with a value of less than one indicating less modeled variability. It is represented in the plot by the radial distance from the origin (0,0).
- Unbiased Root-Mean-Square Error or standard deviation of the error, normalized with the standard deviation of the corresponding measurements (uRMSE*). It is represented in the plot by the grey contours, whose values are proportional to the radial distance from the target (black star).

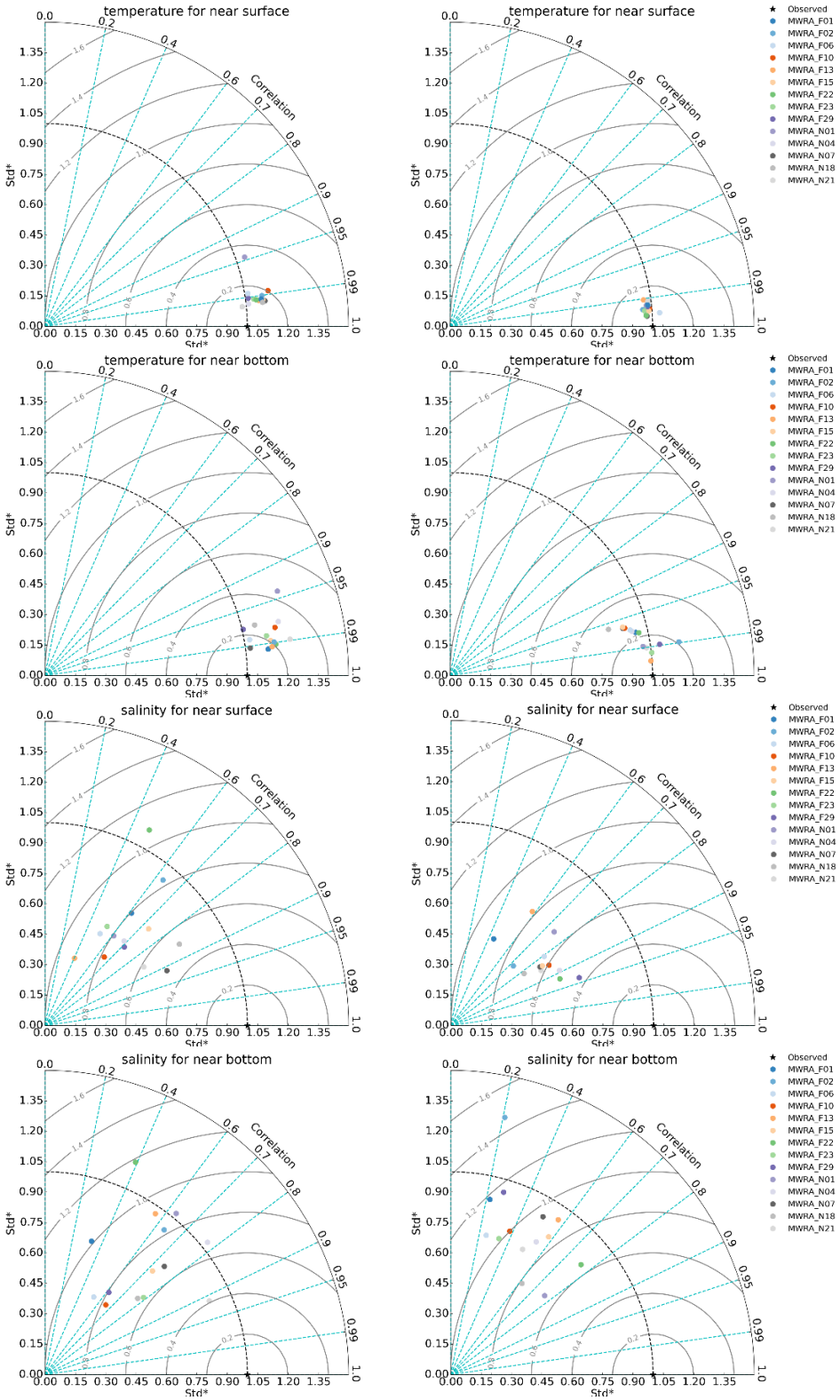

Figure 4-1 Taylor diagrams of model quality for MWRA vessel-based survey observations.

Temperature (upper frames), salinity (lower frames); 2012-2016 validation period (left column) and 2018 simulation (right column).

4.2 Model-observation comparisons

The simulation for 2018 was compared to observations to assess the level of agreement between them for temperature and salinity, both in time and space.

4.2.1 Time series of temperature and salinity

For eight observation stations in Massachusetts Bay and Cape Cod Bay, simulation timeseries of the surface (less than 5 m deep) and bottom (within 5 m of seafloor) temperature and salinity are presented in Figure 4-2 and Figure 4-4. Additionally, a comparison at three levels within the water column, between the surface and seafloor, is given in Figure 4-3 and Figure 4-5 (described below).

In these figures, vessel-based observations by MWRA surveys are included as individual symbols. The locations of the observation stations are given on a bathymetric map in the upper left frame. They include four stations generally surrounding the outfall (N01, N07, N18, and F13), one to the south (F06), one farther offshore (F22), one at the mouth of Boston Harbor (F23), and one in central Cape Cod Bay (F02).

In Figure 4-3 and Figure 4-5, showing results from within the water column, the depths vary from station to station and survey to survey but are nominally at 25%, 50%, and 75% of the water depth. The model output between surveys is not shown on these figures because the depths used, set by the observations, differ from survey to survey.

Overall, the seasonal cycle and most events were well captured by the model. Simulated stratification was similar to observations. At most stations, the onset of temperature stratification occurred in mid-April and it was strongest in June, July and August. The water column started to become mixed again between mid-September and mid-October. Salinity stratification in 2018 was limited compared to other years. Both sea surface as seafloor salinities were rather constant around 32.0 PSU. No sudden complete mixing of the water column due to storm events occurred. In the shallower stations N01, N18, F02 and F13 a sudden increase in bottom temperature (and decrease in surface temperature) was visible in mid-August and early September. The first event coincided with one of the vessel surveys, and there was good agreement between the model and the observations at most stations. However, the model-observation difference at N18 was larger, with an underestimation of the model of about 2°C. At other stations model-observation differences for temperature were less than 1°C at the surface and seafloor, and slightly larger within the water column. Simulated salinity showed a bias of about 0.50-0.75 PSU (as discussed in Deltares, 2021), but because this bias was present throughout the water column, salinity stratification was well represented. In general, the model-observation differences were larger in the upper part of the water column and during the summer, when stratification occurred.

4.2.2 Spatial representation of temperature and salinity

To assess the simulation spatially, maps have been plotted for surface and seafloor conditions, with the mean of the modeled results averaged over a period of 5 days centered on the observation dates. The five presented periods span the seasonal cycle of stratification. This is given in Figure 4-6 and Figure 4-7 for temperature and in Figure 4-8 and Figure 4-9 for salinity. For the model-observation comparison, the available observations are plotted over the simulation fields as colored symbols. Note that the presented simulation fields are the average over 5 days, where the observations are instantaneous values, usually measured in the morning. This might introduce a bias.

These figures show a good agreement between the simulation and observations. The spatial variation at both the surface and bottom was comparable, with near-shore temperatures warmer in summer and

colder in winter. At both depths, salinities were generally fresher near the coast. In contrast with other years no large freshwater plume was present in the spring or summer of 2018. This can be linked to the low river discharges in May, June and July (Figure 3-4 and Figure 3-5). Model-observation differences for temperature and salinity were largest in June with an underestimation of about 2°C and an overestimation of a bit more than 0.5 PSU at the surface. In other months, model-observation differences were at most 1°C and 0.5 PSU. An exception occurred in August when the temperature near the diffuser at station N18 was underestimated by about 5°C. This can be linked to the mixing event at day 232 that is visible in Figure 4-2, due to the strong Nor'easter storm (Figure 4-12, described below).

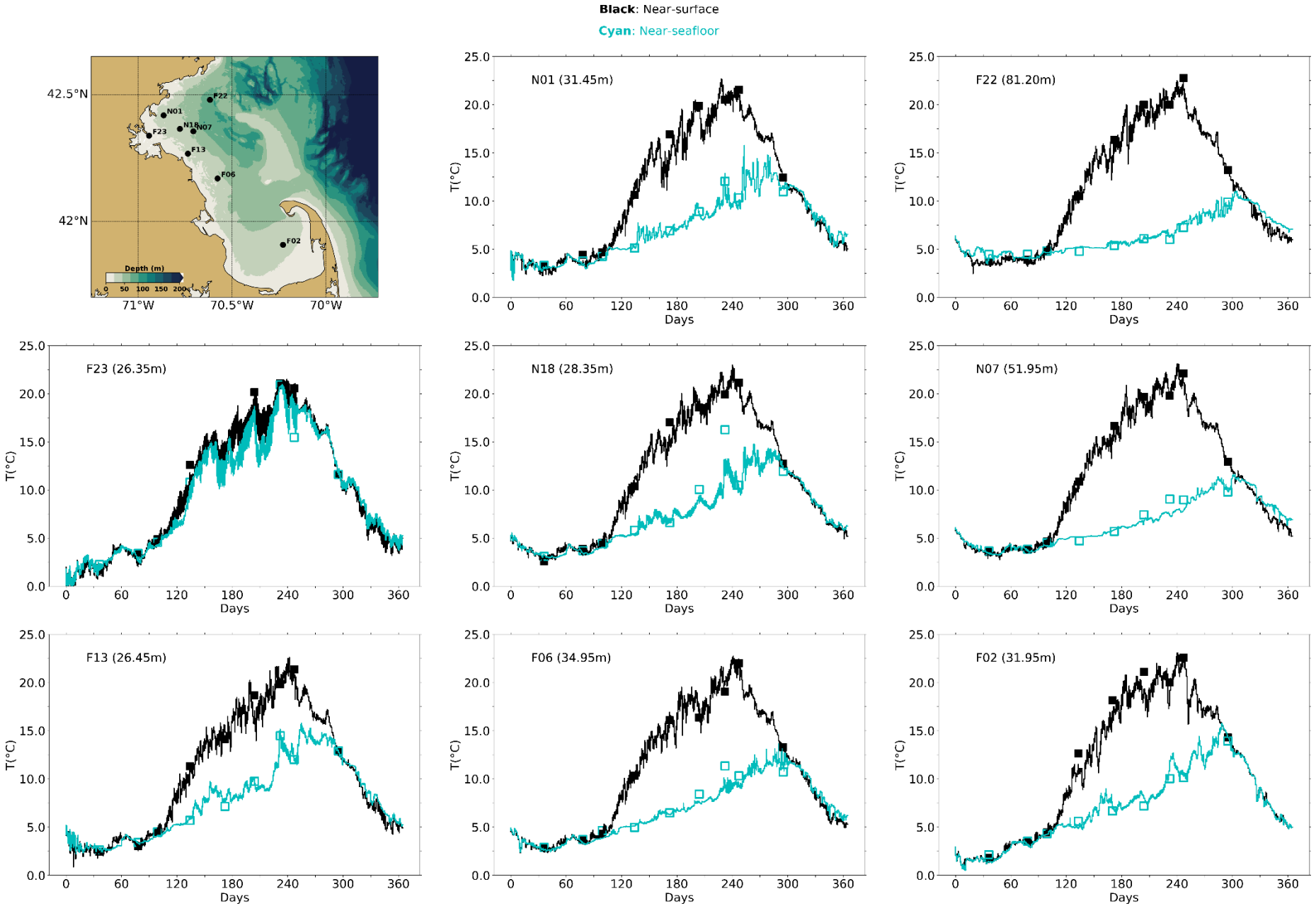

Figure 4-2 Temperature time series, model-observation comparison near surface (black) and seafloor (cyan).

Model results: lines. MWRA vessel-based survey observations: symbols.

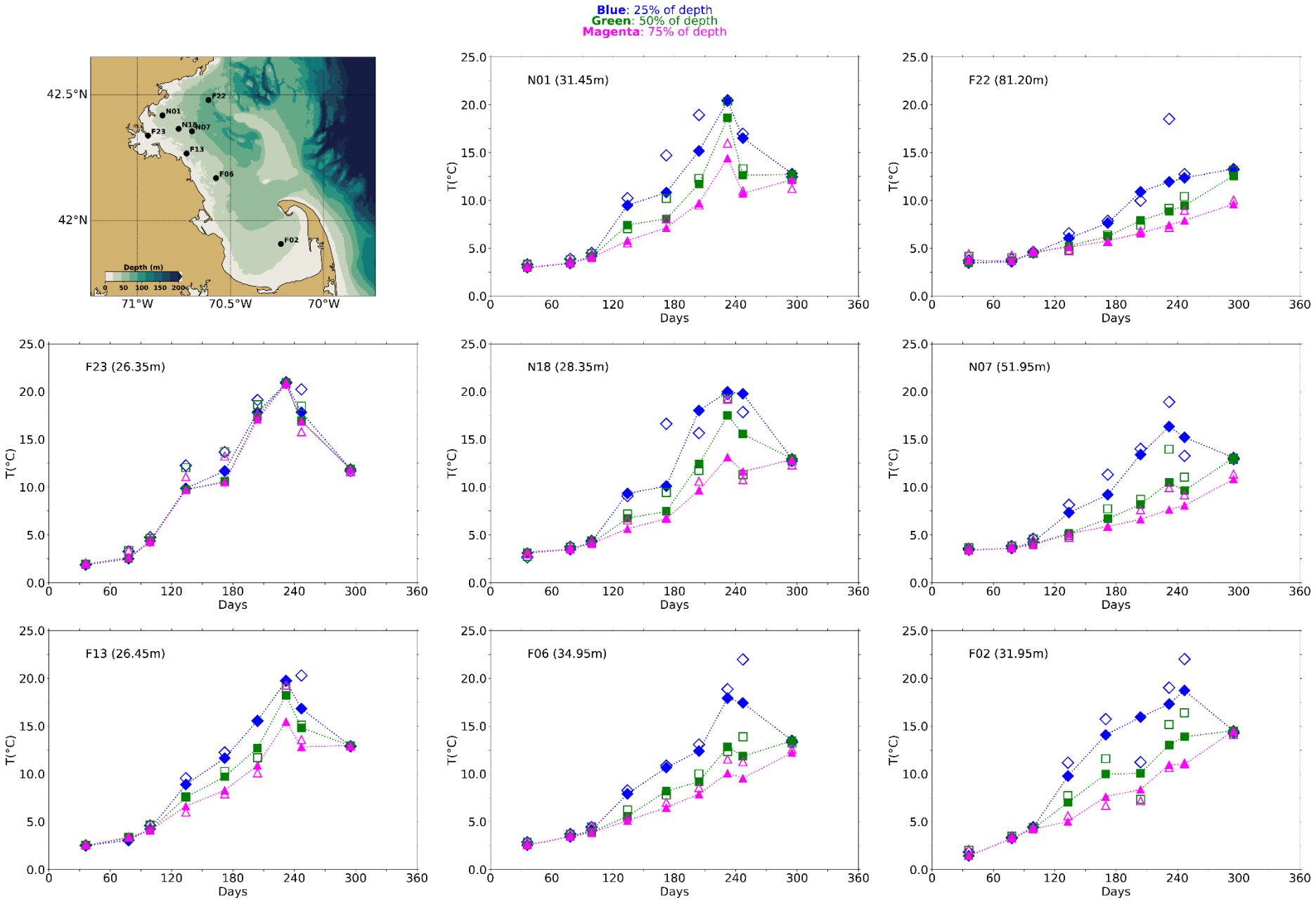

Figure 4-3 Temperature time series, model-observation comparison within water column (between surface and seafloor).

Model results: lines with filled symbols. MWRA vessel-based survey observations: open symbols.

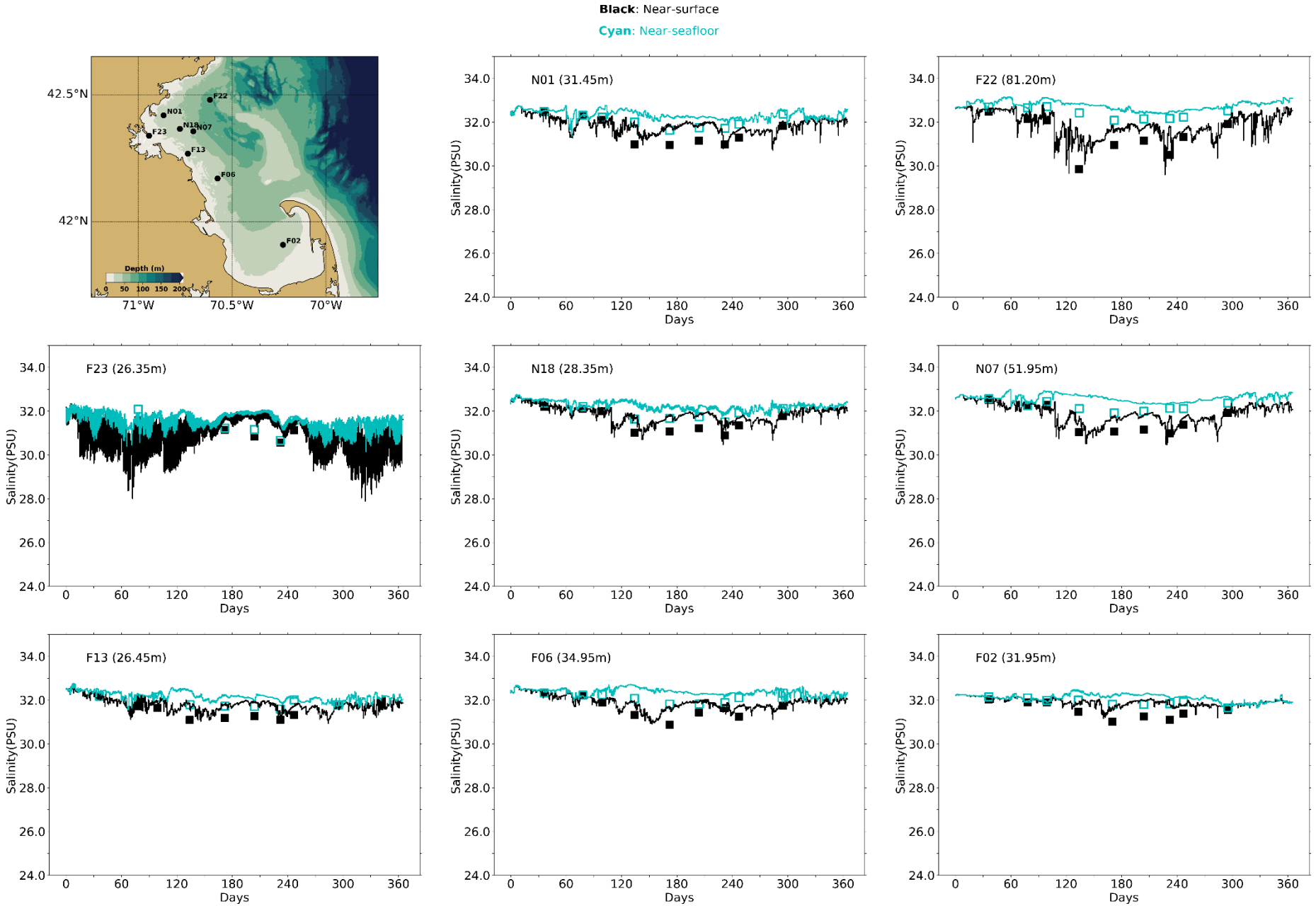

Figure 4-4 Salinity time series, model-observation comparison near surface (black) and seafloor (cyan).

Model results: lines. MWRA vessel-based survey observations: symbols.

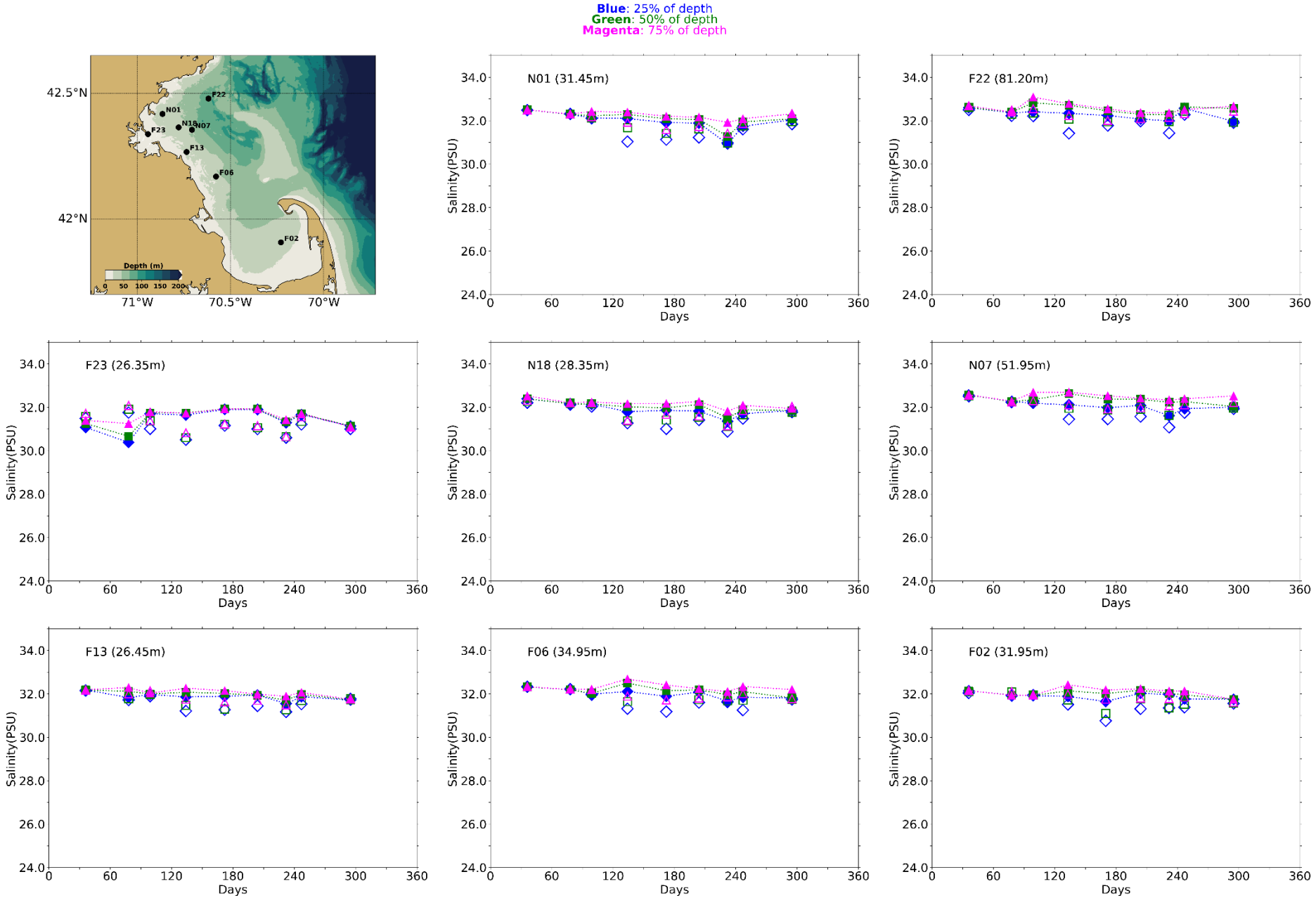

Figure 4-5 Salinity time series, model-observation comparison within water column (between surface and seafloor).

Model results: lines with filled symbols. MWRA vessel-based survey observations: open symbols.

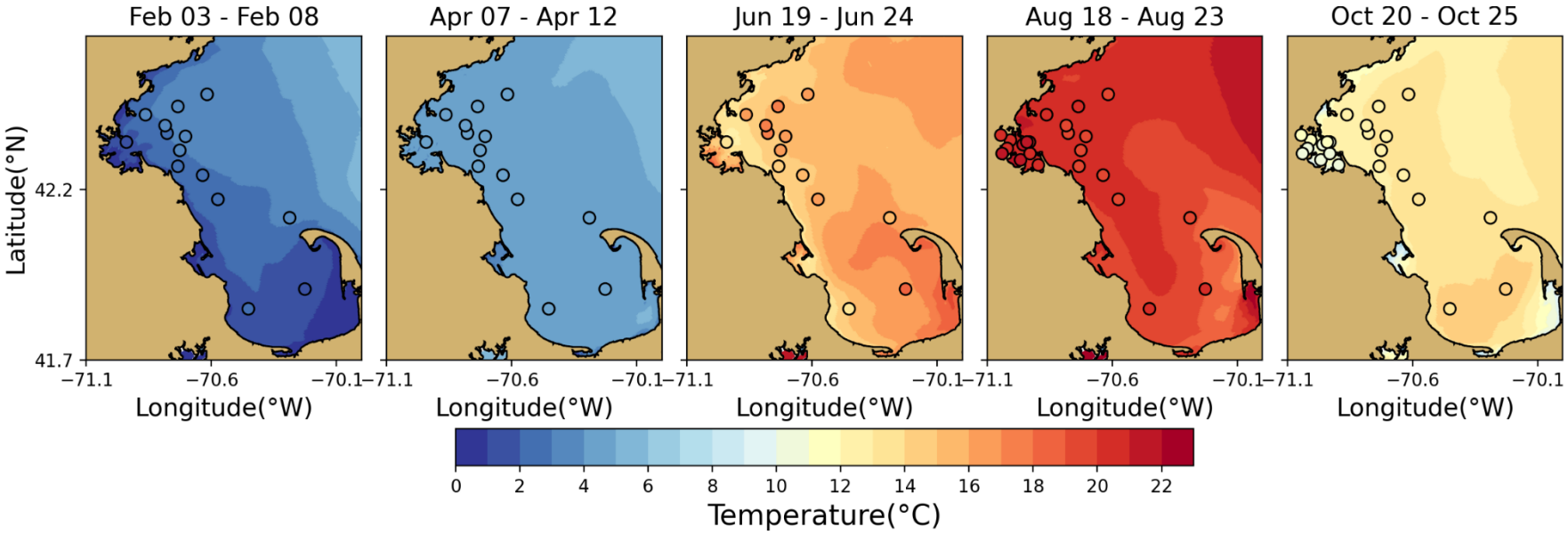

Figure 4-6 Temperature spatial structure, at/near sea surface, model-observation comparison.

Model results: background. MWRA vessel-based survey observations: symbols. Model results are averaged over the 5-day period centered on the measurement date.

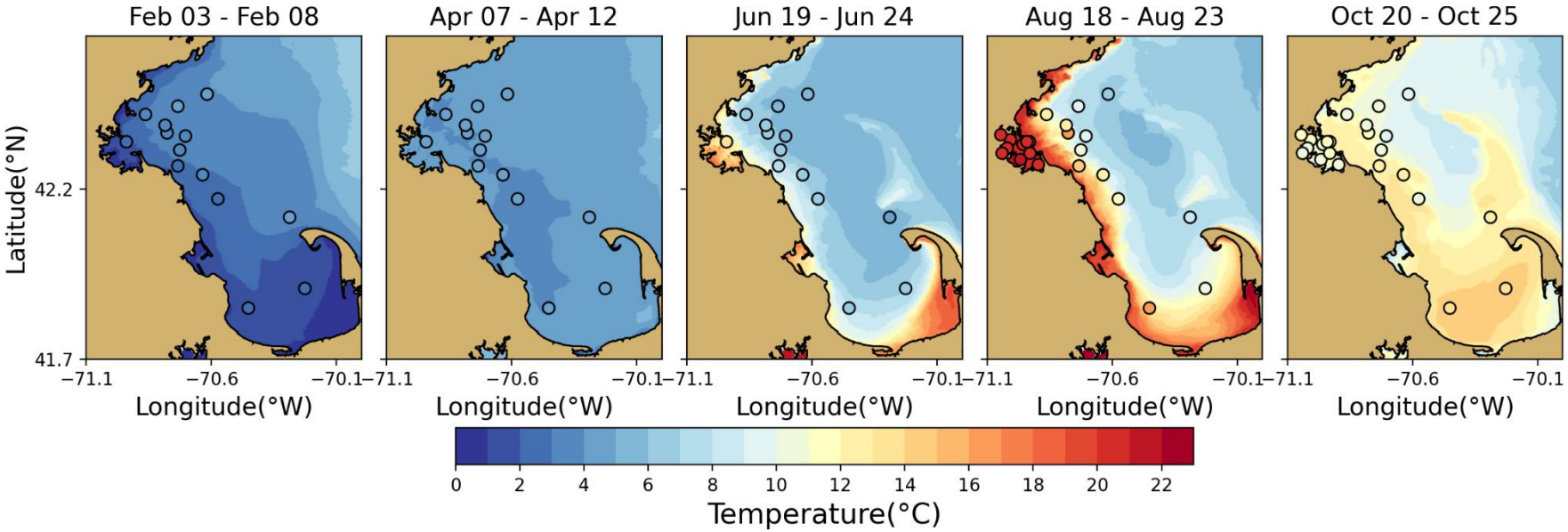

Figure 4-7 Temperature spatial structure, at/near seafloor, model-observation comparison.

Model results: background. MWRA vessel-based survey observations: symbols. Model results are averaged over the 5-day period centered on the measurement date.

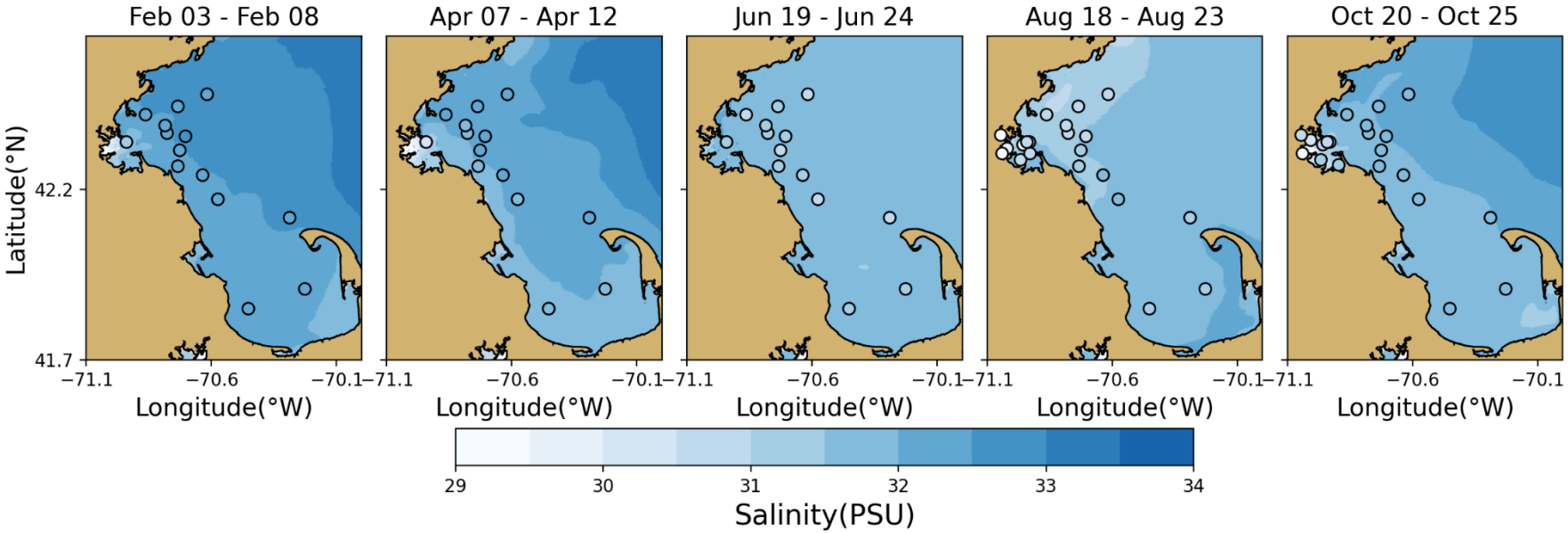

Figure 4-8 Salinity spatial structure, at/near sea surface, model-observation comparison.

Model results: background. MWRA vessel-based survey observations: symbols. Model results are averaged over the 5-day period centered on the measurement date.

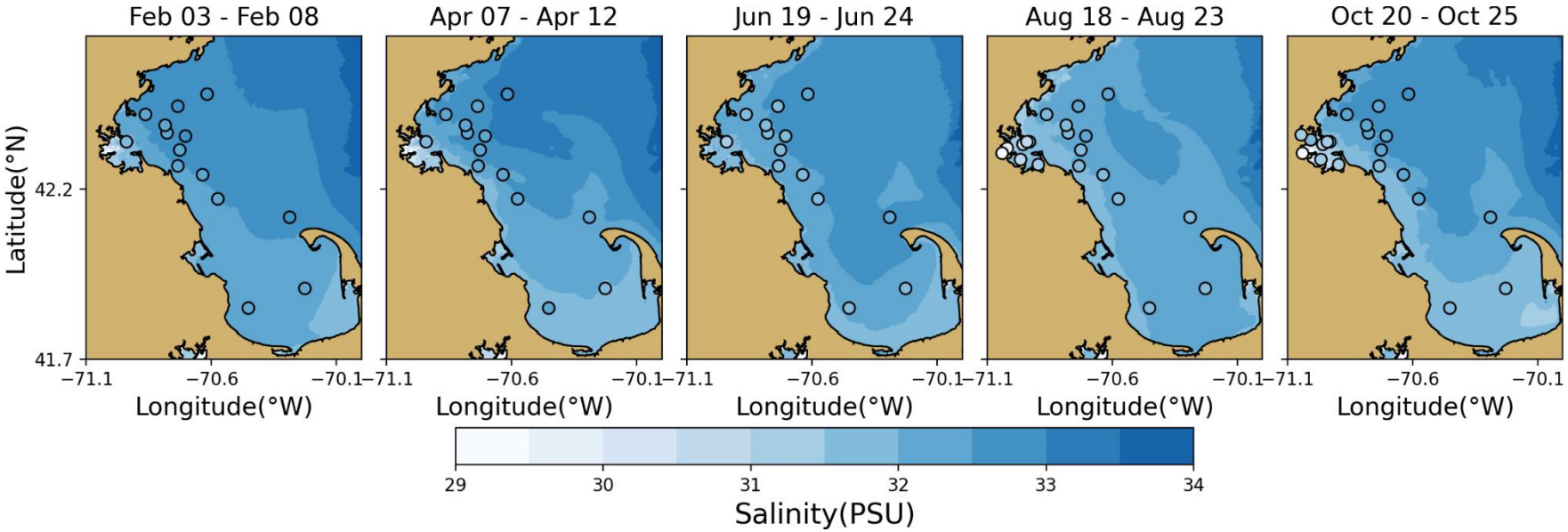

Figure 4-9 Salinity spatial structure, at/near seafloor, model-observation comparison.

Model results: background. MWRA vessel-based survey observations: symbols. Model results are averaged over the 5-day period centered on the measurement date.

4.2.3 Continuous measurements of temperature and salinity

Continuous hourly measurements were available from Mooring A01 at multiple depths. This station is located south of Cape Ann, northeast from MWRA station F22. To provide a more complete assessment of the model-observation comparison in time, timeseries for this station are presented in Figure 4-10. For three depths (1m, 20m and 50m) the simulated and observed temperature and salinity are given. This is also done for the vertical temperature and salinity difference between 1m and 20 m as well as 1m and 50 m, as a measure of stratification. In the measurements some outliers were present, visible as spikes in the salinity and bottom temperature.

The time series compare well, showing that the model captured the strength and timing of the seasonal cycle of temperature and salinity, as well as the stratification of these quantities. Furthermore, many observed event-based changes in stratification on timescales of days to weeks occurred in the model. The bias of 0.50-0.75 PSU more saline water in the simulation, throughout the water column as explained in Deltares (2021), is clear in the second frame of the figure; no such bias occurs for the salinity stratification (fourth frame). The simulated stratification was slightly better represented for temperature than for salinity, but overall the model captures stratification well. This is important for the water quality simulation because stratification is a main influence on vertical transport.

4.2.4 Continuous measurements of non-tidal currents

For Mooring A01, observed currents were available as well, although surface currents in the last three months were missing. In Figure 4-11 and Figure 4-12 a model-observation comparison is presented for the first and second halves of the year, respectively. In the top frame, time series of wind from the meteorological product used to force the model is given for context. In the frames below, simulated and observed time series of non-tidal currents at four depths (2m, 10m, 22m and 50m) are given alternately. To remove the tidal variability, timeseries have been filtered using a low-pass filter with a 33h filter half amplitude (Alessi, 1985). The resulting signal consists mainly of weather-related and seasonal changes. For plotting this has been subsampled to a 6h resolution.

The time series of the filtered wind shows wind in all directions. Winds were generally changing on timescales of multiple days. In general, the wind speeds were lower during the calmer summer months. Winds included a dominantly eastward component year-round, with a mostly southward component in winter and a dominant northward component in summer.

The simulated and observed non-tidal currents showed a similar pattern with a prevailing direction to the southwest. In the first four months of the year the simulated currents included a stronger and more frequent northward component than was observed. In the same period observed current magnitudes throughout the entire water column were higher than in the model. Individual storm events occurred in the model with a similar timing and resulting current direction, but their magnitudes were lower. The model-observation difference was largest in early March, due to sudden peaks in southward direction in the observations. The storm season during the last three months of the year cannot be assessed properly, because of the missing observation data at the surface. During these months, the observations at 10m depth had slightly larger magnitudes but were overall similar to the simulation results. This model-observation comparison at a specific location is a challenging test of the hydrodynamic simulation performance. The agreement between the two was sufficient to conclude that the representation of processes in the hydrodynamic model was adequate to support water quality modeling.

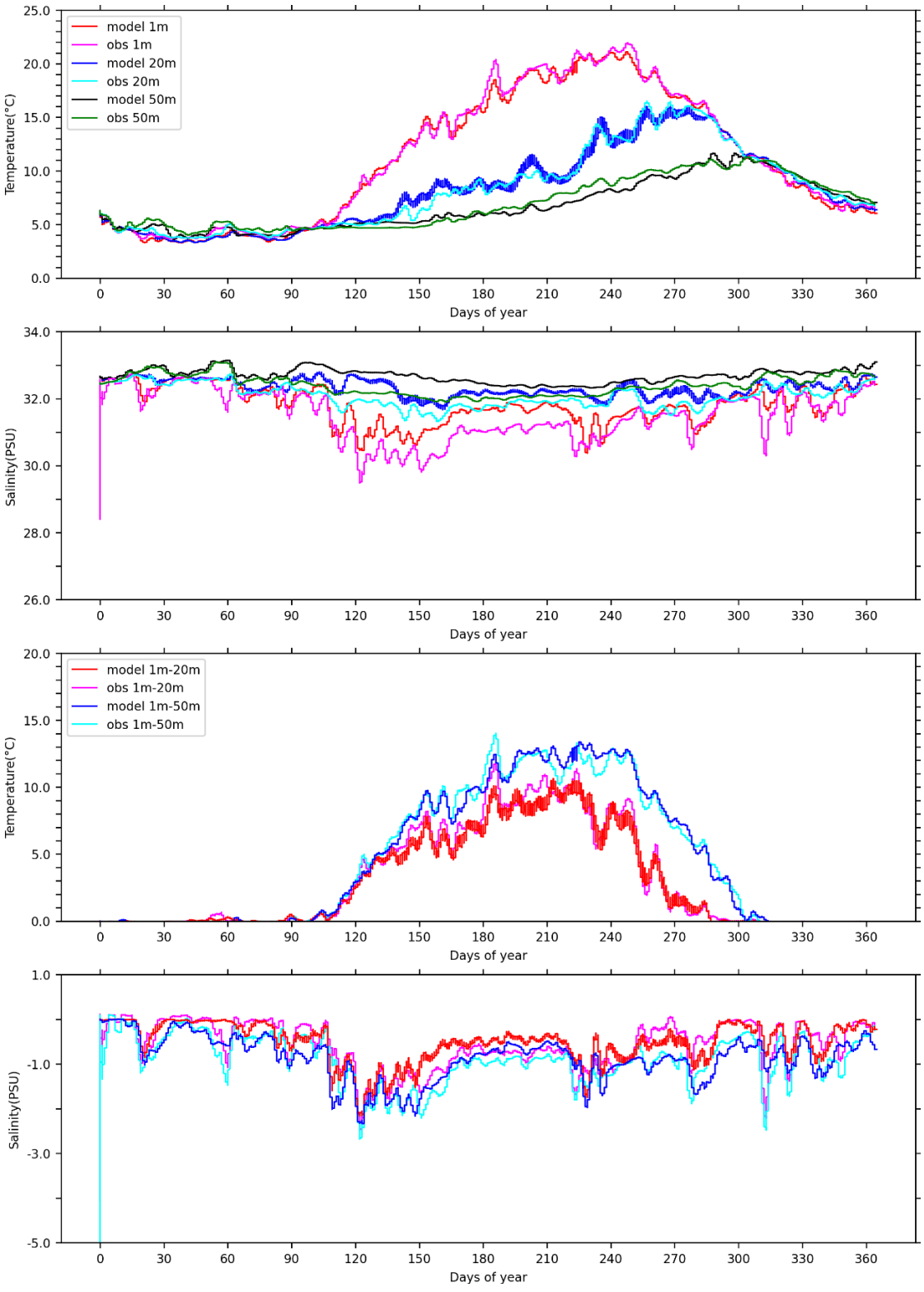

Figure 4-10 Time series Mooring A01 temperature/salinity model-observation comparison (3-day means), three depths and two stratification levels.

Temperature (upper frames), salinity (lower frames).

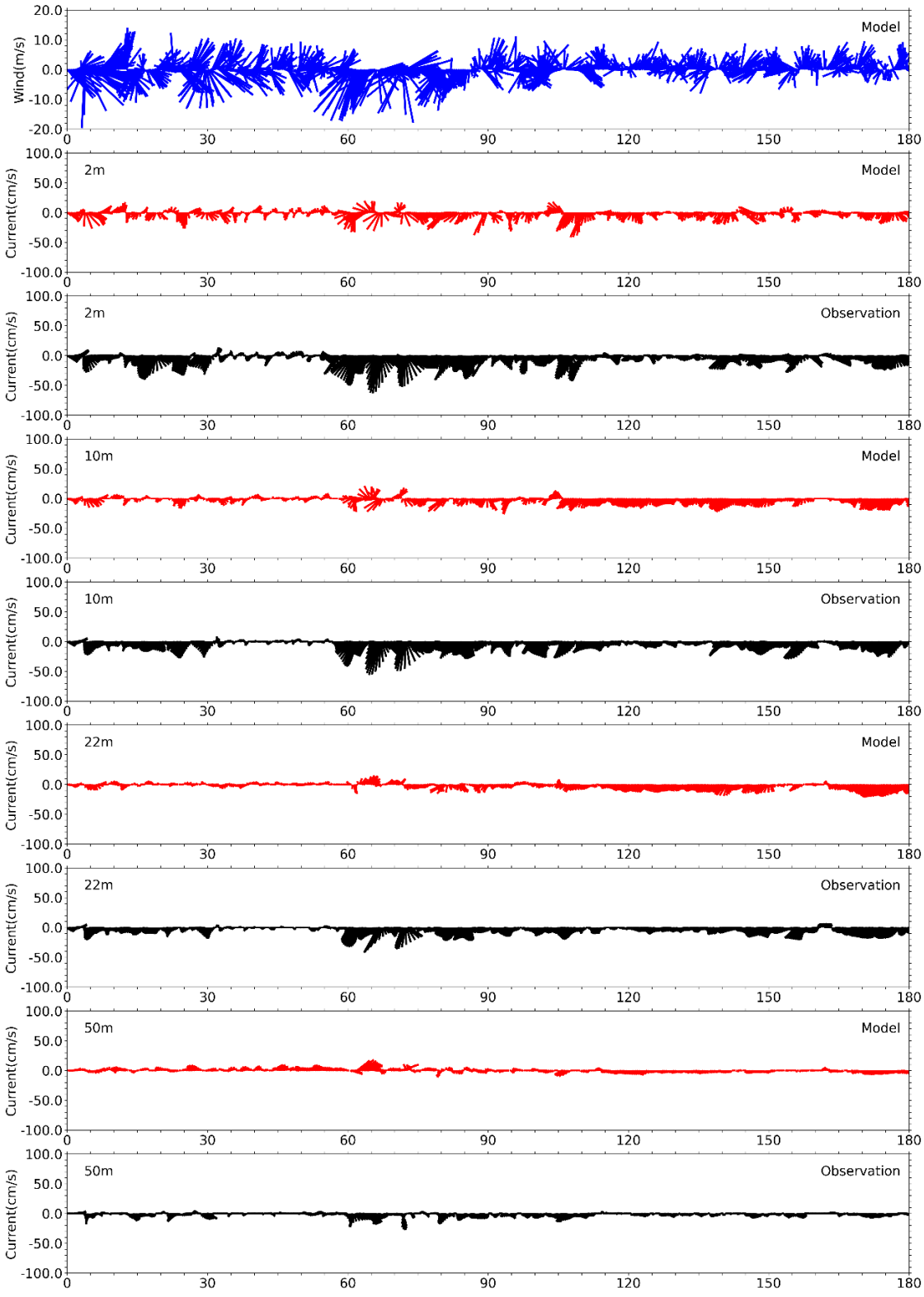

Figure 4-11 Currents time series model-observation comparison, Jan – Jun.

Sticks point in the direction of flow, away from zero line; north/eastward flow up/rightward.

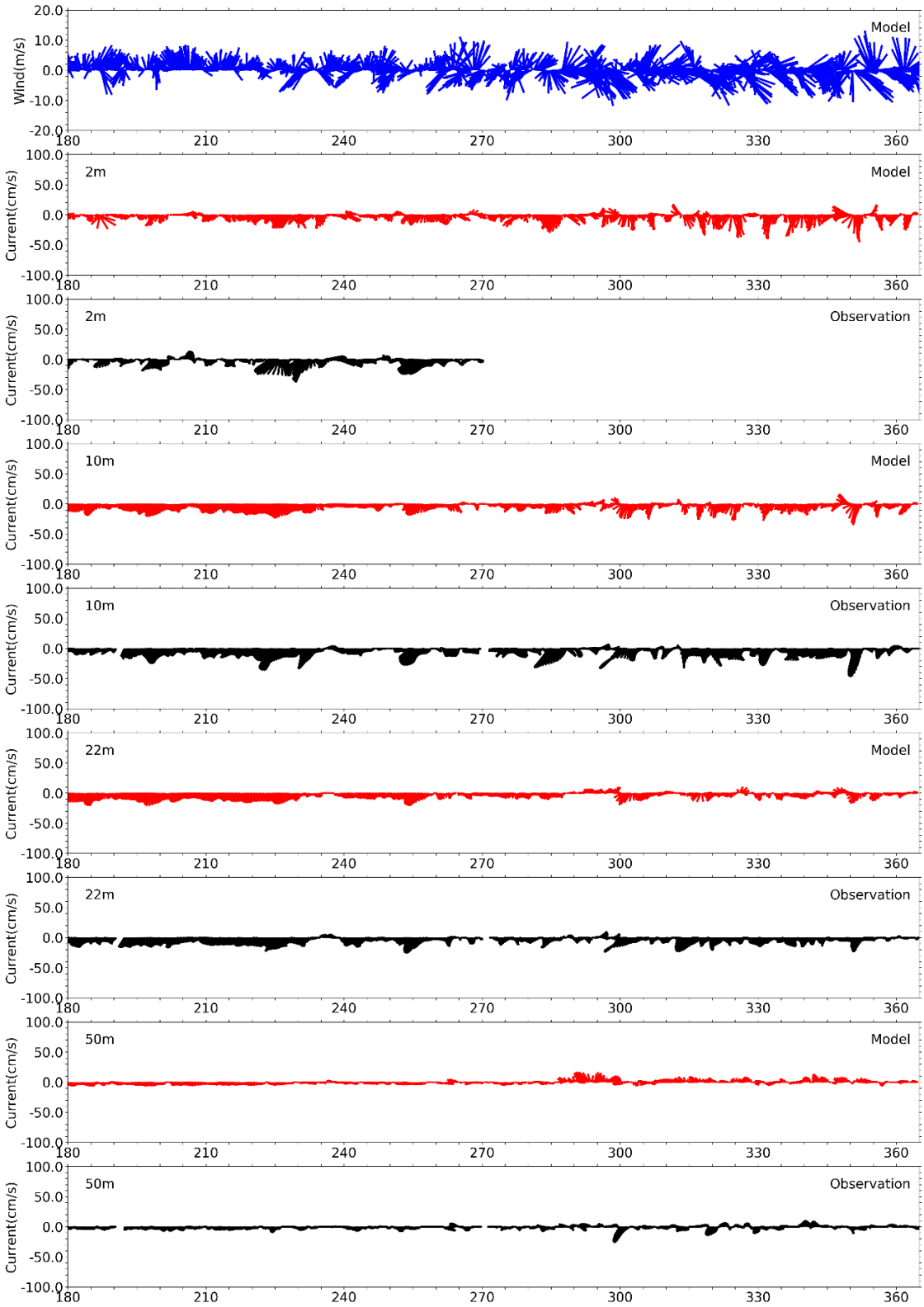

Figure 4-12 Currents time series model-observation comparison, Jul – Dec.

Sticks point in the direction of flow, away from zero line; north/eastward flow up/rightward.

4.3 Model monthly-mean circulation

Figure 4-13 and Figure 4-14 present the simulated monthly-mean currents at the surface and at a depth of 15m. Flow was largely consistent with the general circulation pattern recognized to hold (Figure 1-1).

This schematic pattern was most apparent in the residual surface currents in spring (March to June), autumn (October to December) and to a smaller extent in August. In other months residual currents were weak or the Western Maine Coastal Current did not intrude the Massachusetts Bay. Surface currents were largest off Cape Ann and Cape Cod with largest magnitudes in March, reaching up to 0.35-0.40 m s^{-1}. Within Massachusetts Bay, they were strongest in March (near the coast south of Boston Harbor) and in October to December (near North Passage and South Passage), with magnitudes up to 0.15 m s^{-1}. During the rest of the year surface currents were calmer and stayed well below 0.10 m s^{-1}.

The circulation pattern at 15 m depth (Figure 4-14) showed less influence of the surface forcing. In general, the expected general circulation pattern was more distinguishable throughout the year than at the surface. Current magnitudes were lower than at the surface, with maxima in March of up to 0.30 m s^{-1} at Cape Cod. Near North Passage and South Passage, 15m deep currents were slightly stronger than at the surface, reaching up to 0.20 m s^{-1}. In Cape Cod Bay, 15m deep currents were weaker than elsewhere, as expected due to its limited depth and sheltered geometry.

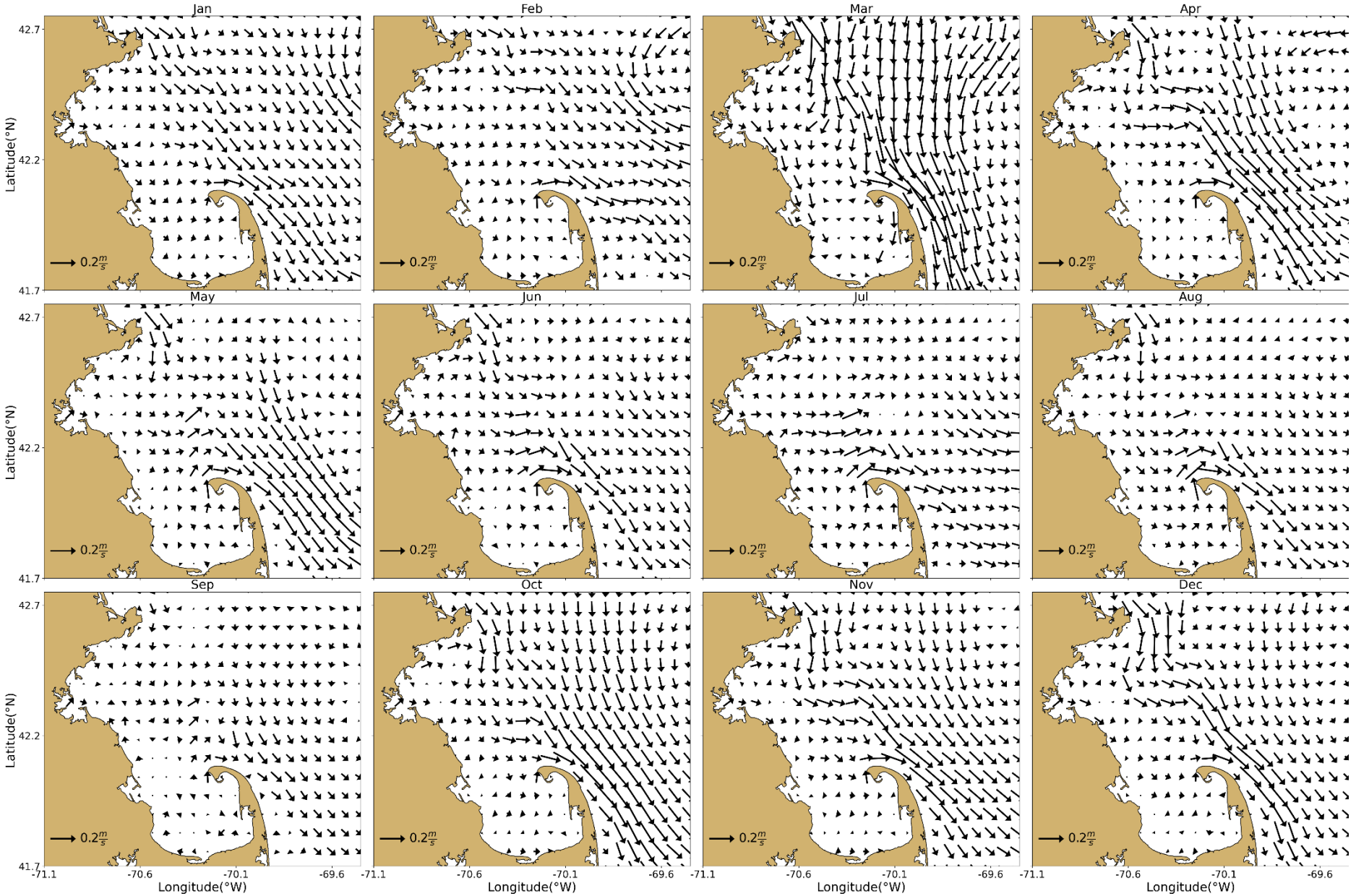

Figure 4-13 Model currents, monthly-mean spatial structure, at sea surface.

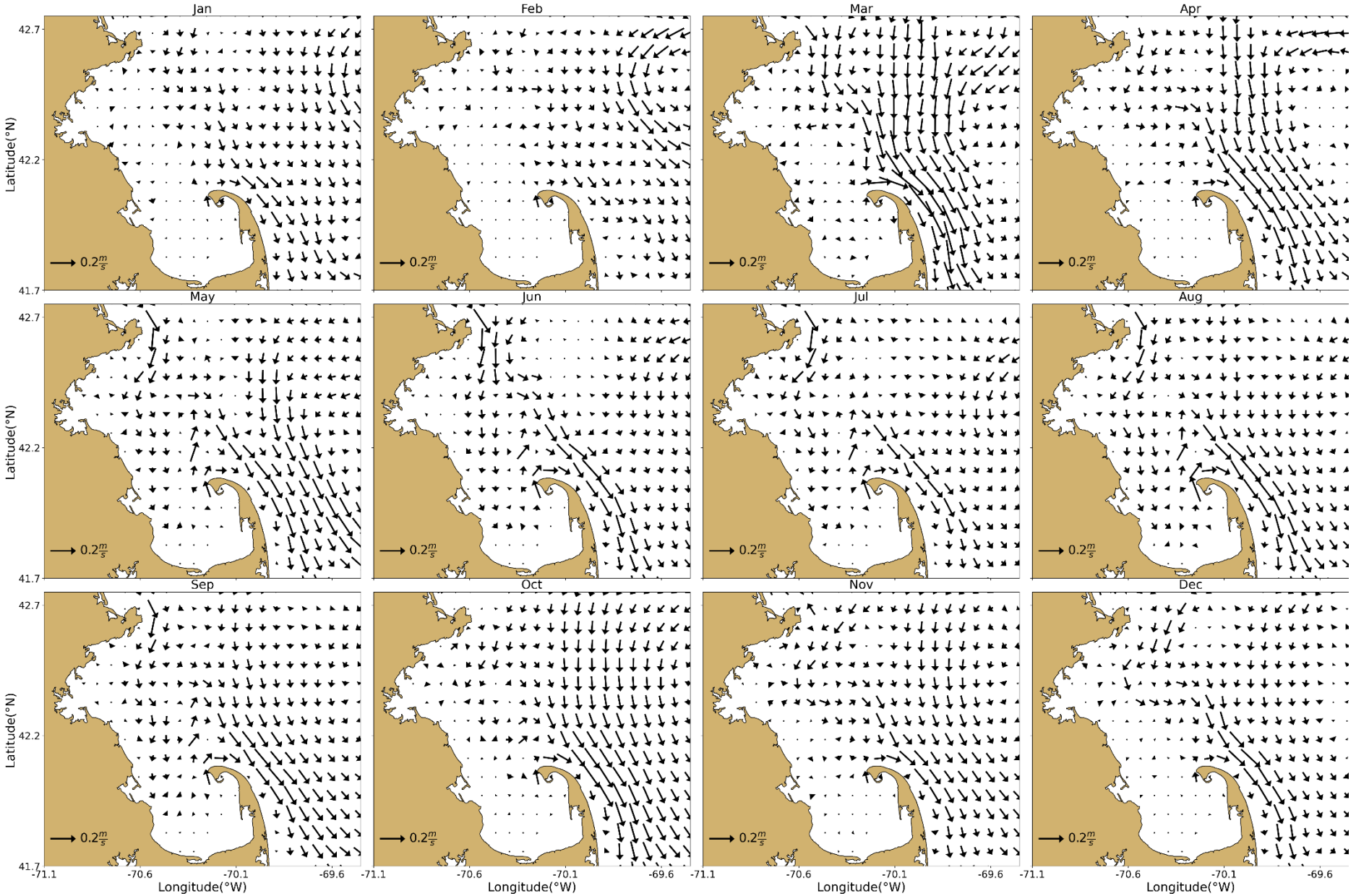

Figure 4-14 Model currents, monthly-mean spatial structure, 15 m deep.

5 Water Quality Model

In this section the performance of the water quality model is discussed, and its results are compared to measurements.

5.1 Verification of model performance

To demonstrate that the model performance during 2018 was comparable to the performance for the calibration and validation period 2012-2016, skill metrics were calculated and plotted on Taylor diagrams as in Section 4. Station N21 directly on top of the outfall was excluded, as a comparison to field data is of limited value for this station, as discussed by Deltares (2021). Information on how to interpret Taylor diagrams can be found in section 4.1 (box “How to read a Taylor diagram”).

Taylor diagrams are plotted for the light extinction coefficient and dissolved inorganic nitrogen (DIN) in Figure 5-1, and for chlorophyll a and dissolved oxygen (DO) in Figure 5-2. These parameters were selected because they are key drivers of ecosystem functioning. Statistics for the period 2012-2016 are plotted on the left side and statistics for 2018 on the right side. For reference, the 2017 simulation report (Deltares, 2022a) provides similar diagrams for the individual years 2012 to 2016. The plots show statistics for three clusters of monitoring stations: Northern Bay stations (F22, N01, N04, N07, F10, N18, F15, F13 and F23), Southern Bay and Cape Cod stations (F06, F29, F01 and F02) and harbor stations (024, 140, 142, 139 and 124) (see Figure 2-4 for station locations).

Extinction skill metrics (Figure 5-1) are comparable in 2018 to the calibration period 2012-2016, with weak correlations, and variability sometimes overestimated (mostly at North stations) and sometimes underestimated (mostly at Harbor stations). Dimensionless unbiased RMSE errors are somewhat higher in 2018, notably at stations F13 and N01, but the time series plots in section 5.2.1 below indicate the values are within ranges that do not indicate a problem with model performance.

Skill metrics for DIN (Figure 5-1) show that for most stations dimensionless unbiased RMSE errors are within the range observed in 2012-2016. The correlation and the variability show more differences from station to station than the 2012-2016 results. The higher than observed variability at some stations is the result of overestimated winter concentrations (e.g. station F29).

Skill metrics for chlorophyll a (Figure 5-2) show smaller dimensionless unbiased RMSE errors than in 2012-2016, mostly because of a smaller simulated than observed variability. This is similar to the 2017 results and was diagnosed as a result of the low sampling frequency in combination with the highly transient character of algae blooms (Deltares, 2022a).

DO skill metrics (Figure 5-2) are comparable to those for 2012-2016 with better correlations than in 2012-2016.

Overall, the figures presented here serve to verify that the performance of the water quality model in the simulations of 2018 does not deviate substantially from its performance during the calibration and validation period 2012-2016.

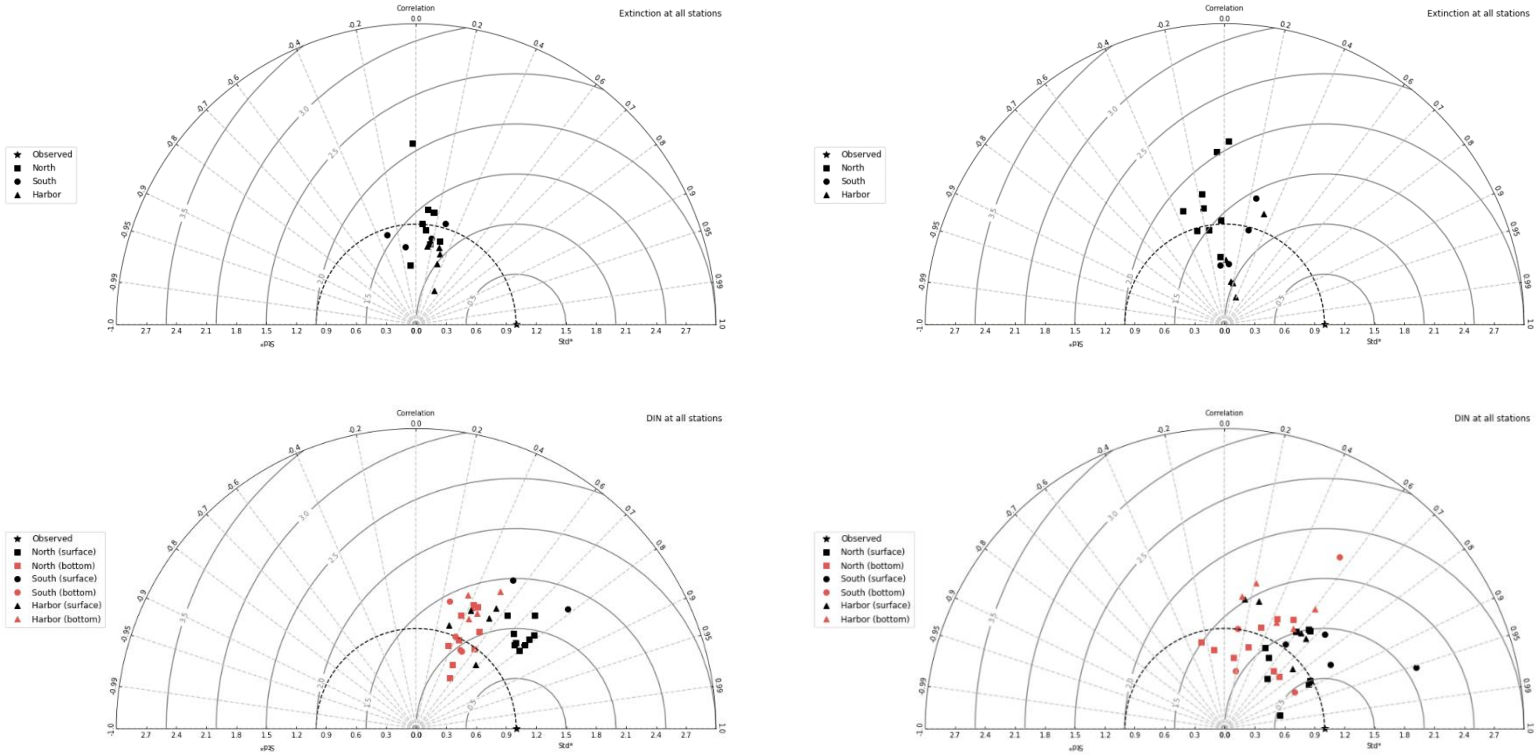

Figure 5-1: Taylor diagrams for MWRA vessel-based survey observations. Top panels show the parameter Extinction and bottom panels Dissolved Inorganic Nitrogen. Left panels show results for the simulation period 2012-2016 and right panels for the year 2018.

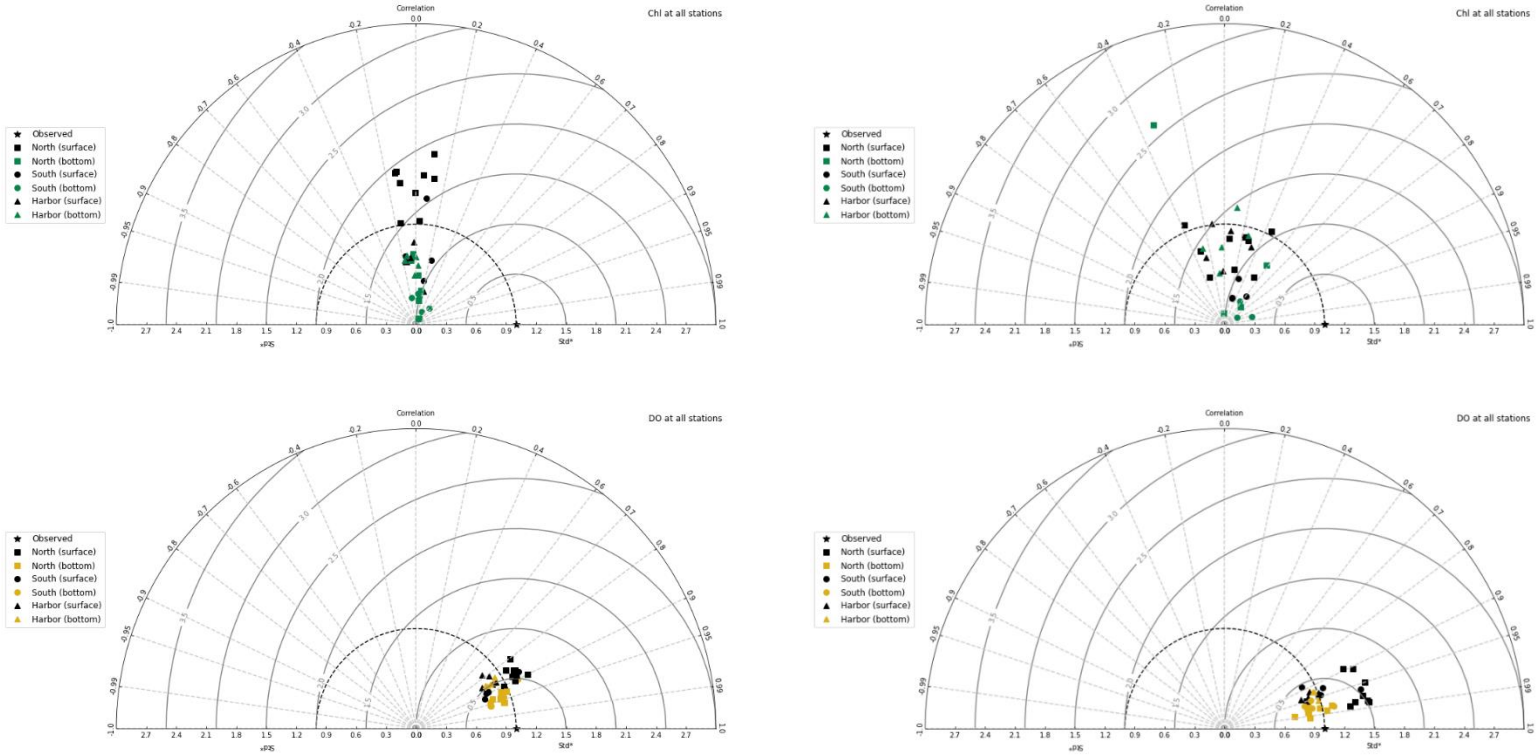

Figure 5-2: Taylor diagrams for MWRA vessel-based survey observations. Top panels show the parameter Chlorophyll-a and bottom panels Dissolved Oxygen. Left panels show results for the simulation period 2012-2016 and right panels for the year 2018.

5.2 Model-observation comparisons

In this section model-observation comparisons in the same format as for the hydrodynamic model (Section 4) are provided. For time series plots, a 3-day moving average is applied to the model outputs to smooth high-frequency variability.

To assess the simulation spatially, vertical transects have been plotted along North-South (N-S) and West-East (W-E) transects (Figure 2-4). Model results in these figures are 5-day averages centered around the field sampling date indicated in each plot.

5.2.1 Light extinction

Measured extinction for the year 2018 (Figure 5-3) ranged from 0.1 to 0.4 at all stations, except at F23, near the harbor, where it ranged between 0.3 and 0.6. This was similar to previous years for which higher and more variable extinction was observed at harbor stations (e.g. Zhao et al., 2017). The model reproduced the extinction range and variability well at most plotted stations. Extinction was generally underestimated at station F23. The model predicted lower extinction in winter (when there are no surveys) than during the rest of the year, associated with lower phytoplankton levels. At stations F23, F13 and F06, simulated extinction showed sharp peaks in the first part of 2018, probably due to storm resuspension of sediment.

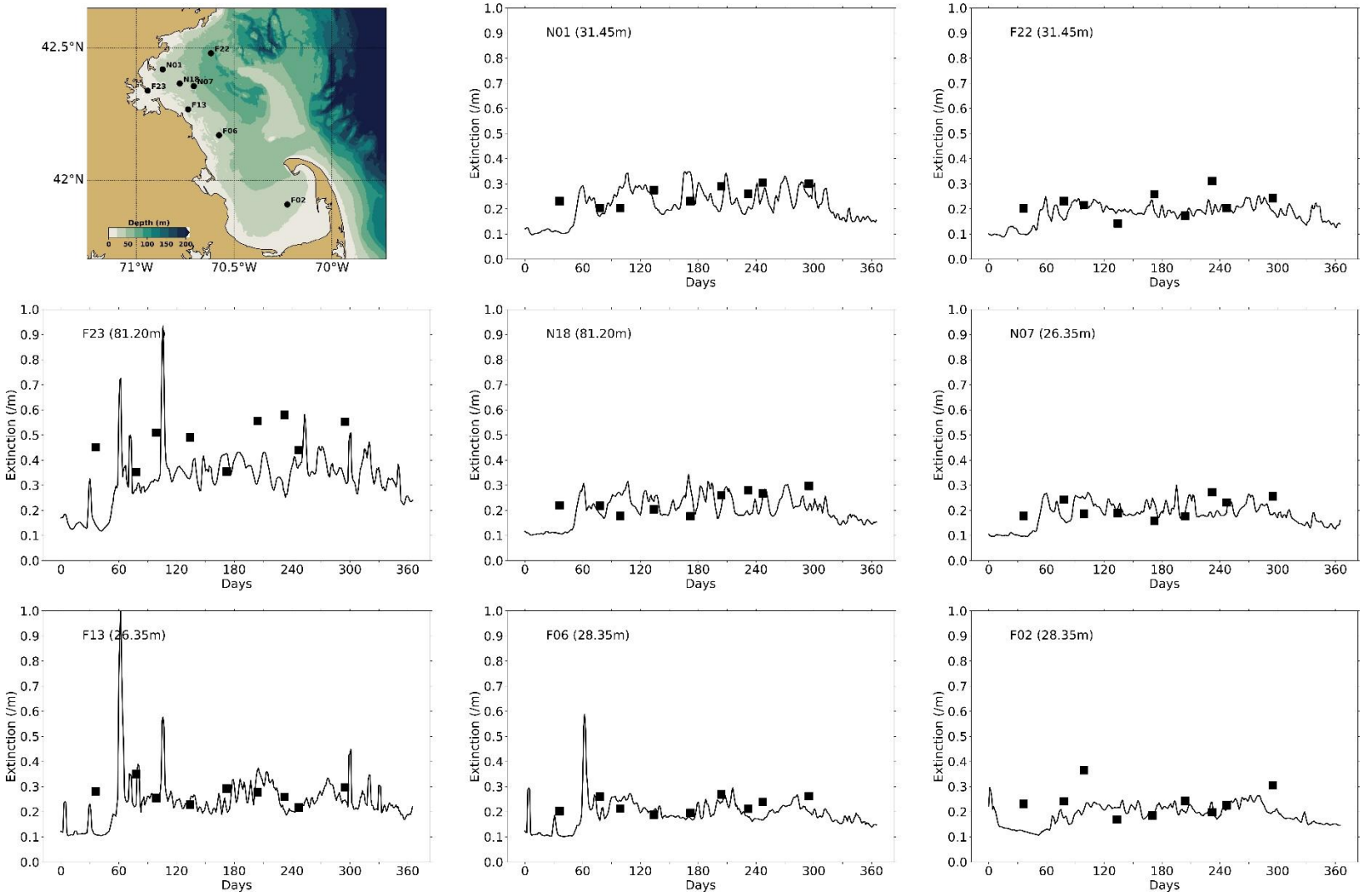

Figure 5-3: Extinction time series, model-observation comparison for 2018. Model: lines. MWRA vessel-based survey observations: symbols.

5.2.2 Dissolved inorganic nitrogen

Seasonal variations of surface and bottom DIN concentrations in 2018 were similar to those observed and simulated for previous years (Figure 5-4). Surface and bottom were comparable in winter, when the water column was well mixed. Surface DIN concentrations declined in April and were depleted throughout the rest of spring and summer, before increasing again in autumn. Bottom concentrations declined to a much lesser degree in spring and summer. The model generally reproduced these observed seasonal variations and vertical differences. In the early spring period, the model shows fluctuating levels of DIN that seem to be driven by early stratification in deeper waters towards the Gulf of Maine (station F22). For the other stations shown, the onset of stratification is well-reproduced. At the southern stations near bottom DIN was slightly overestimated during summer. Observed variations at intermediate depths in the water column were also generally reproduced by the model (Figure 5-5).

According to the model results, the signature of the outfall in terms of DIN concentrations was visible all year round, leading to increased concentrations up to a distance of about 10 km or more (Figure 5-6). This increased DIN remained in the lower layers of the water column during the period of stratification (May-October). During the other months, the effluent led to an increase in DIN concentrations throughout the water column over the outfall (station N21). This was similar to simulations of previous years. In the model during stratified periods, the highest concentrations at N21 (directly over the outfall) were always simulated at the bottom of the water column, while the highest measured concentrations were sometimes higher up in the water column (e.g. June 22nd and August 21st).

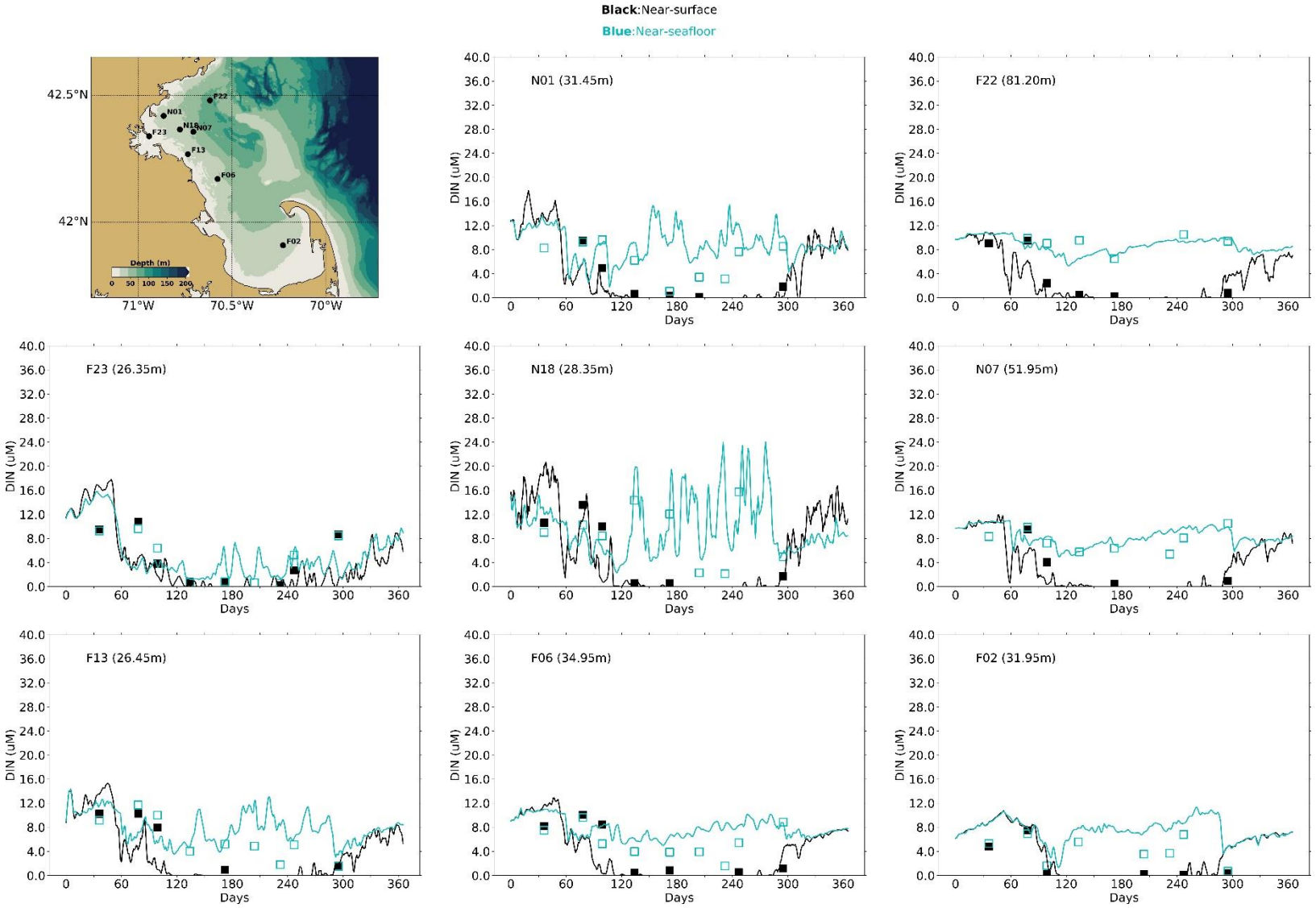

Figure 5-4: Dissolved Inorganic Nitrogen time series, model-observation comparison near surface (black) and seafloor (cyan). Model results: lines. MWRA vessel-based survey observations: symbols.

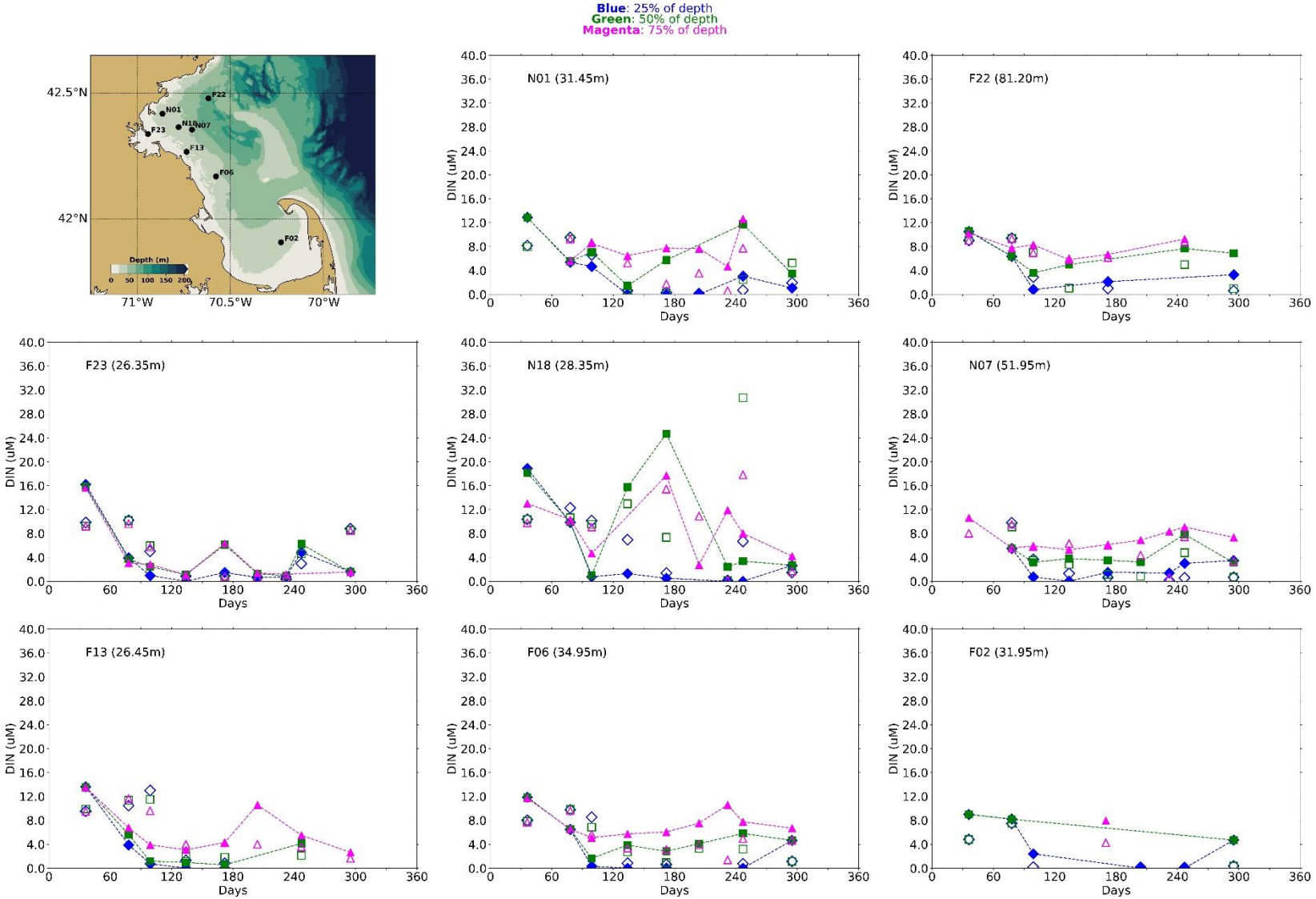

Figure 5-5: Dissolved Inorganic Nitrogen time series, model-observation comparison within water column (between surface and seafloor). Model results: lines and full symbols. MWRA vessel-based survey observations: open symbols.

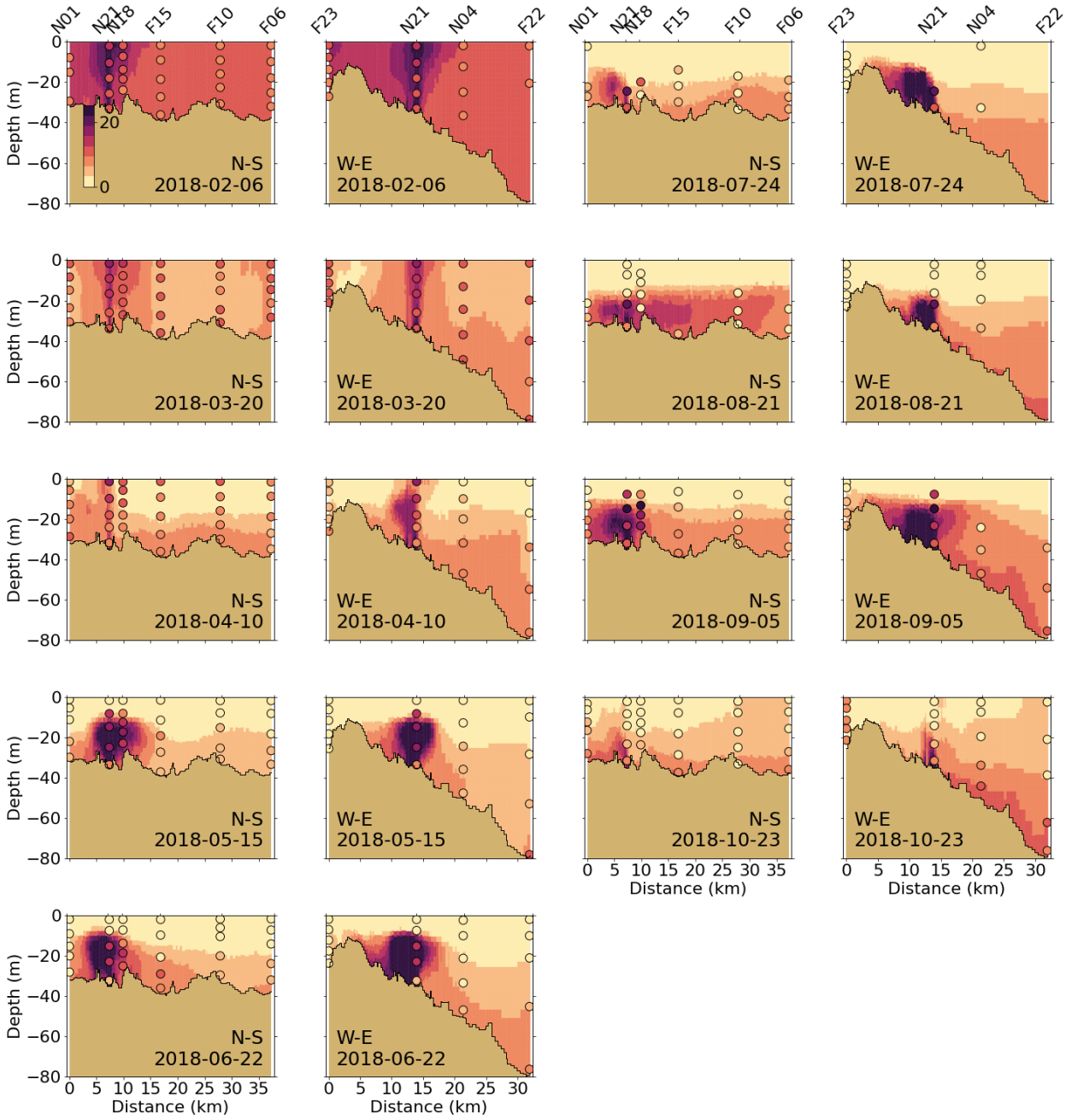

Figure 5-6: Dissolved Inorganic Nitrogen (µM) for 2018 along North-South (N-S) and West-East (W-E) transects (Figure 2-4). MWRA measurements are plotted with round symbols. Model results are 5-day averages around sampling date.

5.2.3 Chlorophyll a

Seasonal variations of chlorophyll a observations in 2018 showed increased values mostly in spring and autumn (Figure 5-7), though the sampling frequency of the MWRA observations makes it difficult to see a clear seasonal pattern. Highest concentrations were observed in fall in northern Massachusetts Bay (N01, N07 and N18), while at the other stations also spring peaks occurred (e.g. F02, F13, F22, F23). Bottom chlorophyll a concentrations were very small at the deeper F22 station, and closer to surface concentrations at some other stations (F23, N18 and F02). The model simulated the higher chlorophyll a peaks in spring and at the end of fall (Figure 5-7). It simulated smaller chlorophyll a summer peaks at some stations (e.g. F23, N01 and F13). As in the simulations for previous years, near surface simulated concentrations were in the same range as observations, while the temporal variability was not always reproduced. This was to some extent related to the relatively low field sampling frequency and the high temporal variability. As in the simulations for previous years, simulated bottom chlorophyll a was underestimated at many stations. Chlorophyll a concentrations in summer and in the beginning of fall were underestimated at the observation stations at intermediate depths as well (Figure 5-7 and Figure 5-8).

Simulated chlorophyll a concentrations decreased eastward from the coast (Figure 5-9). Early spring increases occurred throughout the water column as it was relatively well mixed. During the more stratified months, simulated bottom chlorophyll a remained low and highest values occurred in the subsurface. The observations generally showed that chlorophyll a concentrations declined in March and April (both along the North-South and West-East transects) before increasing again. Highest observed concentrations occurred in late summer, from the surface to depths of ~30 m or more, which was not captured by the model.

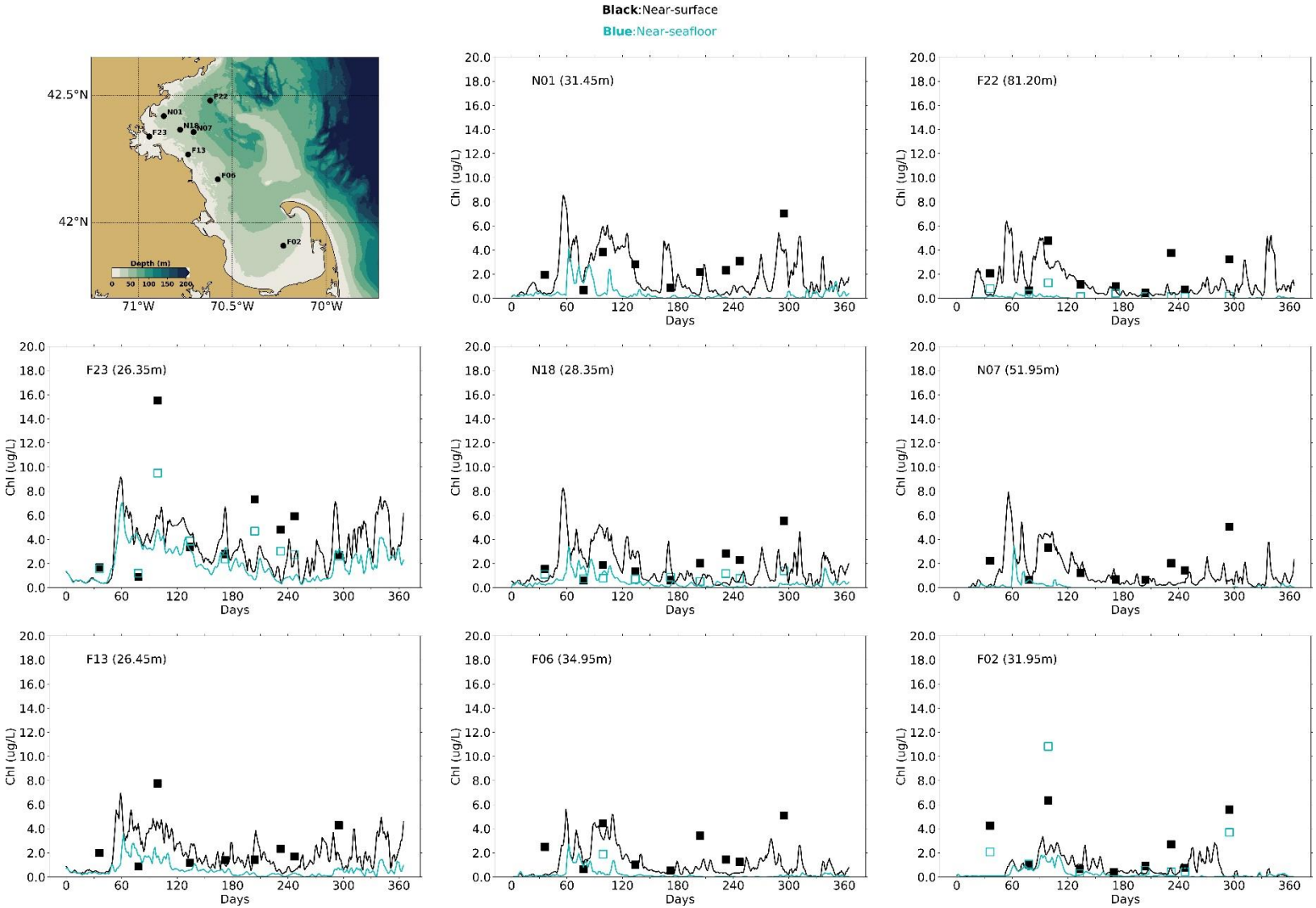

Figure 5-7: Chlorophyll a time series, model-observation comparison near surface and seafloor. Model results: lines. MWRA vessel-based survey observations: symbols.

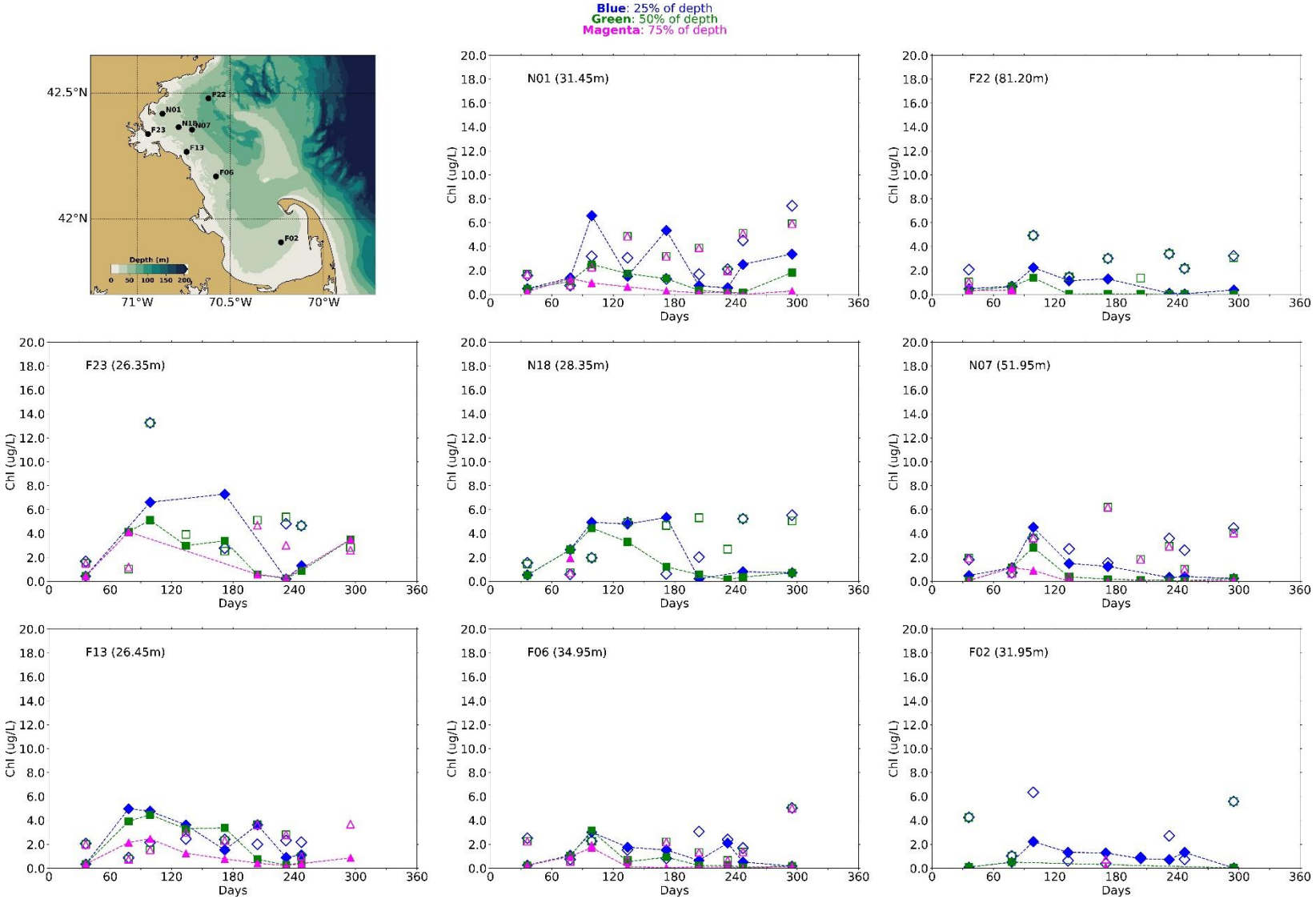

Figure 5-8: Chlorophyll a time series, model-observation comparison within water column (between surface and seafloor). Model results: lines and full symbols. MWRA vessel-based survey observations: empty symbols.

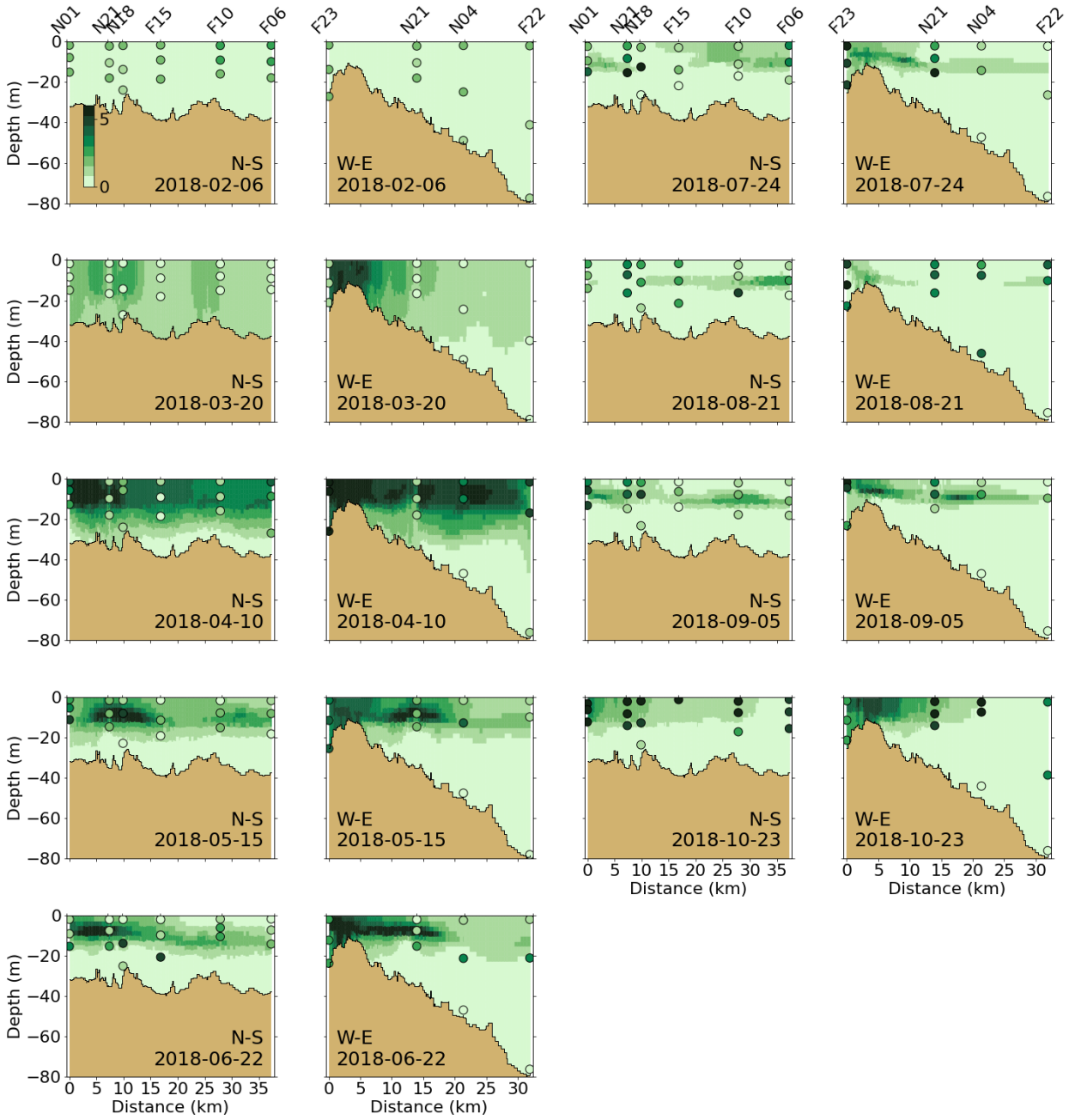

Figure 5-9: Chlorophyll a (µg/L) for 2018 along North-South (N-S) and West-East (W-E) transects (Figure 2-4). MWRA measurements are plotted with round symbols. Model results are 5-day averages around the sampling date.

5.2.4 Particulate organic carbon

POC concentrations at the observation stations were extremely variable and it was difficult to identify a clear seasonal pattern (Figure 5-10). Concentrations were, however, slightly lower in winter and early spring than the rest of the year. Among the plotted stations, POC concentrations were highest at F23, closer to the harbor, likely due to the high river POC inputs (see Figure 3-6). Concentrations were significantly lower near the bottom than at the surface.

The model generally captured POC concentration ranges, variability and vertical gradients at the plotted locations (Figure 5-10 and Figure 5-11). POC concentrations were, however, overestimated at F23, closer to the harbor.

According to the model results, POC concentrations increased from the coast eastward (Figure 5-12). The signature of the outfall was not visible along either the North-South or the West-East transects. This was consistent with the fact that the MWRA outfall only represented a small part of the total non-oceanic OC inputs to the study area (Figure 3-6). Highest simulated concentrations occurred in June, in the subsurface in the northwest. High concentrations were measured in July and August along both transects and quite deep throughout the water column (~30 m). This was not fully captured by the model and was most likely due to the underestimation of phytoplankton biomass (chlorophyll a) for that period.

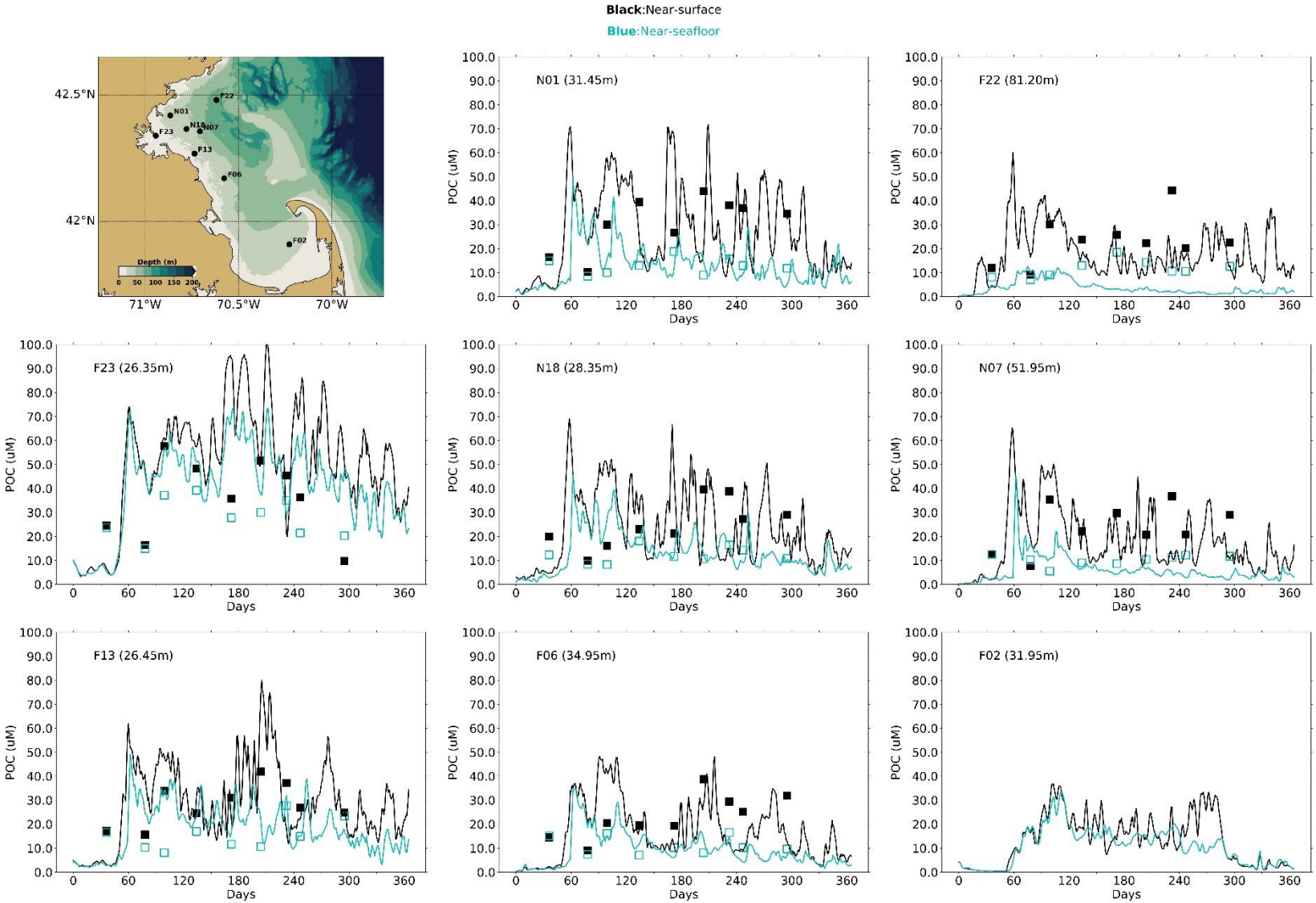

Figure 5-10: Particulate Organic Carbon time series, model-observation comparison near surface and seafloor. Model results: lines. MWRA vessel-based survey observations: symbols.

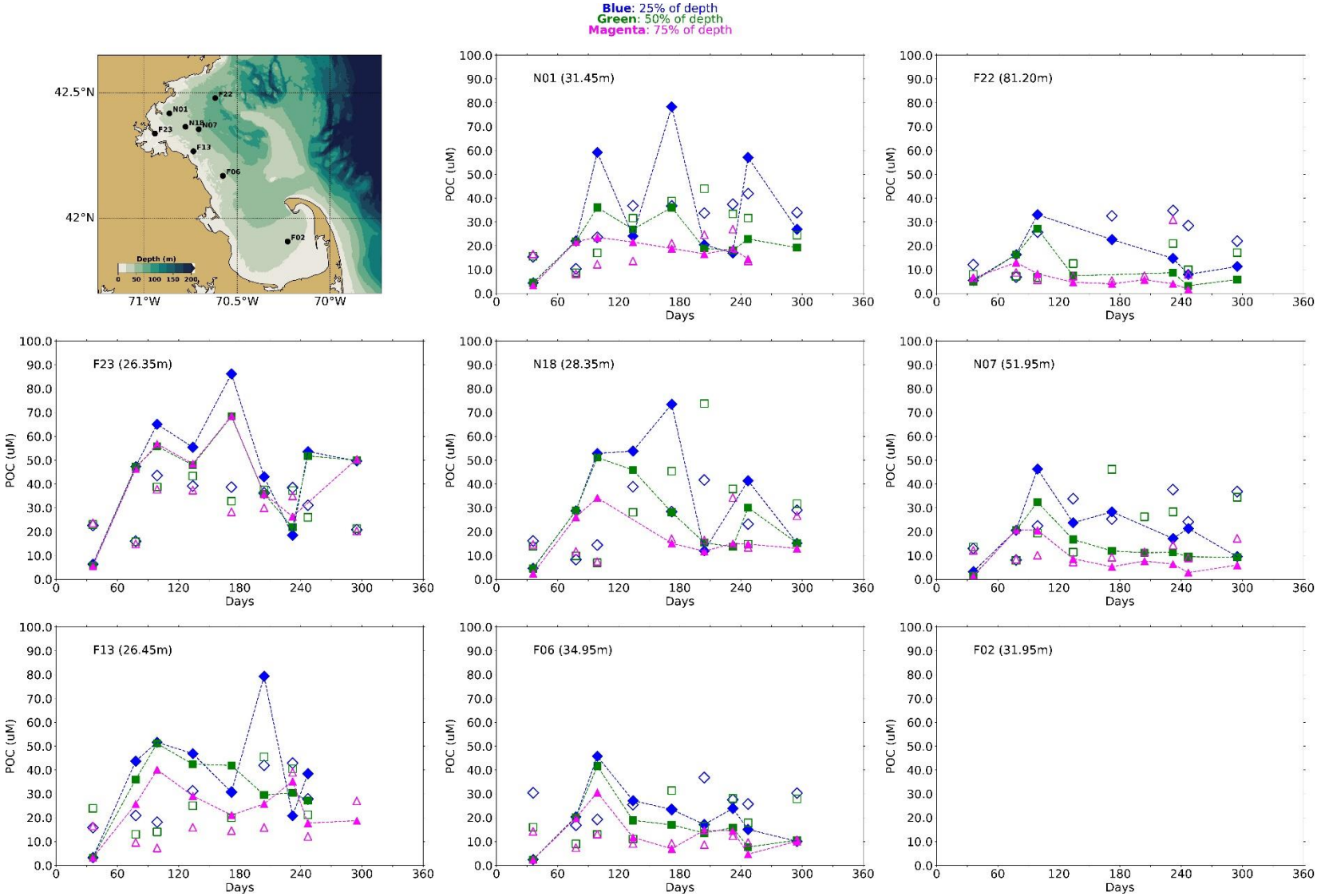

Figure 5-11: Particulate Organic Carbon time series, model-observation comparison within water column (between surface and seafloor). Model results: lines and full symbols. MWRA vessel-based survey observations: empty symbols.

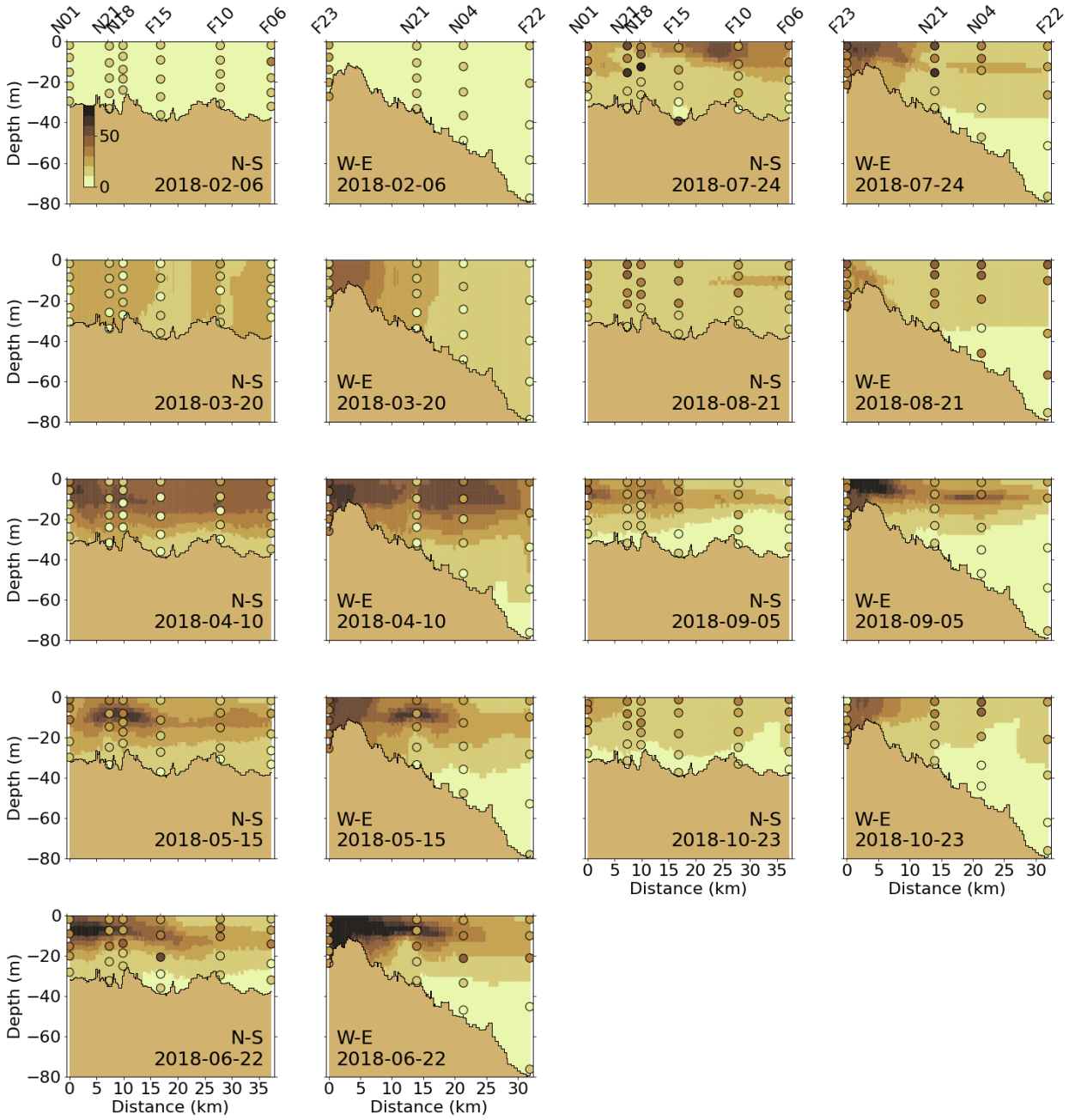

Figure 5-12: Particulate Organic Carbon (µM) for 2018 along North-South (N-S) and West-East (W-E) transects (Figure 2-4). MWRA measurements are plotted with round symbols. Model results are 5-day averages around the sampling date.

5.2.5 Dissolved oxygen

The observed 2018 seasonal variations of DO concentrations were well reproduced by the model, with maximum concentrations at the end of winter and beginning of spring, followed by decreases until fall before rising again (Figure 5-13). While winter concentrations at the surface and the bottom were comparable, bottom concentrations dropped lower at the end of the summer and beginning of fall. Differences between top and bottom concentrations reached about 2 mg/L at the end of October at several stations. As for previous years, the model reproduces minimum observed values at some stations, but not all. The model-observation comparison at intermediate water depths showed similar behavior: summer concentrations at depths nearer the surface were slightly underestimated at most stations, as was the fall decline in DO deeper in the water column (Figure 5-14).

At the A01 mooring station, the model reproduced the seasonal pattern in the observed DO very well, though it again somewhat overestimated the end of autumn minimum (Figure 5-15).

The North-South and West-East cross-section plots show that DO generally had weak vertical gradients (Figure 5-16). Concentrations were higher at the end of winter and beginning of spring and decreased until fall. Higher concentrations were observed and simulated in the subsurface in periods with higher primary production (April-July). In months with visible vertical gradients in DO concentrations, the model captured them well, for example the high subsurface concentrations in June and July.

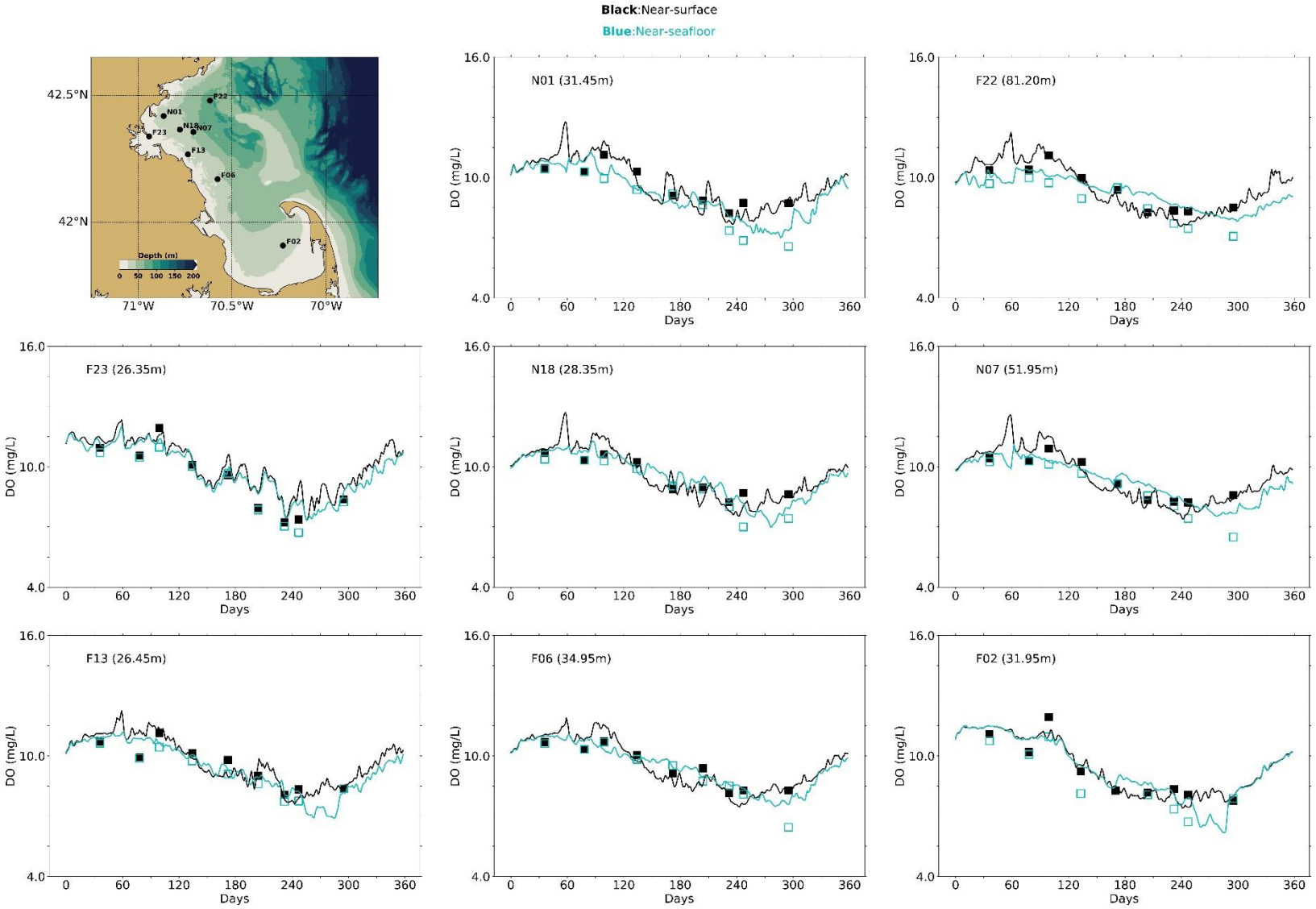

Figure 5-13: Dissolved Oxygen time series, model-observation comparison near surface and seafloor. Model results: lines. MWRA vessel-based survey observations: symbols.

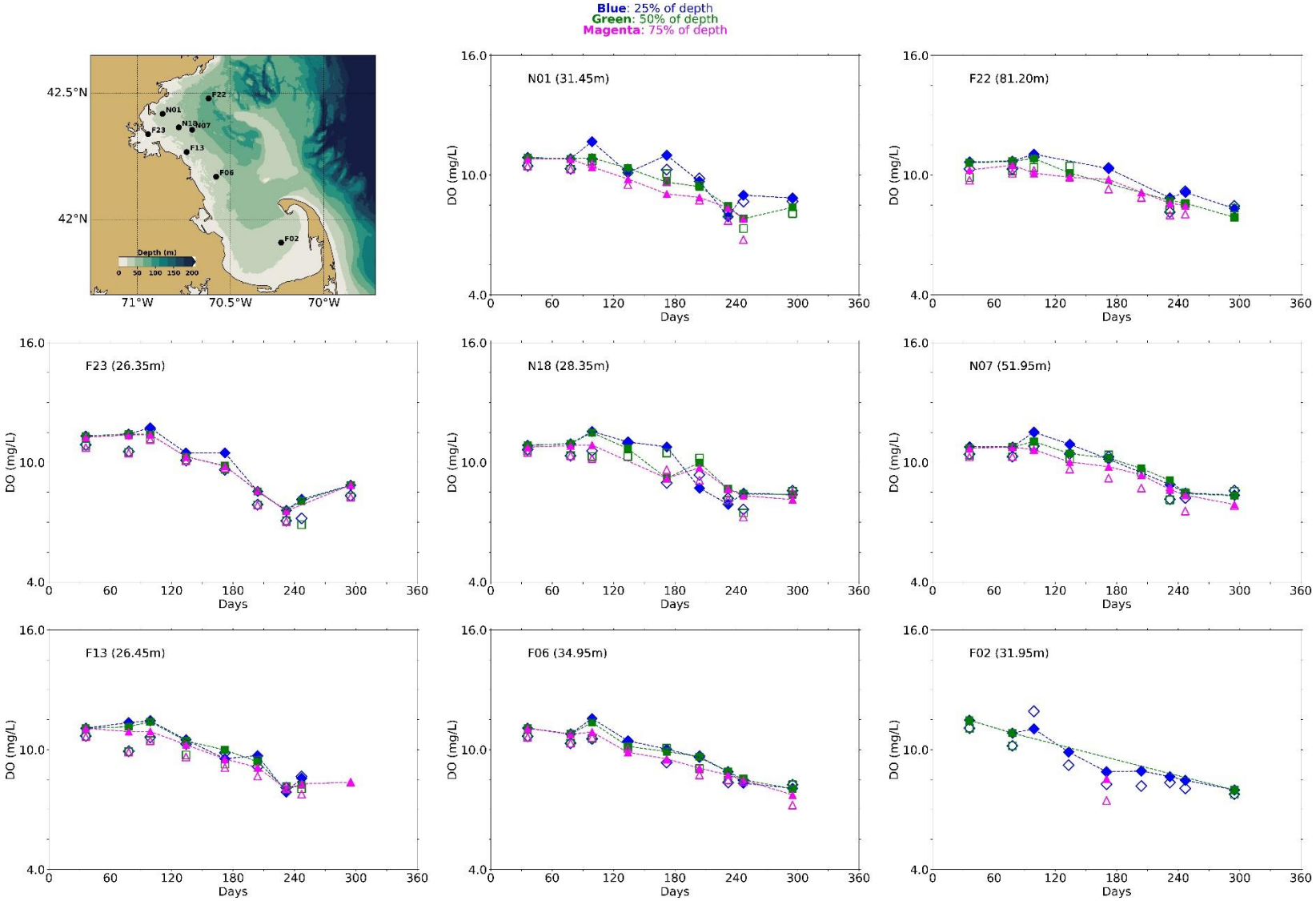

Figure 5-14: Dissolved Oxygen time series, model-observation comparison in water column. Model results: lines and full symbols. MWRA vessel-based survey observations: open symbols.

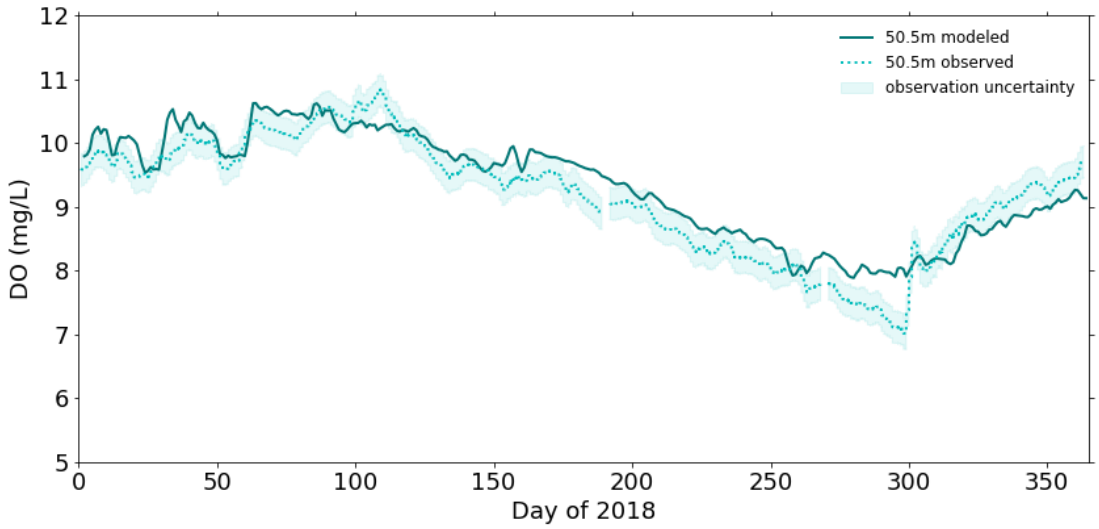

Figure 5-15: Dissolved Oxygen time series 50.5m deep at A01 mooring site, model-observation comparison for 2018.

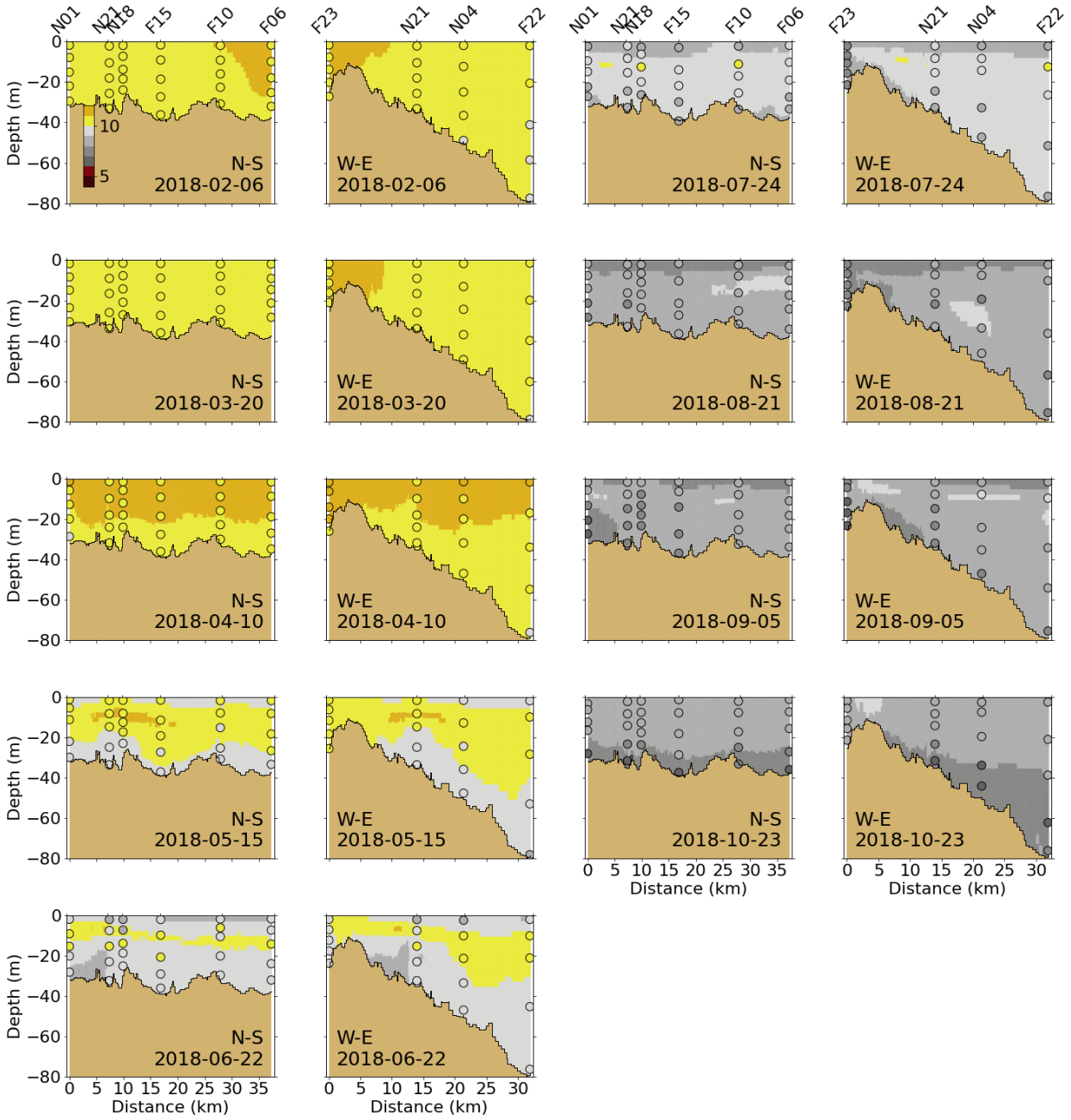

Figure 5-16: Dissolved Oxygen (mg/L) for 2018 along North-South (N-S) and West-East (W-E) transects (Figure 2-4). MWRA measurements are plotted with round symbols. Model results are 5-day averages around the sampling date.

5.2.6 Primary production

Simulated primary production was compared to historical measurements at three monitoring locations (Figure 5-17). Box whiskers represent the 9th, 25th, 50th, 75th and 91st percentiles of primary productions observations over the period 1995-2010 (Keay et al., 2012). Primary production in 2018 was in the range of historical measurements for the entire year at F23, N04, N18. It was also quite typical in comparison to the years 2012 to 2016, with no exceptional peaks (such as in 2012 and 2014 at F23; see Deltares 2021) nor prolonged periods of exceptionally low production.

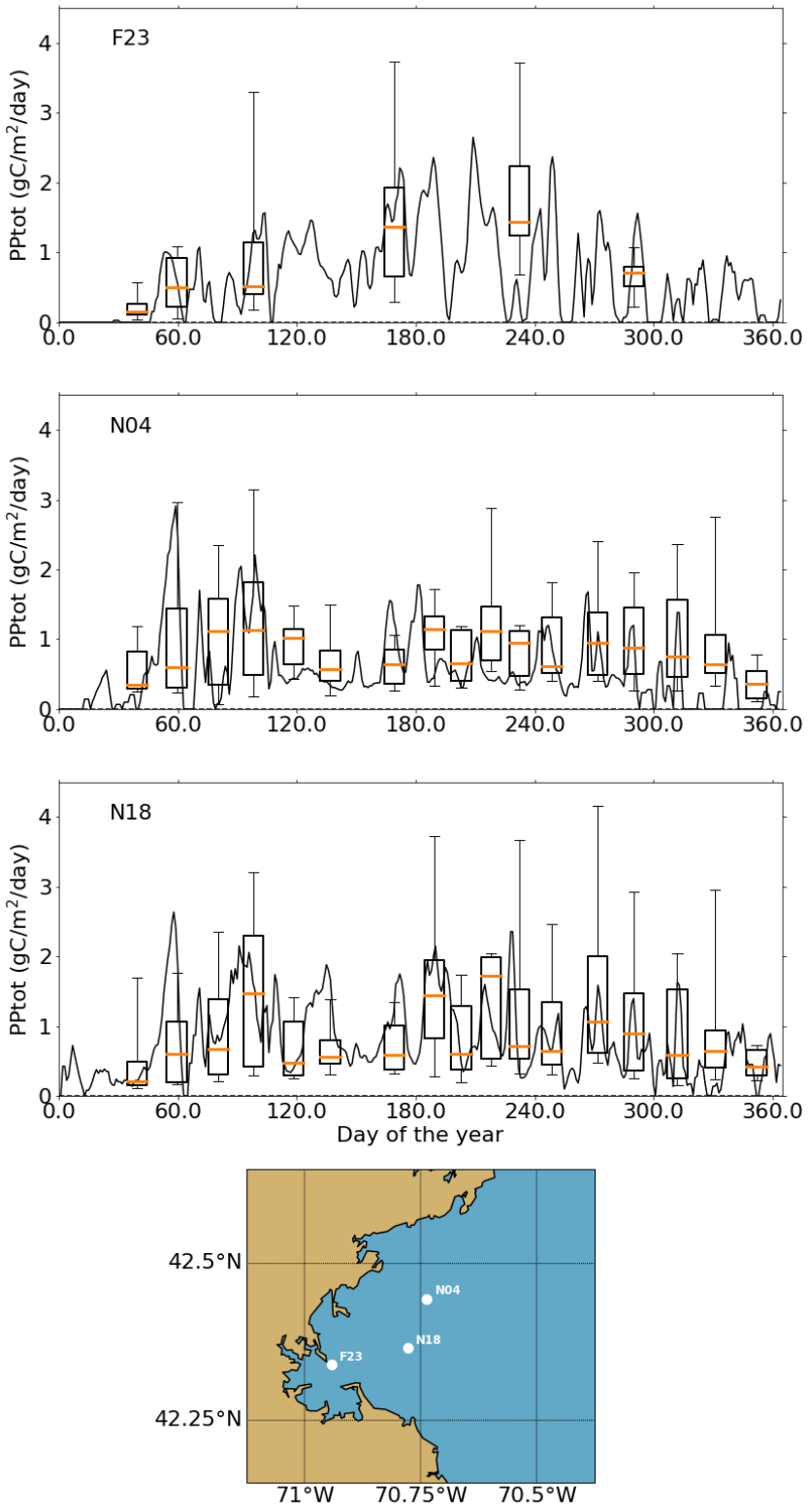

Figure 5-17: Simulated (lines; 2018) and observed (box-whiskers; 1995-2010) primary production.

5.2.7 Sediment fluxes

Sediment NH_4 fluxes (Figure 5-18) and sediment oxygen demand (Figure 5-19) outputs from the model were compared to measurements from the 2001-2010 period from Tucker et al. (2010) at stations located in Boston Harbor and Massachusetts Bay using plots in the same format as Figure 5-17.

Simulated sediment fluxes were low in winter and peaked in the summer due to higher temperatures favorable to biogeochemical activity which mineralizes of organic matter in the sediment. Sediment fluxes were higher in the harbor area than in Massachusetts Bay, which was captured by the model. Results for the year 2018 were similar to those from the individual years 2012 to 2016. These were mostly in the range of historical measurements, except for NH_4 sediment fluxes at the Mass Bay stations (MB01, MB03 and MB05). This discrepancy is related to the simplified representation of sediment biogeochemical processes (see Deltares, 2021).

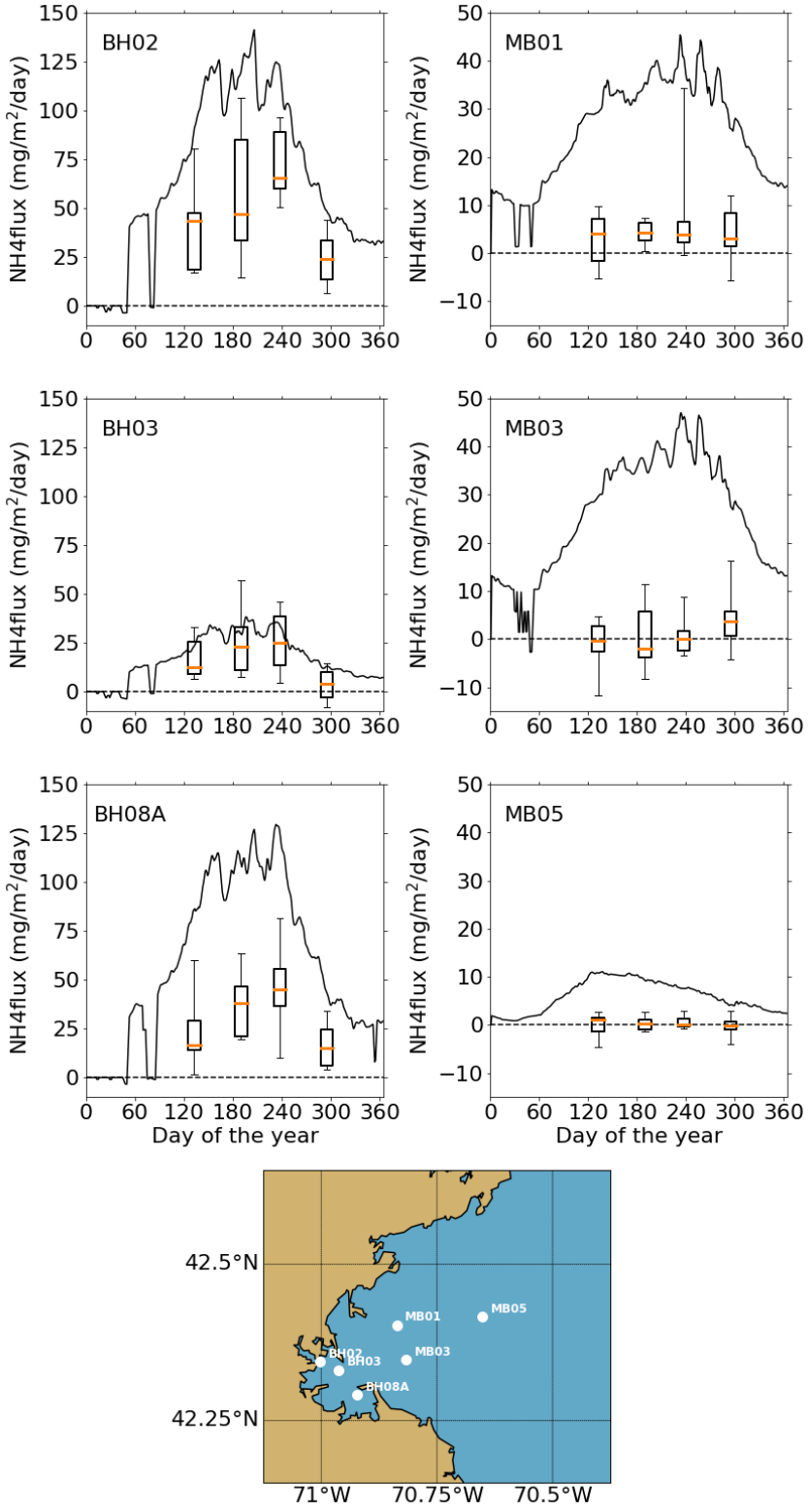

Figure 5-18: Simulated (line; 2018) and observed (box-whiskers; 2001-2010) sediment flux of ammonium. Note change of scale between the Boston Harbor stations (left) and Mass Bay stations (right).

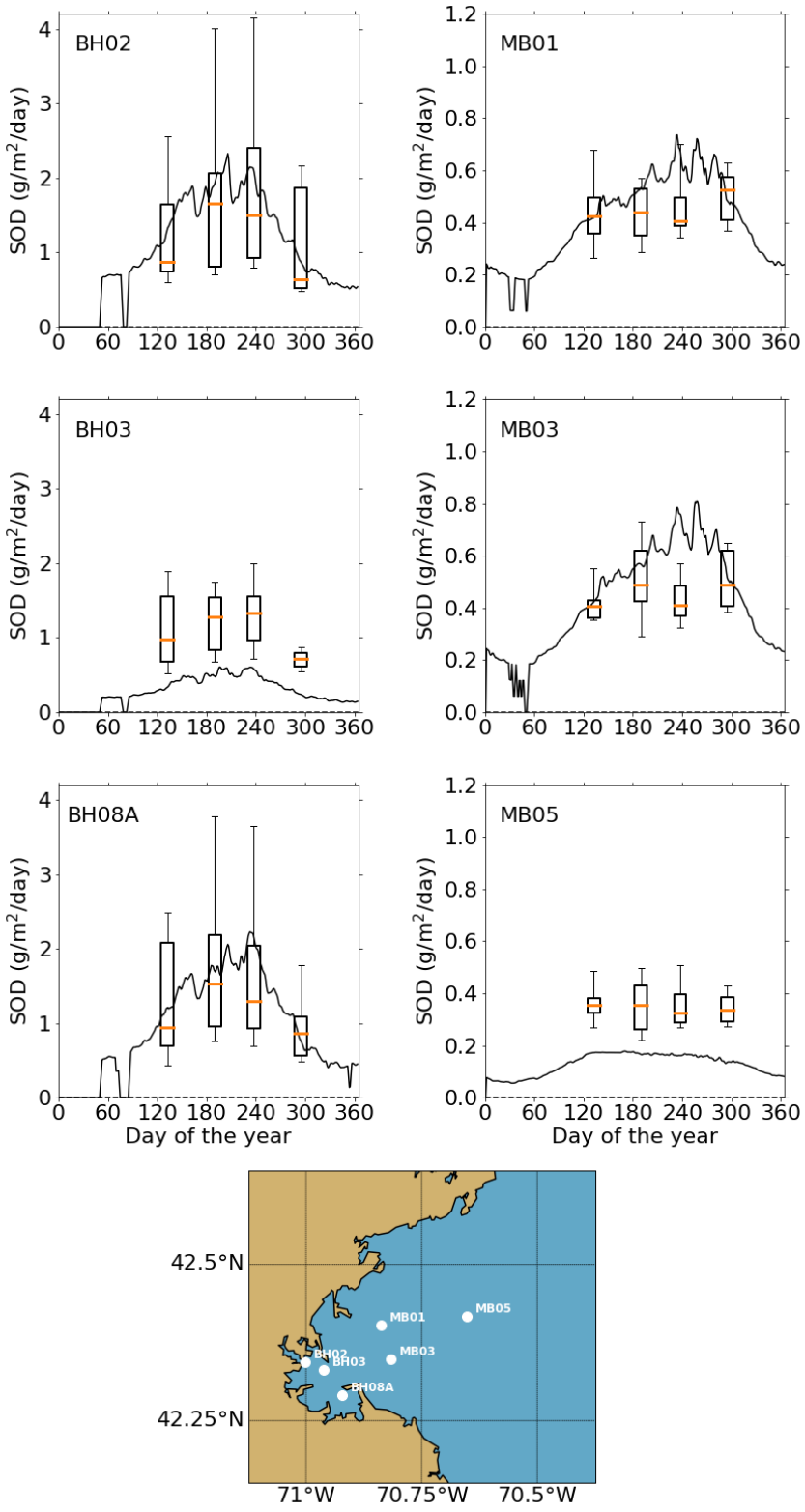

Figure 5-19: Simulated (line; 2018) and observed (box-whiskers; 2001-2010) sediment oxygen demand. Note change of scale between the Boston Harbor stations (left) and Mass Bay stations (right).

5.3 Phytoplankton community composition

Model phytoplankton community/species composition was not validated against field observations during model setup and calibration/validation. However, it is of interest to verify that its main characteristics in the model are not inconsistent with general patterns known to characterize the bays, based on monitoring observations.

The phytoplankton sub-module (BLOOM) simulated the dynamics of 4 functional groups and their adaptation to changing environmental conditions (i.e. light and nutrient limitation). BLOOM simulates the rapid shifts in phytoplankton communities due to these changes, using linear programming to optimize whole-community net primary production (Los, 2009). Simulated phytoplankton groups include: diatoms, dinoflagellates, other marine flagellates, and *Phaeocystis*. Their parameterization was initially based on that used in the North Sea eutrophication model (Blauw et al., 2009) and tuned during the BEM calibration process to better represent chlorophyll a as well as observed PON:POC ratios at MWRA monitoring locations (see Appendix B of Deltares, 2021).

Figure 5-20 shows the share of the different simulated phytoplankton groups in the total phytoplankton biomass near the water surface. Although total phytoplankton biomass temporal dynamics differed from station to station for the year 2018, phytoplankton composition showed similar temporal patterns. Marine diatoms dominated in the winter period and were succeeded in spring by marine flagellates. Dinoflagellates clearly dominated from June to the end of October. These were typical characteristics of community composition seen in monitoring observations.

Observations from the routine monthly surveys in 2018 did not capture a large *Phaeocystis* bloom, but a modest *Phaeocystis* bloom was measured during springtime in Cape Cod Bay. Simulated *Phaeocystis* biomass in the model remained low except for an increase during the spring flagellate bloom period (April-May) at the Cape Cod Bay station F02 and to a lesser extent at F06. Therefore the 2018 model results for *Phaeocystis* agree acceptably well with available observations.

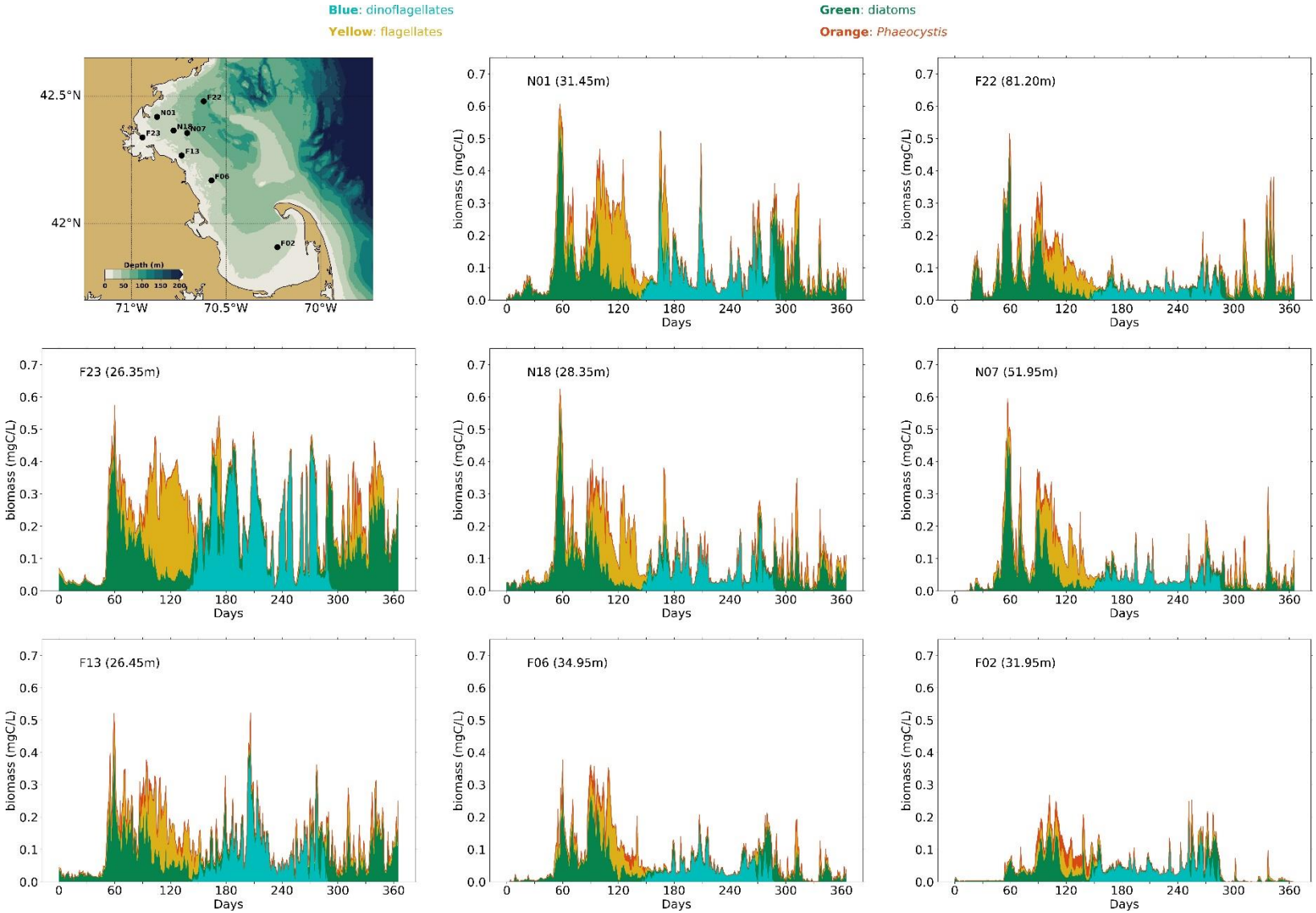

Figure 5-20: Simulated phytoplankton biomass time-series. Biomasses of the 4 simulated species groups (dinoflagellates, other flagellates, diatoms and Phaeocystis*) are stacked.*

5.4 Conditions on West-East transect through outfall

The signature of the outfall in terms of DIN concentrations was visible all year round, with increased concentrations up to a distance of about 10 km (Figure 5-21). This increased DIN was trapped in the lower layers of the water column in the period of stratification (April-October). During the other months, the effluent led to an increase in surface DIN concentrations as well. These temporal patterns were similar to those observed in previous years.

All year round, chlorophyll a concentrations were higher nearshore (Figure 5-22). This was most likely due to the nutrient inputs from rivers to the harbor area, promoting algal growth. Further offshore, highest chlorophyll a concentrations were simulated in spring and, during the summer months, maximum chlorophyll a concentrations occurred at a depth of ~15 m. As for DIN, these patterns were similar to those simulated for previous years. Any effect of the outfall on chlorophyll a concentrations was difficult to detect.

The vertical cross-sections of DO concentrations for 2018 showed similar temporal and spatial patterns as for previous years (Figure 5-23), with the highest concentrations occurring near the surface between February and May. The highest concentrations occurred slightly under the surface between April and July, which corresponded to the depths at which chlorophyll a was the highest. As for chlorophyll a, no effect of the outfall on DO concentrations was visible in the plotted cross sections.

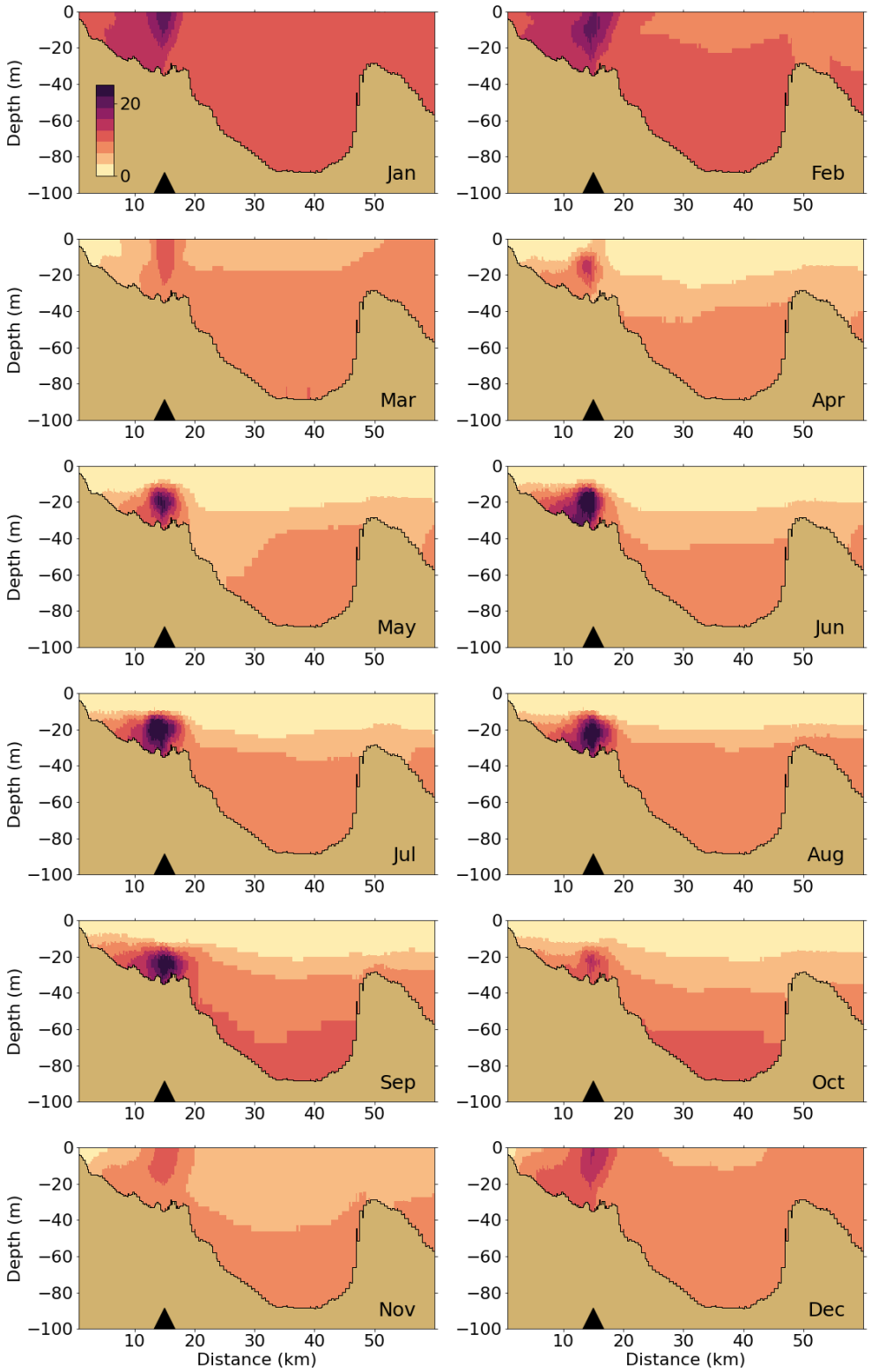

Figure 5-21: Dissolved Inorganic Nitrogen (µM) for 2018 along east-west transect (Figure 2-4). Horizontal axis is distance eastward from coast; black triangle indicates the location of the outfall on the seafloor.

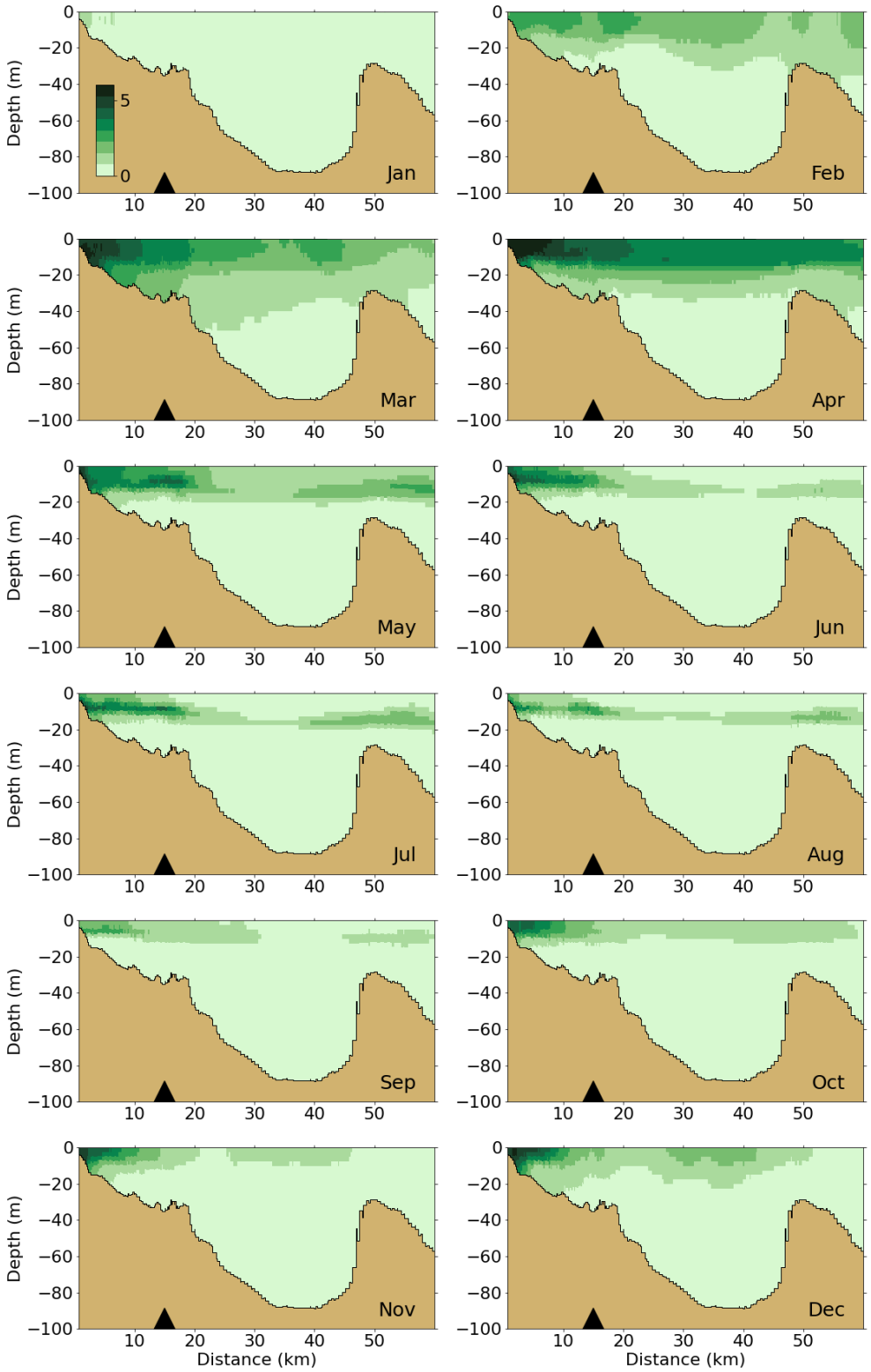

Figure 5-22: Chlorophyll a (µg/L) for 2018 along east-west transect (Figure 2-4). Horizontal axis is distance eastward from coast; black triangle indicates the location of the outfall on the seafloor.

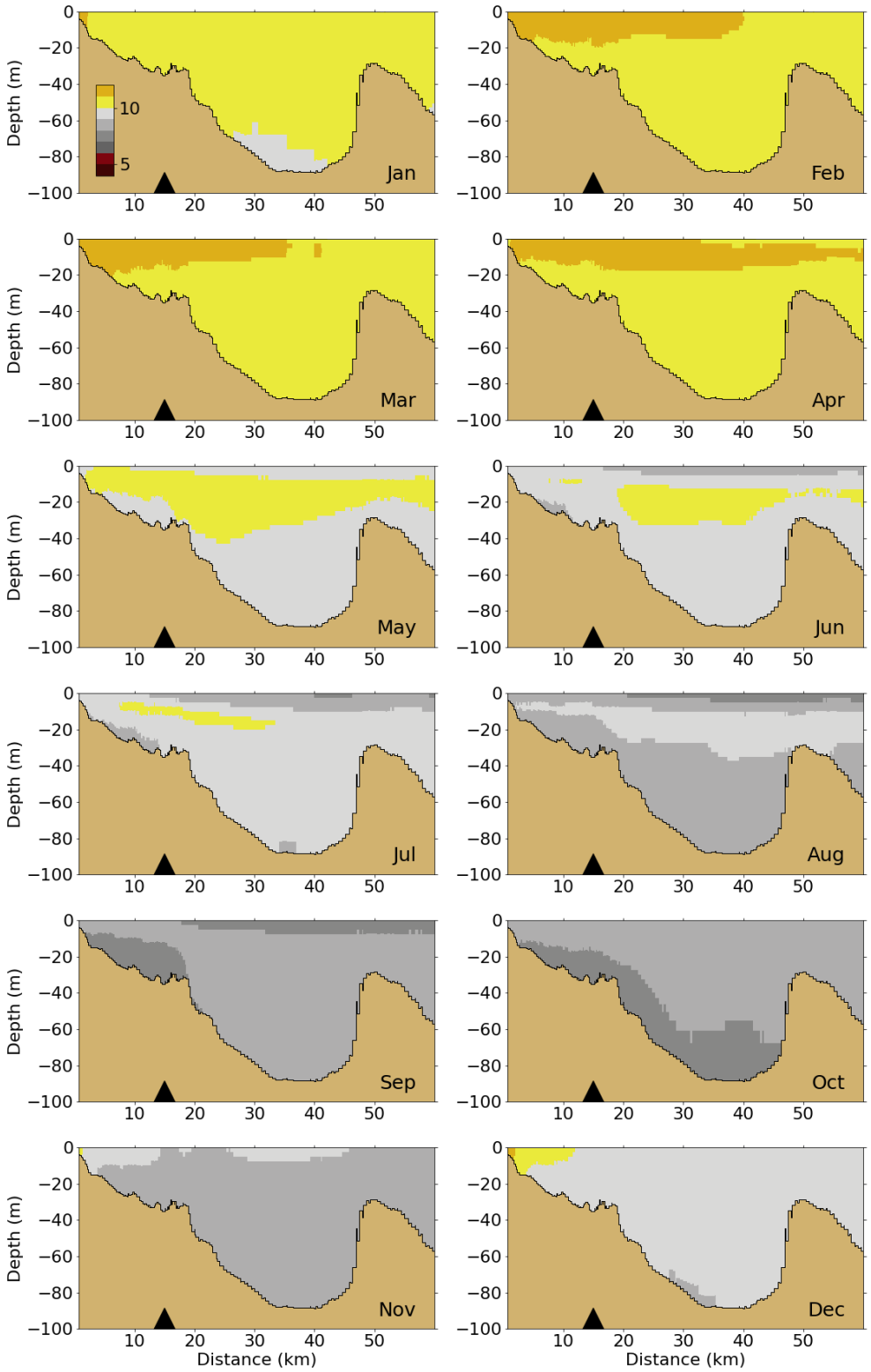

Figure 5-23: Dissolved Oxygen for 2018 along east-west transect (Figure 2-4). Horizontal axis is distance eastward from coast; black triangle indicates the location of the outfall on the seafloor.

6 Synthesis/Application

Two synthesis/application topics are included here: refined nitrogen budgets and effluent dilution. They both use results from the 2017 simulation (Deltares 2022a) because results from the 2018 simulation were not yet final when these analyses were begun.

6.1 Refined nitrogen budgets

A prior report, based on simulations of 2012-2016, details the development and calibration of the current Bays Eutrophication Model and presents 2016 simulation results for annual-mean mass balances of total nitrogen and total phosphorous in the combined Massachusetts Bay and Cape Cod Bay domain (Deltares, 2021; Section B.4.5.4). The balances were dominated by inflows from the Gulf of Maine, which for total nitrogen and total phosphorous were 12 and 23 times as high, respectively, as the combined load of other sources (effluent, rivers, and atmosphere).

This section presents results for the total nitrogen (TN) water column mass balance, using the 2017 simulation, but refined in the following ways relative to that earlier analysis:

- Balances are reported for both the combined Massachusetts and Cape Cod Bays domain, and the Cape Cod Bay domain alone;
- Results are included for each of the individual fluxes (boundaries, effluent, rivers, atmosphere, and internal biogeochemical processes in water column and sediment);
- Monthly-mean results are examined, in addition to annual means.

Methods. Results are from mass balance outputs saved at daily resolution during the simulation of 2017. Figure 6-1 shows the regions analyzed. The first set of mass balance results applies to the area spanning Massachusetts and Cape Cod Bays together (combined areas Mass Bay North, Mass Bay South, and Cape Cod Bay in figure). The second set of results applies to the Cape Cod Bay area only.

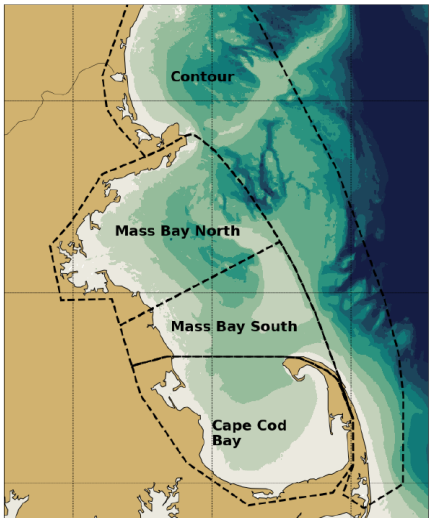

Figure 6-1. Areas used in total nitrogen mass balance calculations.

For each domain the mass balance includes the following terms: fluxes across boundaries with adjacent domains, inputs from external sources (effluent, rivers, and atmosphere), and fluxes due to internal biogeochemical processes. The mass balance equation is

$$M(t_2) - M(t_1) = T_{21} + S_{21} + P_{21}$$

where M is the standing stock or mass of total nitrogen throughout the domain, t_1 and t_2 are the start and end times of the period, T_{21} is the net change of mass at time t_2 relative to t_1 due to boundary transports, and similarly S_{21} and P_{21} are the net changes in mass due to sources and biogeochemical processes, respectively. The net decrease in mass, $M(t_1) - M(t_2)$ is referred to as storage (to denote mass that has been removed from the system of interest and "stored" outside of it) and can be positive (mass decreases) or negative (mass increases).

Fluxes across boundaries between domains are the total time-integrated fluxes, including the effects of tides, through the fixed vertical transect dividing the two domains from each other. For the mass balance of the combined Massachusetts and Cape Cod Bays domain, based on the general pattern of non-tidal flow expected to dominate transport (see Section 4), the influx from offshore and export to offshore were assumed to occur through the “Mass Bay North”/”Contour” interface and the “Mass Bay South”/”Contour” interface, respectively. Such an assumption is necessary in order to compute, in addition to the net flux through the transect, the individual input and output fluxes through it. The net flux between the offshore area and the combined Massachusetts and Cape Cod Bays domain is computed as the difference between the inflow and outflow fluxes. This is consistent with the method used in Deltares (2021) on budgets of the 2016 run, and also consistent with the method used to assess the oceanic inputs of organic carbon and total nitrogen and phosphorus to the study area in annual BEM reports (e.g., Section 3.2 above). For the Cape Cod Bay domain alone, only the net flux between it and Massachusetts Bay to the north is computed, not individual input and output fluxes, because the basis on which to divide the transect into portions where the inflow and outflow occur is less clear.

The internal biogeochemical processes flux is divided into water column and sediment components. The sediment component includes settling and resuspension of organic matter, denitrification and production of ammonium through mineralization in the sediment.

Results: Combined Massachusetts and Cape Cod Bays domain. Table 6-1 presents annual mean and monthly mean results for standing stock and all flux terms broken out individually. The largest individual terms (Table 6-1) are the input and output boundary fluxes, with each typically 10-20 times as large as the magnitude of their sum, the net boundary flux. Source loads have magnitude comparable to the latter, with the effluent contribution dominating over river and atmospheric loads. Net biogeochemical fluxes are substantially smaller than net sources, and dominated by the sediments contribution.

Table 6-1. Combined Massachusetts Bay and Cape Cod Bay domain, annual and monthly means, mass balance results for all individual flux terms and standing stock. Units “t” are metric tons; fluxes are given in thousands of metric tons per year or per month.

Period	Standing stock [t]	Fluxes [10^3 t per period]									
		Offshore boundary			Storage	MWRA load*	Rivers load	Atmos load	Biogeochemical fluxes		
		Input	Output	Net					Water	Sediment	Net
2017	34,216	190	-202	-12.06	1.13	12.33	0.92	1.56	0.58	-4.46	-3.88
January	38,148	15.9	-16.6	-0.68	-0.39	1.06	0.12	0.13	0.08	-0.32	-0.23
February	38,181	21.0	-21.9	-0.88	0.83	1.03	0.10	0.12	0.05	-1.24	-1.19
March	36,796	22.2	-22.8	-0.70	1.58	1.05	0.10	0.13	0.08	-2.24	-2.15
April	34,679	22.6	-24.3	-1.73	2.28	1.09	0.18	0.13	0.06	-2.00	-1.94
May	31,521	33.8	-38.7	-4.93	3.79	1.13	0.12	0.13	0.03	-0.26	-0.24
June	28,681	25.4	-26.1	-0.68	-1.26	1.00	0.11	0.13	0.04	0.67	0.70
July	30,718	20.0	-21.4	-1.38	-0.02	0.96	0.04	0.13	0.03	0.25	0.27
August	31,668	15.7	-12.4	3.28	-4.88	0.97	0.02	0.13	0.01	0.48	0.48
September	34,150	11.5	-15.6	-4.10	2.44	1.04	0.01	0.13	0.10	0.37	0.47
October	33,917	0.23	3.37	3.60	-5.19	1.11	0.03	0.13	0.04	0.28	0.31
November	36,616	-0.91	0.08	-0.84	0.26	0.91	0.05	0.13	0.03	-0.55	-0.52
December	35,810	2.45	-5.47	-3.02	1.69	1.00	0.05	0.13	0.04	0.11	0.15

* This value for annual total TN load is computed using a method different than the EPA method MWRA uses to calculate and test the Contingency Plan nitrogen load threshold.

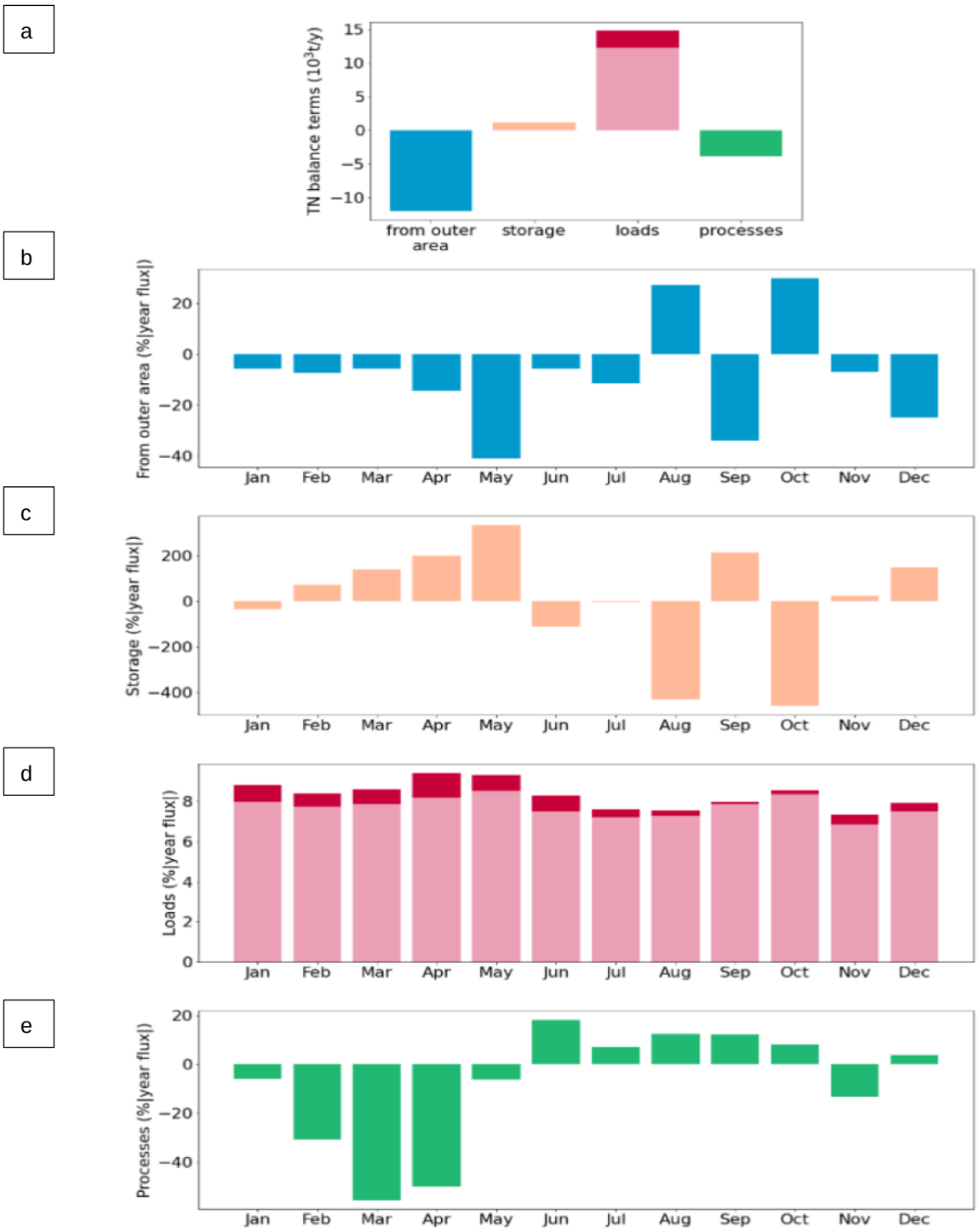

Figure 6-2. Combined Massachusetts and Cape Cod Bays domain, four selected terms of TN mass balance: net offshore input, storage, net loads (effluent in lighter red), and net processes. a: Annual means. b, c, d, and e: Monthly means, as percentage of annual means, for each of the four terms. Note different scales on vertical axes of frames.*
** The individual input and output boundary fluxes have not been included in the figure because they are so large they would require changing the scale, and would make the other terms hard to see.*

The large individual input and output boundary fluxes dominate the mass balance overall. Offshore conditions are the strongest control on total nitrogen within both Massachusetts and Cape Cod Bays. Detailed causes of variability in the boundary flux terms within the year, for example the lower magnitudes during some fall months, have not been examined but the strongest influences are probably circulation processes such as unusual residual currents, offshore flow patterns, or storm impacts.

Figure 6-2 graphically presents a subset of the information in Table 6-1. The individual input and output boundary fluxes have not been included in the figure because they are so large they would require changing the scale, and would make the other terms hard to see. The figure shows the annual means and monthly variations for storage and three net terms, computed as the sum of other individual terms:

- Net offshore input: The sum of boundary input (positive) and boundary output (negative).
- Loads: The sum of load from rivers, atmosphere, and effluent.
- Processes: Net sum of internal biogeochemical process fluxes in water column and sediments.

Among the four terms shown in the annual mass balance of Figure 6-2a the two largest are the net offshore input, which is negative (indicating a net export of total nitrogen offshore), and the net loads, which is positive and largely consists of effluent (lighter red component, in figure). The storage term is small and positive, meaning removal of nitrogen. The biogeochemical processes term is modest and negative.

Overall these results, from the 2017 simulation, are similar to the earlier results from the 2016 simulation. In general, this implies inter-annual variations in these budgets are not dominant, suggesting results presented here may be representative of most years.

Regarding monthly variations, for offshore input (Figure 6-2b) they are relatively large with no clear seasonality; this term is relatively small and negative (minor export to offshore, from the bays) for most of the year, but larger and positive (substantial input to the bays from offshore) in some months (August, October) while larger and negative in others (May, September, and December). These variations are mainly due to changes in non-tidal currents across the boundary. In contrast, monthly variations in loads (Figure 6-2d) are relatively weak because loads are dominated by effluent which does not have strong seasonality. Monthly variations in net biogeochemical processes include a seasonal cycle (Figure 6-2e) with larger negative values (removal of nitrogen) in the spring due mainly to settling of organic matter from spring phytoplankton production, and more modest positive values (input of nitrogen) in fall mainly due to sediment remineralization. The monthly variations in storage (Figure 6-2c) reflect the summed monthly variations of the other terms.

Results: Cape Cod Bay domain alone. Table 6-2 and Figure 6-3 show results for Cape Cod Bay alone. They are presented similarly to Table 6-1 and Figure 6-2 except that the boundary is with Massachusetts Bay (Cape Cod Bay is not adjacent to the offshore area), there is no effluent source, and there is net boundary flux but not individual input and output boundary fluxes (see above). The influence of nitrogen from the MWRA outfall affects this Cape Cod Bay domain as a contribution to the Massachusetts Bay boundary term.

The annual results in Table 6-2 show sediment flux as the largest term followed by atmospheric load, storage, water column flux, and input from Massachusetts Bay. For most monthly-mean results, the ranking of terms by magnitude is similar.

Figure 6-3 graphically presents four terms, a subset of the results in Table 6-2: net flux from Massachusetts Bay, storage, net loads (river and atmospheric), and net biogeochemical processes (water column and sediment). The annual-mean results (Figure 6-3a) show net biogeochemical processes as the largest single term. It is negative, mainly due to settling of organic matter and processing in the sediment, similar to the result for the combined Massachusetts and Cape Cod Bay results described above. The other three terms are positive; net sources, which is dominantly due to atmospheric input, is largest followed by storage, and finally input from Massachusetts Bay (within which the nitrogen from MWRA effluent is one contribution).

Table 6-2. As Table 6-1 but for Cape Cod Bay domain only.

Period	Standing stock [t]	Fluxes [10^3 t per period]						
		Mass Bay boundary	Storage	Rivers load	Atmos load	Biogeochemical fluxes		
		Net				Water	Sediment	Net
2017	7,737	0.22	0.38	0.02	0.54	0.28	-1.45	-1.17
January	8,801	0.05	-0.06	0.00	0.05	0.02	-0.07	-0.05
February	9,008	0.15	0.14	0.00	0.04	0.03	-0.36	-0.33
March	8,428	0.18	0.58	0.00	0.05	0.04	-0.85	-0.81
April	7,977	0.57	0.21	0.00	0.04	0.02	-0.85	-0.83
May	7,178	-0.72	0.80	0.00	0.05	0.01	-0.14	-0.13
June	6,537	-0.06	-0.26	0.00	0.04	0.01	0.26	0.27
July	7,217	0.10	-0.16	0.00	0.05	0.01	0.00	0.01
August	7,339	0.76	-1.06	0.00	0.05	0.01	0.25	0.25
September	7,810	-0.68	0.40	0.00	0.04	0.06	0.18	0.23
October	7,427	-0.17	-0.06	0.00	0.05	0.01	0.18	0.19
November	7,538	0.15	-0.10	0.00	0.04	0.03	-0.12	-0.10
December	7,666	-0.11	-0.05	0.00	0.05	0.03	0.09	0.12

With respect to monthly variations, Massachusetts Bay inputs shows large changes (Figure 6-3b) of both signs, with no clear seasonality, indicative that changing currents are the main driving influence as is consistent with above results for the offshore boundary. Monthly variability of net sources (Figure 6-3d) is minimal, as it is dominated by atmospheric input which is assumed constant in the model (Deltares, 2021). Monthly variability of net biogeochemical fluxes (Figure 6-3e) has a similar seasonal pattern as described above. The monthly variations in storage (Figure 6-3c) are the resultant of the other terms.

Conclusions. For the combined Massachusetts and Cape Cod Bays domain, the refined approach presented here confirms prior understanding that the TN budget is dominated by input and output across the boundary with the offshore area. It also builds on prior understanding, to reveal that settling organic matter overcomes sediment remineralization so biogeochemical processes cause net removal of nitrogen on an annual basis. Finally, it shows the nature of month-to-month variability of fluxes. Monthly variability of net transport from the offshore boundary is irregular, as controlled by currents. The net of sources (effluent, rivers, and atmospheric deposition) has weak monthly variations because it is dominated by effluent, which is relatively stable from month to month. Monthly changes in biogeochemical fluxes show a clear seasonal cycle, with removal by settling organic matter through spring, followed by more modest sediment remineralization input later in the year. Results for the Cape Cod Bay domain alone show that biogeochemical removal of TN, which has a similar seasonal cycle to that just described, has the largest magnitude. Atmospheric load is the largest input and input from the boundary with Massachusetts Bay, which includes a contribution from MWRA effluent, is smaller.

a

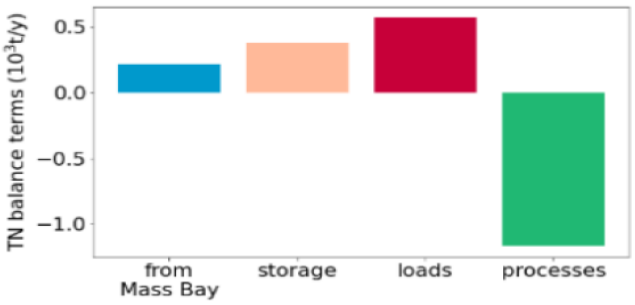

b

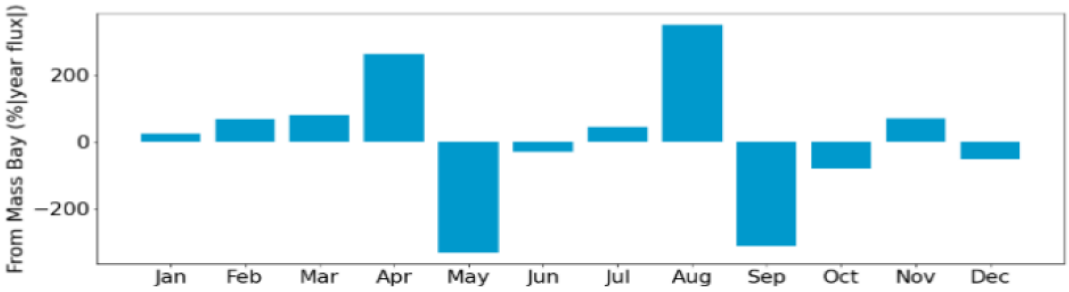

c

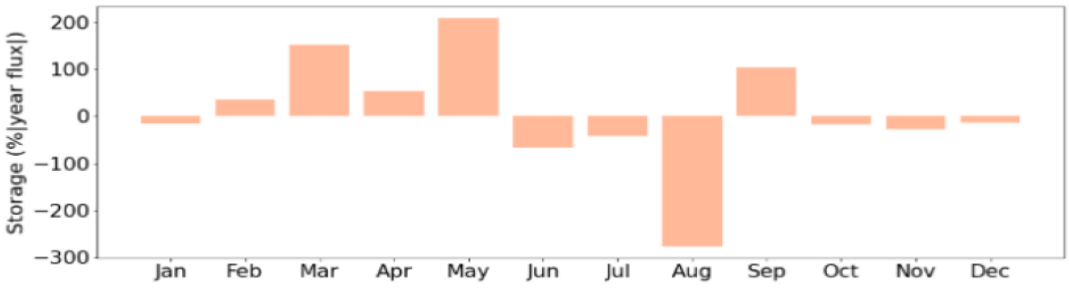

d

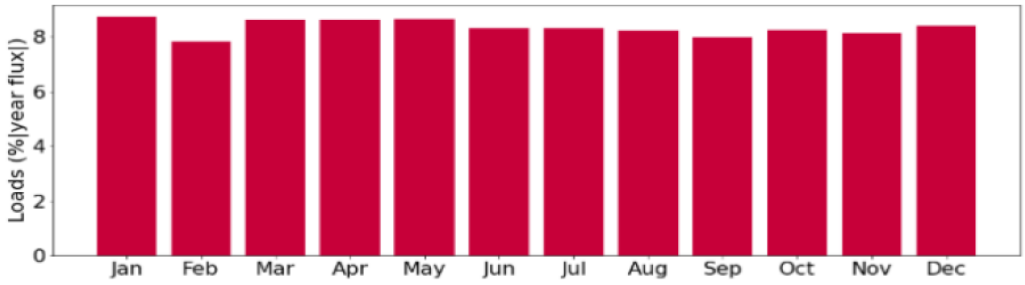

e

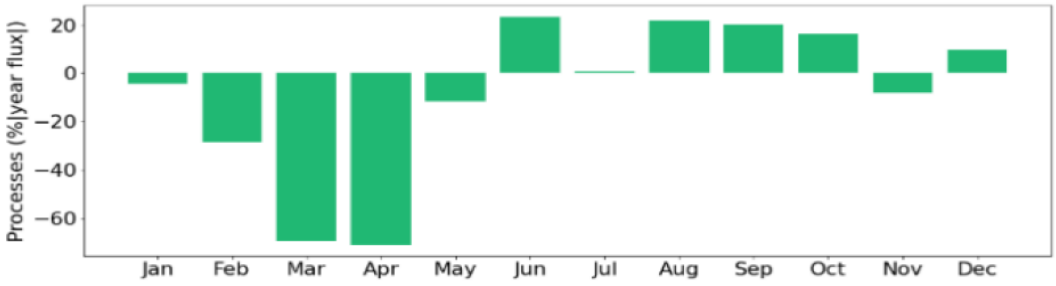

Figure 6-3. Cape Cod Bay domain alone, four selected terms of TN mass balance: input from Massachusetts Bay, storage, net loads (atmosphere and river), and net (sediment and water column) biogeochemical processes. a: Annual means. b, c, d, and e: Monthly means, as percentage of annual means, for each of the four terms. Note different scales on vertical axes of frames.

6.2 Effluent dilution

Modeling studies from the 1990s during the outfall planning process examined effluent dilution using precursor models to the Bays Eutrophication Model (e.g., Signell, 2007). They showed a seasonal pattern. In summer, dilution was weakest at depth below the pycnocline where stratification trapped the effluent plume, and strongest shallower than the pycnocline. In winter when stratification was weak the effluent plume extended to the surface so dilution was relatively strong and more uniform throughout the water column. These early studies also revealed spatial patterns including an area of relatively weaker dilution extending from the outfall westward then southward along the south shore towards Cape Cod Bay, mainly during the well-mixed (unstratified) winter season. The purpose of this section is to revisit earlier dilution studies using the updated BEM, because it incorporates a number of improvements over the prior model, including a higher-resolution grid.

Methods. The 2017 simulation was run with a conservative tracer added to the effluent at a constant concentration. Note that the tracer was added throughout the two-year duration spin-up of the model. The dilution factor is the ratio of the tracer concentration in the effluent to the tracer concentration in each model grid cell. The daily-mean dilution factor was saved at every grid cell throughout the year. From those daily-mean results, the monthly average and monthly minimum dilution factor were computed at every grid cell. Results are presented as maps of monthly-mean dilution at the surface, at the seafloor, and at 20 m deep which is representative of the pycnocline depth when it is present from roughly April through September. Monthly-mean and monthly-minimum dilution are also presented on vertical slices along two transects that pass through the outfall and selected MWRA monitoring stations: one transect with roughly west-east orientation and the other with roughly north-south orientation (Figure 6-4).

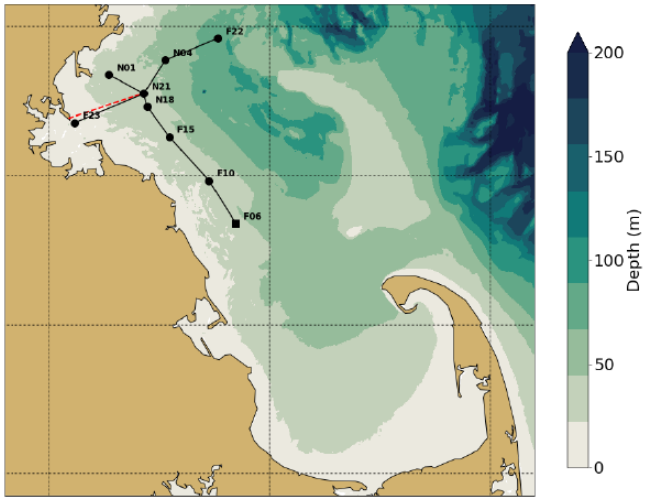

Figure 6-4. . Map showing two transects (black lines) along which vertical slices of dilution factor are shown in below figures. The west-east transect starts at F23 and ends at F22, passing through the outfall at N21. The north-south transect starts at N01 and ends at F06, also passing through the outfall. Red line is tunnel from Deer Island to the outfall.

Because the purpose of BEM is to improve understanding of potential eutrophication across the Massachusetts and Cape Cod Bays on scales of many kilometers, it is a far-field model. In contrast, near-field mixing models focus on the detailed processes of effluent plume mixing and behavior on scales of meters or less, within a few 100 meters of the outfall. As a far-field model with horizontal grid resolution of 250 m near the outfall, BEM gives dilution results within about 500 meters of the outfall that are generally underestimates (as discussed in Deltares 2021) and are not in full agreement with more accurate values from near-field mixing models (e.g., Deltares 2022b) which have been verified against dye study field measurements. The BEM dilution results are more accurate throughout the areas of interest, farther than 500 meters from the outfall, where calibration of the model has demonstrated agreement with extensive observations.

Results. Monthly-mean dilution factors (Figure 6-5 shows maps; Figure 6-6 shows vertical slices) are generally at least about 100 throughout the domain at all times. They reach minima as low as 50-100 in areas directly over the outfall that do not extend more than a few kilometers away. As noted, because BEM is a far-field model the values within about 500 m of the outfall are known to be lower

than more accurate dilution estimates from field measurements and near-field mixing models. These lowest values extend from surface to seafloor from about December through April while in the other months they remain at the pycnocline depth and deeper, and during late summer they can be slightly lower than the lowest December through April values.

Areas with higher monthly-mean dilution that remains less than 500 extend somewhat farther from the outfall, to a confined region within Massachusetts Bay that varies from month to month, with similar seasonality of its vertical structure. In January, this region is largest and extends westward to Boston Harbor and some of the south shore. It is smallest during some stratified months, confined to near the outfall, and during other stratified months can extend away from the outfall in different directions.

Consider next the area with monthly-mean dilution more than 500 but less than 1000, which is distinctly seasonal. From about January through March, it extends throughout the water column and south from the outfall in a wide region from along the south shore to Cape Cod Bay. In April, it still extends to the surface in the coastal area nearest the south shore and throughout Cape Cod Bay, but is confined to depths near and below the pycnocline on the east-west transects. In May, the area where it extends to the surface is confined to parts of Cape Cod Bay, and during remaining months of the year it remains at the pycnocline or deeper and within smaller parts of Massachusetts Bay generally to the north, west, or south of the outfall.

Finally, there are areas where monthly-mean dilution is at least 1000. These include regions offshore and to the north year-round, as well as Cape Cod Bay from June through December.

In order to provide an indication of the within-month variability, in Figure 6-7 the monthly-minima of the daily-mean values at each grid cell are shown on the vertical-slice transects. Comparing these to the monthly-mean values in Figure 6-6 demonstrates the extent to which individual daily-mean results can be lower than the monthly means. The spatial and temporal patterns of the monthly-minima results are generally similar to those of the monthly-means described above. The monthly minima are as low as 10-100 in areas over and very near the outfall; as noted above, because BEM is a far-field model, within about 500 meters of the outfall they are lower than more accurate results from near-field mixing models (e.g. Deltares 2022b) which have been validated against observations.

Conclusions. These effluent dilution results are based on more modern modeling methods, and provide greater spatial and temporal detail, than similar calculations from the 1990s. However, they show similar overall patterns in terms of the seasonality, vertical structure, and geographic patterns of dilution. In addition, the quantitative dilution factor results are generally similar to past studies. In Massachusetts Bay within 10-20 km of the outfall the monthly-mean dilution is typically at least 200. During winter and spring, dilution remains less than 500 in an area extending from the outfall westward to Boston Harbor and along the south shore extending to Cape Cod Bay. During summer, areas with dilution less than 500 are confined to Massachusetts Bay and beneath the pycnocline.

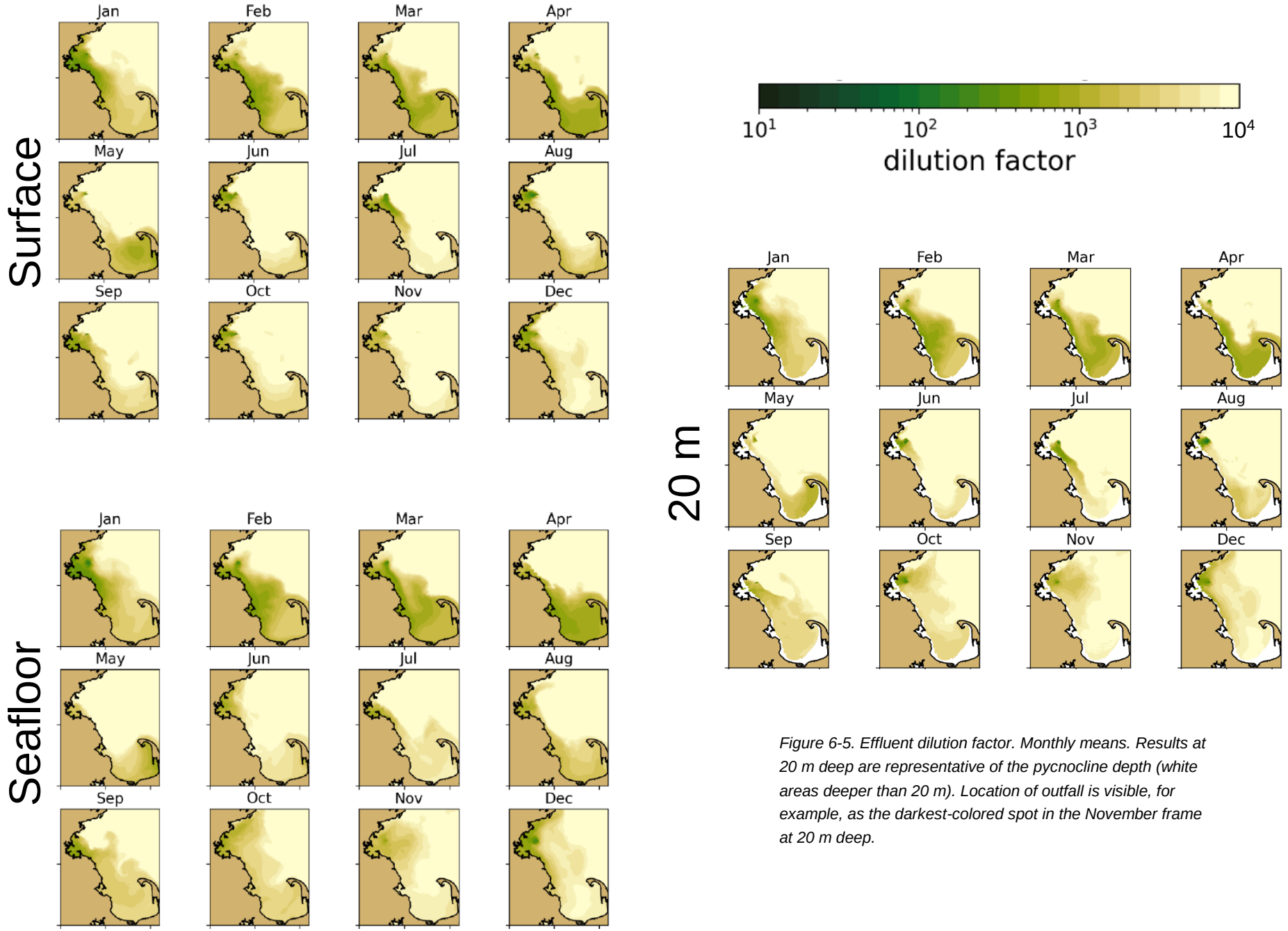

Figure 6-5. Effluent dilution factor. Monthly means. Results at 20 m deep are representative of the pycnocline depth (white areas deeper than 20 m). Location of outfall is visible, for example, as the darkest-colored spot in the November frame at 20 m deep.

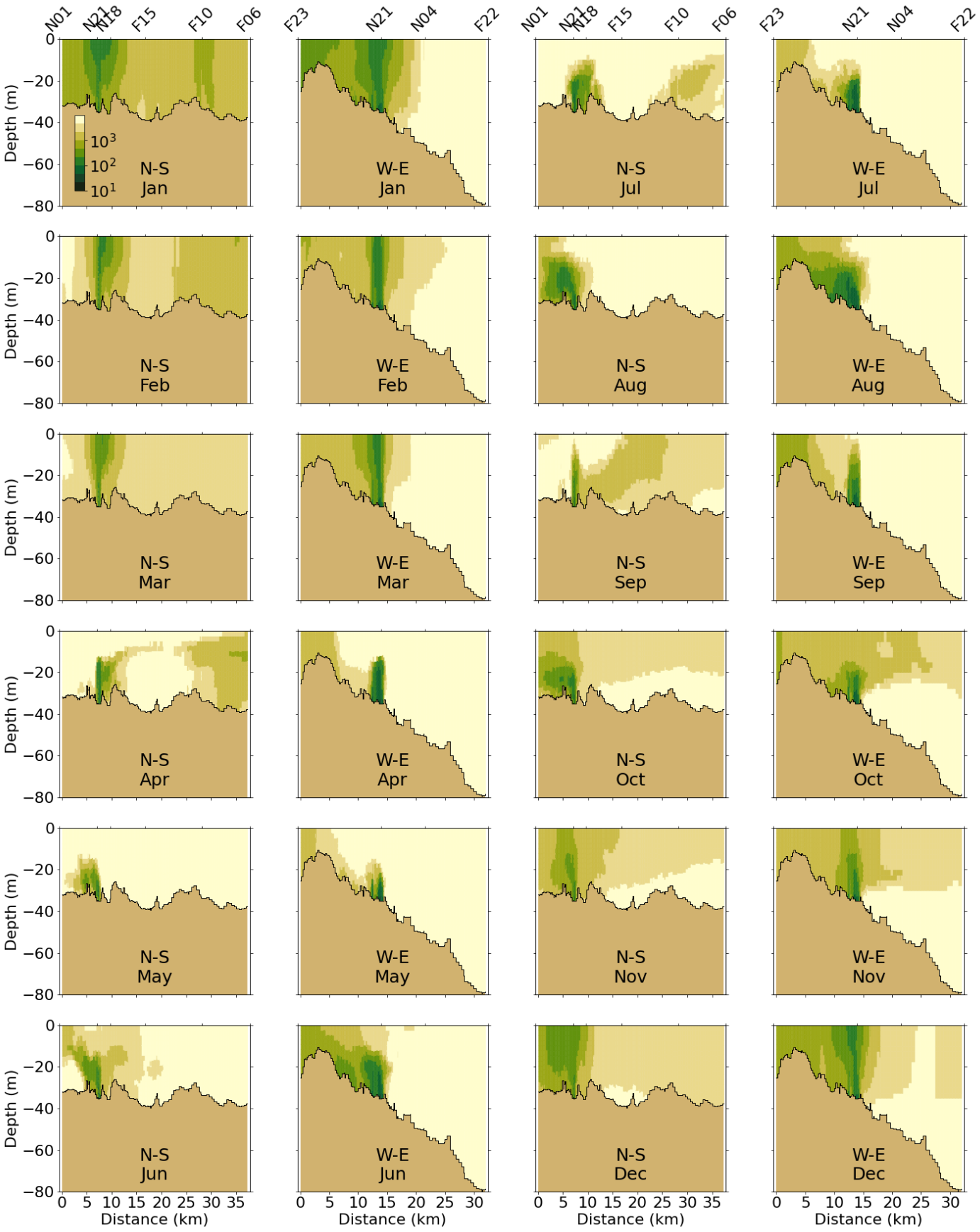

Figure 6-6. Monthly mean dilution. Vertical slices on transects in Fig. 6-4. Scale bar top left panel.

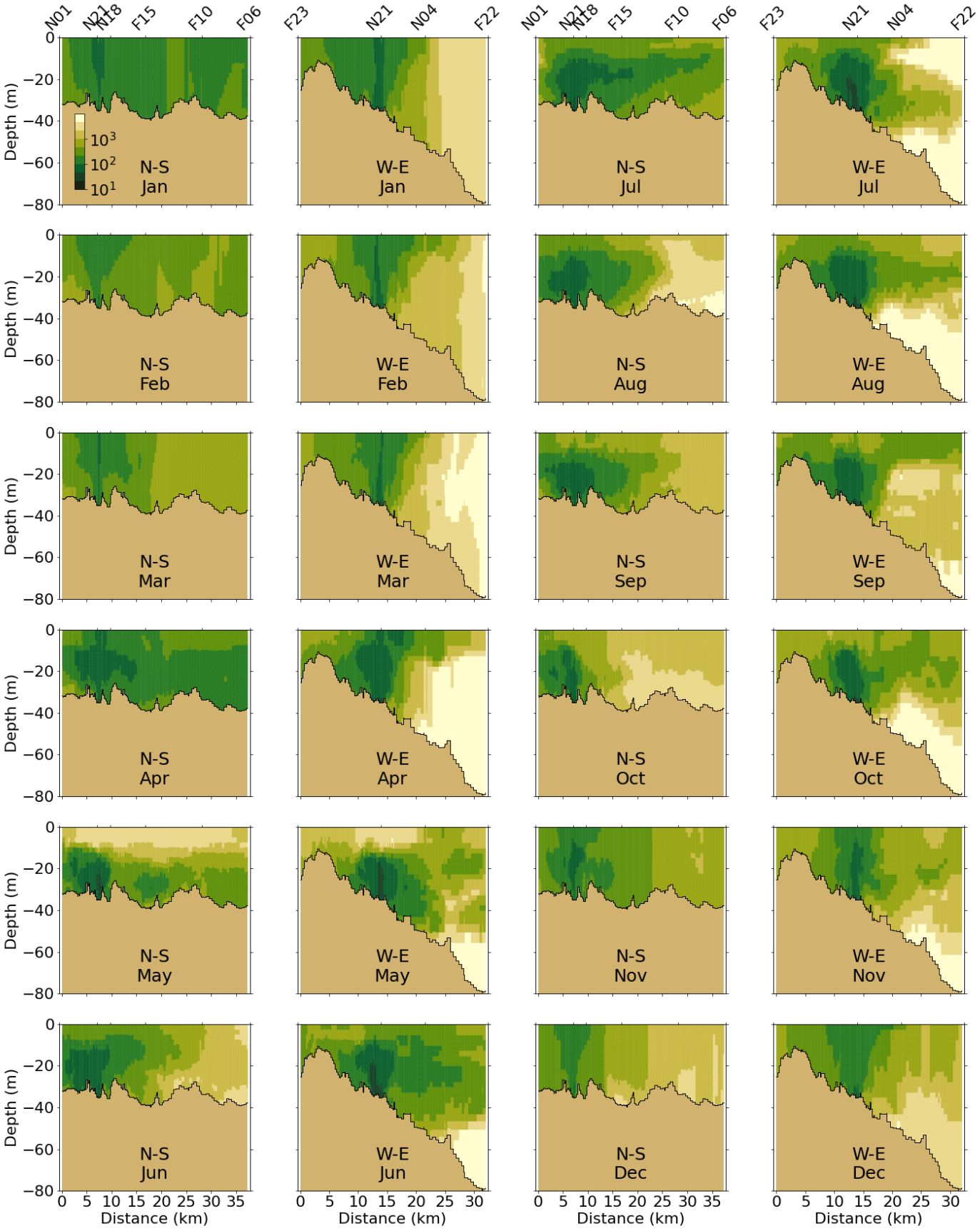

Figure 6-7. Monthly minimum dilution. Shown as in Figure 6-6.

7 Conclusion

The meteorological and hydrological forcing conditions in the year 2018 were not substantially different from the long-term mean over the previous 20 years. Wind speeds and heat fluxes showed no large deviation. However, the effect of storms in January and March was visible in the wind speed and mainly in the North-South wind stress, and a storm in November affected the monthly-mean wind speed, but not the North-South wind stress. The total discharged volume from the rivers in Massachusetts Bay and Cape Cod Bay was above the long-term mean due to multiple flow events in November and December.

Oceanic input was the dominant source of organic carbon (OC), nitrogen and phosphorus (both in organic and inorganic forms), accounting for > 90% of their total inputs. Rivers were the second largest source of OC, accounting for 86% of the non-oceanic input. MWRA loads constitute the main non-oceanic source of TN and total phosphorus (TP). These occur mainly in the inorganic form for nitrogen and in the organic form for phosphorus. Atmospheric deposition accounted for approximately 10% of the non-oceanic TN inputs. Finally, rivers are the smallest source of TN and TP to Massachusetts and Cape Cod Bays, representing 9% and 6% of non-oceanic inputs, respectively. The 2018 OC loads from the MWRA effluent were slightly higher than in the preceding years 2012-2017. The 2018 TN and TP effluent loads were in the middle of the range of loads from the preceding years 2012-2017. River loads were higher in 2018 than they were in 2017 due to higher than average river discharges.

The performance of the hydrodynamic model was similar to previous years. Temperatures performed slightly better than in previous years, especially at the surface. Model salinity showed a similar performance as for previous years. At most stations, temperature stratification was present from mid-April until mid-October with its maximum in June, July and August. Salinity stratification in 2018 was very limited. Sudden peaks in bottom temperature (and a minor drop in surface temperature) were visible in both the observations and the model in mid-August and early September.

Non-tidal currents were mostly well represented by the model. A slight deviation was visible for sudden southward directed flow events in March. Looking at a larger scale, the expected circulation pattern driven by the Western Maine Coastal Current was visible in the model. In general, the agreement between the hydrodynamic model and the observations was sufficient to conclude that the representation of processes was adequate to support water quality modeling.

Water quality conditions in 2018 where not exceptional compared to previous years, with respect to nutrient and oxygen concentrations and seasonal patterns. Overall, the water quality model accurately represented temporal dynamics and vertical gradients of the different water quality variables, e.g. DIN, POC, DO and light conditions. Skill metrics were mostly comparable to previous years.

Extinction for the year 2018 was similar to previous years. The model reproduced the extinction range and variability well at most plotted stations. The model predicted lower extinction in winter than during the rest of the year, in association with lower phytoplankton levels.

Seasonal variations of surface and bottom DIN concentrations in 2018 were similar to those observed and simulated for previous years. Surface and bottom were comparable in winter, when the water column was well mixed. Surface DIN concentrations declined in April and were depleted throughout

the rest of spring and summer, before increasing again in autumn. Bottom concentrations declined to a much lesser degree in spring and summer. The model generally reproduced these observed seasonal variations and vertical differences. In the early spring period, the model showed fluctuating levels of DIN that seem to be driven by early stratification in deeper waters towards the Gulf of Maine. For other stations, the observed onset of stratification was reproduced well by the model. At the southern stations near-bottom DIN was slightly overestimated during summer. Observed variations at intermediate depths in the water column were also generally reproduced by the model.

Seasonal variations of chlorophyll a observations in 2018 showed increased values mostly in spring and autumn. Highest concentrations were observed in fall in northern Massachusetts Bay. The model generally simulated the higher chlorophyll a peaks in spring and at the end of fall. It simulated smaller chlorophyll a summer peaks at some stations. As in the simulations for previous years, near surface simulated concentrations were in the same range as observations. Temporal variability was not always reproduced, which was diagnosed to be related to the relatively low field sampling frequency and the high temporal variability. As in the simulations for previous years, the model tends to underestimate bottom chlorophyll a at a number of stations.

POC concentrations at the observation stations were extremely variable and it was difficult to identify any clear seasonal pattern. Concentrations were, however, slightly lower in winter and early spring than the rest of the year. Measured POC concentrations were highest closer to the harbor, likely due to the high river POC inputs. Concentrations were significantly lower near the bottom than at the surface. The model generally captured POC concentration ranges, variability and vertical gradients. POC concentrations were however overestimated closer to the harbor. According to the model results, POC concentrations increased from the coast eastward. Highest simulated concentrations occurred in June, in the subsurface in the northwest. High concentrations were measured in July and August along both transects and quite deep throughout the water column (~30 m). This was not fully captured by the model and was most likely due to the underestimation of phytoplankton biomass (chlorophyll a) for that period.

The vertical cross-sections of DO concentrations for 2018 showed similar temporal and spatial patterns as for previous years, with the highest concentrations occurring near the surface between February and May. The 2018 seasonal variations of DO concentrations were reproduced well by the model, with maximum concentrations occurring at the end of winter and beginning of spring, followed by decreases until fall before rising again. Winter concentrations at the surface and the bottom were comparable, and at the end of the summer and beginning of fall bottom concentrations dropped lower than surface concentrations. As for previous years, the model reproduced minimum observed values at some stations, but not all. The model-observation comparison at intermediate water depths showed similar behavior: summer concentrations at depths nearer the surface were slightly underestimated, as was the decline of DO in fall deeper in the water column. The North-South and West-East cross-section plots show that DO generally had weak vertical gradients. Higher concentrations were observed and simulated in the subsurface in periods with higher primary production (April-July). In months with visible vertical gradients in DO concentrations, the model captured them well, for example high concentrations in the subsurface in June and July.

Primary production in 2018 was generally in the range of historical measurements for the entire year. It was also quite typical in comparison to the years 2012 to 2016, with no exceptional peaks nor prolonged periods of exceptionally low production.

Simulated sediment fluxes were low in winter and peaked in the summer due to higher temperatures, favorable to biogeochemical activity (mineralization of organic matter in the sediment). Sediment

fluxes were higher in the harbor area than in Massachusetts Bay, which was captured by the model. Results for the year 2018 were similar to those from the individual years 2012 to 2016. These were mostly in the range of historical measurements.

Although total phytoplankton biomass temporal dynamics differed from station to station for the year 2018, phytoplankton composition showed similar temporal patterns across all stations. Marine diatoms dominated in the winter period and were succeeded in spring by marine flagellates. Dinoflagellates clearly dominated from June to the end of October. These were typical characteristics of community composition seen in monitoring observations. Simulated *Phaeocystis* biomass in the model showed increased levels during the spring flagellate bloom period (April-May), most strongly at a station in Cape Cod Bay. This is consistent with available observations.

According to the model results, the MWRA outfall did not have visible effects on ecosystem functioning at the Massachusetts Bay scale. The signature of the outfall in terms of DIN concentrations was visible all year round, with increased concentrations up to a distance of about 10 km. The higher DIN concentrations were trapped in the lower layers of the water column during the period of stratification (April-October). During the other months, the effluent led to an increase in surface DIN concentrations as well. These temporal patterns were similar to those observed in previous years. All year round, chlorophyll a concentrations were higher nearshore. This was most likely due to the nutrient inputs from rivers to the harbor area, promoting algal growth. Any effect of the outfall on chlorophyll a concentrations could not be detected. Similar to chlorophyll a, no effect of the outfall on DO concentrations was evident in the model.

References

Alessi, Carol A., Beardsley, Robert C., Limeburner, Richard, Rosenfeld, Leslie K., Lentz, Steven J., Send, Uwe, Winant, Clinton D., Allen, John S., Halliwell, George R., Brown, Wendell S., Irish, James D.,1985. "CODE-2: moored array and large-scale data report", Woods Hole Oceanographic Institution Technical Report 85-35, DOI:10.1575/1912/1641. (https://hdl.handle.net/1912/1641)

Blauw AN, HFJ Los, M Bokhorst and PLA Erftemeijer, 2009. GEM: a Generic Ecological Model for estuaries and coastal waters. Hydrobiologia 618: 175-198.

Deltares, 2019a. D-Flow Flexible Mesh, Technical Reference Manual. Released for: Delft3D FM Suite 2020. Version: 1.1.0 SVN Revision: 63652. December 4, 2019.

Deltares. 2019b. Delft3D Flexible Mesh Suite, D-Flow FM in Delta Shell, User Manual, Version 1.5.0, December 5, 2019 (https://content.oss.deltares.nl/delft3d/manuals/DFlow_FM_User_Manual.pdf)

Deltares, 2021. Demonstration of the updated Bays Eutrophication Model. Boston: Massachusetts Water Resources Authority. Report 2021-02. 138 p. plus appendices. (www.mwra.com/harbor/enquad/pdf/2021-02.pdf)

Deltares, 2022a. Simulations of 2017 Hydrodynamics and Water Quality in the Massachusetts Bay System using the Bays Eutrophication Model. Boston: Massachusetts Water Resources Authority. Report 2021-12. 107 p. (https://www.mwra.com/harbor/enquad/pdf/2021-12.pdf)

Deltares, 2022b. Massachusetts Bay outfall treated effluent discharge plume characteristics from the EPA-supported near-field mixing model. Boston: Massachusetts Water Resources Authority. Report 2022-03. 24 p. (https://www.mwra.com/harbor/enquad/pdf/2022-03.pdf)

Hunt CD, RK Kropp, JJ Fitzpatrick, P Yodzis, and RE Ulanowicz, 1999. A Review of Issues Related to the Development of a Food Web Model for Important Prey of Endangered Species in Massachusetts and Cape Cod Bays. Boston: Massachusetts Water Resources Authority. Report ENQUAD 99-14. 62 p. (http://www.mwra.state.ma.us/harbor/enquad/pdf/1999-14.pdf)

Keay KE, Leo WS, Libby PS. 2012. Comparisons of Model-Predicted and Measured Productivity in Massachusetts Bay. Boston: Massachusetts Water Resources Authority. Report 2012-03. 11 p. plus Appendix. (https://www.mwra.com/harbor/enquad/pdf/2012-03.pdf)

Libby PS, Borkman DG, Geyer WR, Turner JT, Costa AS, Wang J, Codiga D. 2019. 2018 Water Column Monitoring Results. Boston: Massachusetts Water Resources Authority. Report 2019-08. 52p. https://www.mwra.com/harbor/enquad/pdf/2019-08.pdf

Libby PS, Borkman DG, Geyer WR, Turner JT, Costa AS, Taylor DI, Wang J, Codiga DL. 2021. 2020 Water column monitoring results. Boston: Massachusetts Water Resources Authority. Report 2021-07. 57 p. https://www.mwra.com/harbor/enquad/pdf/2021-07.pdf

Los, FJ, 2009. Eco-hydrodynamic modeling of primary production in coastal waters and lakes using BLOOM. Ph.D. Thesis, Wageningen University, 2009.

Signell, R.P., 2007. Effluent Dilution Simulations in Massachusetts Bay: An Evaluation of Relocating Greater Boston's Sewage Outfall. Section 5 in: Processes influencing the transport and fate of contaminated sediments in the coastal ocean—Boston Harbor and Massachusetts Bay: Bothner, M.H., and Butman, B. (eds.), U.S. Geological Survey Circular 1302, 89 p. https://pubs.usgs.gov/circ/2007/1302/sections/CIRC1302_Section5.SewageOutfall.pdf

Tucker J, Kelsey S, Giblin AE. 2010. 2009 benthic nutrient flux annual report. Boston: Massachusetts Water Resources Authority. Report 2010-10. 27 p. https://www.mwra.com/harbor/enquad/pdf/2020-10.pdf

Xue, P, C Chen, J Qi, RC Beardsley, R Tian, L Zhao, and H Lin, 2014. Mechanism studies of seasonal variability of dissolved oxygen in Mass Bay: A multi-scale FVCOM/UG-RCA application. Journal of Marine Systems. 131, 102-119.

Zhao L, Chen C, Leo WS, Mickelson MJ. 2012. Modeling 2011 in Massachusetts Bay using the unstructured-grid Bays Eutrophication Model. Boston: Massachusetts Water Resources Authority. Report 2012-13. 136 p. https://www.mwra.com/harbor/enquad/pdf/2012-13.pdf

Zhao L, Beardsley RC, Chen C, Codiga DL, Wang L. 2017. Simulations of 2016 Hydrodynamics and Water Quality in the Massachusetts Bay System using the Bays Eutrophication Model. Boston: Massachusetts Water Resources Authority. Report 2017-13. 111p.

Massachusetts Water Resources Authority
100 First Avenue • Boston, MA 02129
www.mwra.com
617-242-6000